Improving the Analysis of Radiant Thermal Effects on Children

by

Nour YOUSSEF

MANUSCRIPT-BASED THESIS PRESENTED TO ÉCOLE DE TECHNOLOGIE SUPÉRIEURE IN PARTIAL FULFILLEMENT OF THE REQUIREMENTS FOR THE DEGREE OF DOCTORAT
PH.D.

MONTREAL, DECEMBER 18, 2025

ÉCOLE DE TECHNOLOGIE SUPÉRIEURE
UNIVERSITÉ DU QUÉBEC

BOARD OF EXAMINERS (THESIS PH.D.)

THIS THESIS HAS BEEN EVALUATED

BY THE FOLLOWING BOARD OF EXAMINERS

Mrs. Katherine D'Avignon, Thesis Supervisor
Department of Construction Engineering at École de technologie supérieure

Mr. Kajl Stanislaw, President of the Board of Examiners
Department of Mechanical Engineering at École de technologie supérieure

Mr. Stéphane Hallé, Member of the jury
Department of Mechanical Engineering at École de technologie supérieure

Mrs. Lili Ji, External Evaluator
National Research Council Canada (NRCC)

THIS THESIS WAS PRENSENTED AND DEFENDED

IN THE PRESENCE OF A BOARD OF EXAMINERS AND PUBLIC

ON THE 8TH OF DECEMBER 2025

AT ÉCOLE DE TECHNOLOGIE SUPÉRIEURE

ACKNOWLEDGMENTS

I would like to express my deepest gratitude to my thesis supervisor, Professor Katherine D'Avignon, for her mentorship, support, and guidance throughout my doctoral studies at École de Technologie Supérieure. This thesis would not have been completed without her incomparable dedication and effort, and her belief in my ability to grow as a researcher. I respectfully thank each member of the jury for evaluating this thesis.

I would like to thank and dedicate this thesis to my family and friends, without whom I would not be where I am today. To my mother, my uncle Farouk, my brother Youssef, his wife Sahar, and their children Jawad, Rida and Adam, who always encouraged my academic pursuits. To my brother Fadi, his wife Sawsan, and their two children Aboudi and Ziad, who were my home away from home and who always had a place for me on their couch whenever life was too difficult to bear. To my friends Nada, Ahmad, and Rafi, for nudging me to keep writing to professors even when I faced rejection, and to make a case for myself. To my friends Wajiha, Mostafa, Vincent, and Elias, who made my life in Montreal exciting and my time at ÉTS enjoyable. To my friends Bri, Jelly, and Bea, who always made sure I had a meal to eat and a dog or cat to pet, and who were there for me in the darkest moments of my life. And finally, to my sister Farah who supported me in my studies and in my life in every imaginable way, thank you for listening to me talk about radiation and everything else.

L'amélioration de l'analyse des effets thermiques radiants sur les enfants

Nour YOUSSEF

RÉSUMÉ

Le confort thermique des enfants est un facteur important à prendre en compte dans les écoles et les garderies, car il a une incidence sur leur concentration, leur assiduité et leur bien-être général. De récentes études ont montré que les enfants ne sont pas confortables dans les écoles et que les adultes ne sont pas en mesure de prédire et d'ajuster correctement l'environnement pour répondre à leurs préférences thermiques. Or, ces espaces sont généralement conçus en fonction des charges thermiques d'occupants adultes, et le confort qui en découle est présentement évalué à l'aide de méthodes développées pour les adultes, même dans le cas où ces espaces sont occupés de façon prédominante par de jeunes occupants. Or, la plupart des paramètres de conception et des méthodes d'évaluation appliqués dans ce contexte n'ont pas été validés pour des enfants. L'un de ces paramètres est le facteur de forme, qui est utilisé pour calculer la température moyenne de rayonnement, un indice qui quantifie l'échange thermique radiatif entre l'occupant et son environnement. Cette thèse vise à combler cette lacune en analysant les méthodes utilisées pour prédire et évaluer le confort thermique des enfants, en mettant l'accent sur l'aspect radiatif de leurs échanges thermiques.

À la lumière de l'objectif énoncé, des mannequins numériques détaillés représentant des adultes, similaires aux sujets des expériences pionnières de Fanger, sont générés et utilisés pour évaluer diverses hypothèses méthodologiques. La précision des méthodes de calcul numérique par lancer de rayons (*raytracing*) et hémicube est comparée. L'effet de la pose du mannequin est étudié en position debout et s'avère avoir une influence significative sur la correspondance des données avec la littérature. La posture du mannequin adulte est donc calibrée afin de garantir que les résultats correspondent étroitement à ceux de l'homme moyen issu des expériences de Fanger. Une comparaison approfondie entre trois configurations de sièges démontre que le blocage du rayonnement provenant du sol par un siège est significatif dans tous les cas. La présence d'un siège réduit la température radiante moyenne de 2 °C dans les deux scénarios simulés avec des chaises de bureau et d'école. L'hypothèse de symétrie antérieure/postérieure, actuellement acceptée dans la littérature et utilisée dans toutes les normes de confort thermique, est réfutée en présence de sièges, ce qui nécessitera un changement méthodologique important dans toutes les futures études sur les données de rayonnement humain en position assise. La méthode rigoureuse mise au point comble plusieurs lacunes constatées dans la littérature sur les facteurs de forme, et permet le calcul numérique des facteurs de surface projetée et des facteurs de forme des mannequins numériques pour toute population étudiée.

Cette nouvelle méthode est ensuite appliquée à un mannequin numérique représentant un garçon de 5 ans afin de déterminer si les données relatives au rayonnement chez les enfants diffèrent significativement de celles chez les adultes. Un mannequin représentant un garçon de 5 ans est utilisé pour représenter la tranche d'âge la plus jeune de la population scolaire. Les mannequins représentant des enfants et des adultes sont générés en position debout et assise, avec trois différents types de sièges. En position assise, la différence entre les adultes et les enfants s'avère insignifiante. La taille plus petite et l'ombrage réduit des chaises d'école par

rapport aux chaises de bureau expliquent la plupart des différences observées entre les données de rayonnement des enfants et des adultes. Les résultats indiquent toutefois que les enfants présentent des données de rayonnement distinctes de celles des adultes en position debout. Dans les deux scénarios étudiés, l'un avec un plancher chauffant et l'autre avec un plafond rafraîchissant, les différents facteurs de surface projetée des enfants les conduisent à subir une température radiante moyenne supérieure de 1 °C à celle des adultes, ce qui affecte leur confort thermique.
La thèse conclut que les caractéristiques propres des enfants justifient qu'une attention particulière leur soit accordée dans les normes de confort thermique. En position debout, des facteurs de rayonnement spécifiques aux enfants devraient être utilisés pour la conception et l'évaluation des espaces où ils représentent l'occupant dominant. En position assise, les facteurs de rayonnement utilisé pour les adultes et les enfants devraient être révisés afin de tenir compte de l'effet d'ombrage des sièges, qui seront inévitablement présents. Pour cette position, l'hypothèse de symétrie antérieure/postérieure devrait être abandonnée au profit d'une prise en compte complète des échanges radiatifs entre le corps humain et son environnement. Des recherches supplémentaires doivent être menées sur le confort thermique des enfants, en particulier sur l'applicabilité des équations de vote moyen prévisible (PMV) actuellement utilisées pour évaluer le confort thermique des enfants, et évaluer l'effet des caractéristiques propres des enfants sur d'autres modes d'échange thermique.

Mots clés : enfant, confort thermique, transfert de chaleur par rayonnement, facteurs de forme, température moyenne de rayonnement

Improving the analysis of radiant thermal effects on children

Nour YOUSSEF

ABSTRACT

Children's thermal comfort is an important consideration in schools and daycares due to its impact on their concentration, attendance, and overall happiness. Recent research has shown that children are not thermally comfortable in schools and that adults are unable to correctly predict and adjust the environment to meet their thermal preferences. Yet, these spaces are typically designed according to the heat loads of adult occupants, and their comfort is assessed using methods developed for adults. However, most of the design parameters and evaluation approaches applied in this field have not been validated for children. One of these parameters is the view factor, which are used to calculate the mean radiant temperature, an index that quantifies the radiant thermal exchange between the occupant and its surroundings. This thesis aims to rectify this gap by analyzing the methods used for the prediction and evaluation of children's thermal comfort, with a focus on the radiant aspect of their heat exchange.

In light of the stated goals, detailed numerical manikins of adults, representative of the subjects found in Fanger's seminal experiments, are generated and used to evaluate various methodological assumptions. Raytracing and hemicube numerical calculation methods are compared for accuracy. The effect of manikin pose is investigated in the standing posture, and found to significantly influence data match with literature. The adult manikin pose is thus calibrated to ensure results closely match those of the average male from Fanger's experiments. Through a thorough comparison between three seating configurations, it is demonstrated that a seat's blocking of radiation from the floor is significant in all cases. The presence of a seat is found to lower the mean radiant temperature by up to 2 °C in the two scenarios simulated with office and school chairs. The Anterior/Posterior symmetry assumption, currently accepted in the literature and used in all thermal comfort standards, is debunked in the presence of seats, requiring an important methodological change in all future investigations of human radiation data in the seated posture. The rigorous method developed addresses several gaps found in view factor literature, allowing for numerical calculation of projected area factors and view factors of numerical manikins for any population investigated.

This novel method is then applied to a numerical manikin of a 5-year-old boy in order to investigate whether children's radiation data is significantly different from that of adults. A 5-year-old boy manikin is retained to represent the lower end of the child population found in schools. Both child and adult manikins are generated in the standing and the seated posture combined with three different seating configurations. In the seated posture, the difference between the adult and child is found to be insignificant. The smaller size and reduced shading by school chairs when compared to office chairs explains the majority of the differences found when comparing the child and adult radiation data. The results indicate however that children have distinct radiation data than adults in the standing posture. In the two test scenarios considered, one with radiant floor heating, and another with a chilled ceiling, the child's different projected area factors lead them to experience a mean radiant temperature up to 1 °C greater than the adults', affecting their thermal comfort.

The thesis concludes that children's particular characteristics warrant a special consideration in thermal comfort standards. In the standing posture, child specific radiation data should be used for the design and evaluation of spaces where occupants are primarily children. In the seated posture, the radiation data used for both adults and children should be revised to account for the shading effect of seats that will inevitably be present, and the Anterior/Posterior symmetry assumption should be disposed of in favour of a complete accounting of radiant exchange of the human body with its environment. More research must be done on children's thermal comfort, particularly on the applicability of the predicted mean vote equations currently in use for the evaluation of children's thermal comfort, and to evaluate the particularity of children in other modes of heat exchange.

Keywords: children, thermal comfort, radiant heat exchange, view factors, mean radiant temperature

TABLE OF CONTENTS

LIST OF TABLES

Page

LIST OF FIGURES

Page

LIST OF ABREVIATIONS

3D	Three dimensional
5-B	5-year-old boy manikin
A/P	Anterior/Posterior
A-M	Adult Manikin
A-M, L	Adult male manikin with its arms lowered
A-M, R	Adult male manikin with its arms raised
ASHRAE	American Society of Heating, Refrigerating and Air-Conditioning Engineers
BGT	Black Globe Thermometer
BMI	Body Mass Index
BSA	Body Surface Area
CBE	Center for the Built Environment
CFD	Computational Fluid Dynamics
GPU	Graphics processing unit
HVAC	Heating, Ventilation, and Air Conditioning
ISO	International Organization for Standardization
MRT	Mean Radiant Temperature
NHANES	National Health and Nutrition Examination Survey
PMV	Predicted Mean Vote
PPD	Predicted Percentage Dissatisfied
PR	Parallel ray method
RMR	Resting Metabolic Rate
SA	Solid angle method

SHS	Sitting Height to Stature ratio
TSV	Thermal Sensation Vote
UMTRI	University of Michigan Transportation Research Institute
L/R	Left/Right symmetry

LIST OF SYMBOLS AND UNITS OF MEASUREMENT

A_{DuBois}	Human body surface area calculated using the Du Bois equation, in m^2
q_{ir}	Intensity of radiation emitted by the sun, in W
α_{ir}	Absorptivity of the skin/clothing, unitless
A	Surface area, in m^2
A_{eff}	Effective radiation area, in m^2
A_p	Projected area, in m^2
A_t	Total manikin body surface area, in m^2
c	Distance from occupant's center of mass to the center of rectangular section, in m
EE	Energy Expenditure, in kcal/day
F	View factor, unitless
$F_{m\text{-}ss}$	View factor between a manikin (m) and sphere section (ss), unitless
$F'_{m\text{-}ss}$	Corrected view factor between a manikin (m) and sphere section (ss), unitless
f_c	Correction factor, unitless
f_{cl}	Clothing area factor, unitless
f_{eff}	Effective radiation area factor, unitless
f_p	Projected area factor, unitless
h_c	Convective heat transfer coefficient, in $W/m^2 \cdot K$
M	Metabolic rate, in W/m^2
met	Energy produced per unit body surface area of an average person seated at rest, equal to 58.15 W/m^2
pa	Vapor pressure at ambient temperature, in kPa
r	Sphere radius, in m

R_{lw}	Low-wave radiation emitted by the body, in W/m^2
R_{sw}	Short-wave radiation absorbed from the sun, in W/m^2
S	Distance between surfaces, in m
SD	Standard deviation
t	Temperature, in °C or Kelvin
t_a	Air temperature, in °C
t_{cl}	Clothing surface temperature, in °C
t_g	Globe temperature, in °C
$\overline{t}_r$	Mean radiant temperature, in °C
VF	View factor between the occupant and a surrounding rectangular surface, unitless
W	Rate of mechanical work accomplished, in W/m^2
α	Azimuth, in degrees
β	Altitude, in degrees
Δ	Absolute difference, unitless
Ω	Solid angle, in sr
dA	Differential surface area, in m^2
ε	Emissivity of the skin/clothing, unitless
θ	Angle, in degrees
σ	Stefan-Boltzmann constant, in $W/(m^2 \cdot K^4)$

INTRODUCTION

Context and problematic

Thermal comfort plays an important role in children's school performance, influencing both their concentration and attendance (Zeiler & Boxem, 2009). However, field studies conducted in schools and daycares have consistently shown that children often experience thermal discomfort in these environments (De Giuli et al., 2012; Trebilcock et al., 2014). Several studies have posited that the reason for this discomfort is that classrooms are essentially designed for adults – i.e. using methods and data only validated for adult occupants. This oversight is problematic since adults have been found to have different thermal sensations and preferences than children (De Dear et al., 2015; Haddad et al., 2013; Martinez-Molina et al., 2017; Mors et al., 2011; Teli et al., 2012; Yang et al., 2018). Additionally, adults are unable to accurately predict and adapt the environment to children's preference (Folkerts et al., 2020; Montazami & Nicol, 2013). These issues draw attention to the precarity of relying on current standards for thermal comfort design in classrooms where children are the dominant occupant group.

The PMV method (predicted mean vote) is the most used method for the evaluation of thermal comfort in the indoor environment, is recommended by professional associations such the American Society of Heating, Refrigerating and Air-Conditioning Engineers (ASHRAE) and included in common thermal comfort standards such as ASHRAE Standard 55 (ASHRAE-55, 2017). In that method, the PMV is calculated based on six factors: air temperature, air relative humidity, air velocity, mean radiant temperature (MRT), metabolic rate, and clothing insulation. ASHRAE Standard 55 states that the method itself, as well as the data it provides for the measurement or calculation of each parameter, is based on experiments conducted on adults and is not applicable to children. Consequently, there is a need to examine this method and to analyze its different parameters to assess whether they contribute to the evident discrepancy observed.

Radiation accounts for a large proportion of the heat exchange of occupants in indoor environments (La Gennusa et al., 2005). The MRT is used to represent the radiant thermal effect of an indoor environment on the occupant. ASHRAE Standard 55 (ASHRAE-55, 2017) provides a method for the calculation of the MRT using the view factors provided by Fanger (1970) from his study involving solely adult subjects. View factors are geometrical parameters which are dependent on the shape, size, and posture of the occupant, which indicates that they are likely to be different for young children due to differences in anthropometric characteristics between children and adults (Frisancho, 2008). Presently, there is a gap in the literature with regards to children's view factors; child-specific view factors do not exist in the literature nor have adult view factors been validated for this population, indicating the need for their determination for an accurate calculation of the MRT felt by children.

Several studies have determined the radiation data (i.e. view factors, projected area factors, effective radiation area factors) of occupants in the indoor environment either experimentally or numerically (Bedford, 1935; Calvino et al., 2005, 2009; Chen et al., 2024; Fanger, 1970; Francisco et al., 2012; Havgaard Vorre et al., 2015; Horikoshi et al., 1990; Jones et al., 1998; Kubaha et al., 2004; La Gennusa et al., 2005, 2008; Lo Curcio FP, 2009; Manabe et al., 2004; Park & Tuller, 2011; Rykaczewski et al., 2022; Tanabe et al., 2000; Underwood & Ward, 1966; Y. Wang et al., 2014, 2020; Wei et al., 2004; Xu et al., 2019; Yousaf et al., 2008; Zeng et al., 2024a). With advancements in computing, numerical methods have lately dominated the field, but there remain several issues, assumptions, and points of contestation in the literature on the suitability of the methods used, some dating back as far as the early seminal work by Fanger (1970). In numerical studies, two calculation methods are found, one relying on the parallel ray method and the other on the solid angle method, with some studies claiming that the former is inapplicable to the indoor environment due to the short distance between the occupant and surrounding surfaces (Horikoshi et al., 1990; Kubaha et al., 2004; Tanabe et al., 2000). Additionally, the pose assumed by subjects (i.e., angle of arms in the standing posture, position of arms with regards to the legs in the seated posture, etc.) was found to affect the results, prompting questions on whether the pose of subjects or numerical manikins skew attempts at comparison between studies. One major assumption presented by Fanger (1970) and thereafter

unchallenged in the literature is the Anterior/Posterior symmetry (explained in detail in Chapter 5), which is likely to be inapplicable in the seated posture. The studies which considered occupants in the seated posture have also mostly neglected to account for the shading effect of the seat on the amount of radiation that the occupant can exchange with surrounding surfaces, particularly with the floor. In short, there are many considerations that need to be accounted for in the development of a robust method for the calculation of occupants' radiation data, regardless of whether children or adults are the targeted occupant group.

Main and sub-objectives

In the context detailed above, this thesis has as its general objective the improvement of the analysis of children's radiant exchange with their environment. To accomplish this, the following three sub-objectives are identified:

1- To determine a rigorous and generalizable method for the calculation of radiation data using human numerical manikins.

The determination of such a method requires addressing the following aspects:

   a. Identifying which numerical method (solid angle or parallel ray) is applicable to indoor environments (i.e., for surfaces that are at a close distance from the occupant).
   b. Selecting the pose assumed by the manikin so as to minimise its possible effects on the calculated data.
   c. Verifying the validity of the Anterior/Posterior symmetry, which is commonly assumed in standards and studies of human view factors, particularly for the seated posture.
   d. Quantifying the effect of seat blocking on the radiation received by seated occupants.

2- To investigate the difference in radiation data between adults and children, and whether it is significant in various settings.

3- To provide the needed radiation data, missing from standards and literature, to allow adequate calculation of radiation data for a spectrum of occupants: children in the standing and seated posture, as well as adults in the seated posture with different types of seats.

Structure of thesis

This thesis by article is presented in six chapters. The first chapter presents the first conference paper titled "Evaluating Thermal Comfort for Children: A Perspective on Commonly Used Methods". This paper was presented at the 2021 ASHRAE Annual conference and published in the conference's proceedings (Youssef & D'Avignon, 2021). It explores how children's thermal comfort is currently evaluated in the literature, highlighting aspects where physiological and anthropomorphic differences between adults and children could have an impact, and providing recommendations for improvement. In the present thesis, this chapter provides the reader with a literature review on important elements of thermal comfort evaluation which are paramount to understand the choice to focus on thermal radiation.

After this first chapter, the thesis delves into its topic of focus: calculations of human radiation. In the second chapter, a specific literature review is conducted on the determination of human radiation data. This chapter seeks to provide the rationale for the choice of investigating radiation data numerically rather than experimentally, as well as for the method retained in the following chapters. The third chapter presents the first journal paper titled "Considering child-specific view factors in human thermal balance". This article was published in the journal *Science and Technology for the Built Environment* (Youssef & D'Avignon, 2025). It presents the first full use of the refined method (Obj. 1) and provides a definite answer to the applicability of some common assumptions (a. and b.). It provides children's radiation data in the standing posture (Obj. 3) and a comparison to adult values (Obj. 2), which establishes the significant differences and the need to further investigate radiation effects on child occupants. The fourth chapter presents the second journal paper, titled "Are We Overestimating Radiant Effects? Re-examining View Factors in the Seated Posture", which was published in the journal *Building and Environment*. The paper explores the seated posture of both adults and

children and addresses the assumptions (c. and d.) discussed above. The fifth and final chapter presents a discussion of the main results of the thesis, followed by a general conclusion, and recommendations for future work.

CHAPITRE 1

ARTICLE 1: EVALUATING THERMAL COMFORT OF CHILDREN: A PERSPECTIVE ON COMMONLY USED METHODS

Nour Youssef, Katherine D'Avignon

Département de génie de la construction, École de Technologie Supérieure, 1100 Notre-Dame Ouest, Montréal, Québec, Canada H3C 1K3

Article presented at ASHRAE 2021 Virtual conference, published in ASHRAE Transactions 129 (2), June 2021

The present chapter establishes the broader context of children's thermal comfort and critically examines how it is currently evaluated in the literature. By reviewing commonly used methods and standards which were originally developed and validated for adults, it highlights systematic limitations when these approaches are applied to child occupants. This chapter motivates the thesis by identifying key sources of discrepancy in thermal comfort assessment before narrowing the focus toward the radiative component of heat exchange as a particularly underexplored contributor.

1.1 Introduction

The selection of indoor environment conditions, used by professionals to design, size, and control HVAC systems, is predicated upon an ability to predict occupant thermal sensation. However, field evaluations of thermal comfort in spaces dominated by children (schools, daycares and child development centers) indicate that one of the foremost methods, the predicted mean vote (PMV), fails to adequately estimate the thermal sensation of children (De Dear et al., 2015; Haddad et al., 2013; Martinez-Molina et al., 2017; Mors et al., 2011; Teli et al., 2016; Yang et al., 2018). Reported discomfort in classrooms (De Giuli et al., 2012; Trebilcock et al., 2014) indicates notably different indoor environment conditions could be required for these occupants. Young children's inability to easily adjust their clothing or environment, and evidence (Folkerts et al., 2020; Montazami & Nicol, 2013) that care

providers' attempts to predict children's thermal comfort are ineffective, call into question the reliability of occupants' adaptive comfort behaviors to offset thermal discomfort in early-childhood education facilities. An accurate method to predict thermal sensation of children is needed.

This paper examines thirty-four studies from the literature on the evaluation of children's indoor thermal comfort in early-childhood education facilities to determine if recommendations can be made for a formal method for such occupants. First, we present the recommendations and requirements set forth by the standards. Then, we analyze the methods used in the considered studies to determine environmental factors, with a special focus on their adherence to standard requirements and applicability to child occupants. Similarly, we examine the methods used to determine the metabolic rate and clothing insulation in the considered papers to identify the most promising approaches. Finally, we highlight issues in the examined protocols and present recommendations for future improvements to thermal comfort studies of young children.

1.2 Standards and norms

1.2.1 ASHRAE 55: Thermal environmental conditions for human occupancy

ASHRAE Standard 55 (ASHRAE-55, 2017) specifies that its scope is "limited to healthy adults" as it was developed based on experiments conducted solely on that population. It offers four methods of determining comfort, but in this study, we will study only the analytical method, as it is applicable to most cases of school environments and more detailed than the graphical method. This method uses six factors - four environmental factors (air temperature, air relative humidity, mean radiant temperature, and air velocity) and two personal factors (metabolic rate and clothing insulation) - to predict thermal comfort of occupants using two indexes: the predicted mean vote (PMV), and the predicted percentage dissatisfied (PPD). The PMV is calculated using heat balance principles and represents the prediction of the thermal sensation of occupants - based on the six factors - which can then be compared to ASHRAE's

seven-point scale. The PPD index is calculated from the PMV and predicts the percentage of people who can be expected to be decidedly dissatisfied in a specific thermal environment. The computer code, provided for the calculation of PMV in Standard 55, which was obtainable from Annex D of ISO 7730 (ISO 7730, 2005), is presented in Equation (1.1) in SI units and (1.2) in I-P units and was obtained from the ASHRAE Handbook of Fundamentals (ASHRAE, 2017).

$$\begin{aligned}\mathrm{PMV} = {} & [0.303 \cdot \exp(-0.036\mathbf{M}) + 0.028] \\ & \cdot \{(\mathbf{M} - \mathrm{W}) - 3.05 \cdot 10^{-3} \\ & \cdot [5733 - 6.99 \cdot (\mathbf{M} - \mathrm{W}) - \mathrm{p_a}] - 0.42 \\ & \cdot \left[(\mathbf{M} - \mathrm{W}) - \boxed{58.15}\right] - 1.7 \times 10^{-5}\mathbf{M}(5867 - \mathrm{p_a}) \\ & - 0.0014\mathbf{M}(34 - \mathrm{t_a}) - 3.96 \\ & \cdot 10^{-8}\mathrm{f_{cl}}[(\mathrm{t_{cl}} + 273)^4 - (\overline{\mathrm{t_r}} + 273)^4] - \mathrm{f_{cl}}\mathrm{h_c}(\mathrm{t_{cl}} - \mathrm{t_a})\}\end{aligned} \tag{1.1}$$

$$\begin{aligned}\mathrm{PMV} = {} & 3.155[0.303\exp(-0.114\mathbf{M}) + 0.028] \cdot \{(\mathbf{M} - \mathrm{W}) - 1.196 \\ & \cdot 10^{-9}\mathrm{f_{cl}}[(\mathrm{t_{cl}} + 460)^4 - (\mathrm{t_r} + 460)^4] + \mathrm{f_{cl}}\mathrm{h_c}(\mathrm{t_{cl}} - \mathrm{t_a}) \\ & + 0.97[5.73 - 0.022(\mathbf{M} - \mathrm{W}) - 6.9\mathrm{p_a}] \\ & + 0.42\left[(\mathbf{M} - \mathrm{W}) - \boxed{18.43}\right] + 0.0173\mathrm{M}(5.87 - 6.9\mathrm{p_a}) \\ & + 0.00077\mathbf{M}(93.2 - \mathrm{t_a})\}\end{aligned} \tag{1.2}$$

The metabolic rate (M) is a significant input to the calculation of the PMV and has been identified as a possible cause for the disparity between the PMV and thermal sensation vote (TSV) resulting from surveys of child occupants. Standard-55 (ASHRAE-55, 2017) defines M as the rate of transformation of chemical energy into heat and mechanical work by metabolic activities of a person, per unit of body surface area (W/m^2 or $Btu/h{\cdot}ft^2$). For simplicity, the metabolic rate induced by specific activities has been tabulated in units of "met" to convey their intensity relative to the resting metabolic rate (RMR). Standard-55 presents a table of *met* values applicable to the average adult using an average DuBois body surface area of 1.8 m^2 (19.4 ft^2). The M can then be calculated through Equation (1.4), by multiplying the average adult RMR (i.e., the energy produced per unit body surface area of an average person seated

at rest) of 58.15 W/m^2 (18.43 Btu/h·ft^2) with the *met* value of the task performed. Equations (1.1) and (1.2) shows that the metabolic rate (M) affects the PMV equation in two ways: first as an input to the equation (in bold); second as a constant, where the average adult RMR value of 58.15 W/m^2 (or 18.43 Btu/h·ft^2), hereafter known as RMR_{adult}, appears directly in the equation (framed in a text box). Any attempt to apply the PMV equation to children must stipulate how both terms are to be treated.

The Standard allows several methods to determine the clothing insulation value for the representative occupant. It provides a reference to tabulated values of clothing insulation, for ensembles or individual garments, procured from experimental measurements of adult clothing. It also proposes a correlation relating clothing insulation values to outdoor air temperature at six am. The Standard makes clear that this correlation is based on field studies of adult populations and may not be appropriate for all cultures and occupancy types.
The Standard presents recommendations on the measurement of environmental factors but for brevity, only the protocols and requirements of ISO 7726 (ISO 7726, 1998) are presented in the next section.

1.2.2 ISO 7726: Ergonomics of the thermal environment - Instruments for measuring environmental quantities

ISO 7726 (1998) provides methods for measuring each environmental factor including the required instrument measuring range, response time, and accuracy. It considers the variation of environmental factors in location and time, highlighting the importance of placing sensors relative to the occupant's location in the space. ISO 7726 recommends measuring environmental factors at three different heights (occupants' ankles, abdomen, and head) in order to determine mean values of the environmental parameters. Appropriate sensor heights meeting average adult anthropometric measurements when seated (0.1 m (4 in.), 0.6 m (24 in.), 1.1 m (43 in.)) and standing (0.1 m (4 in.), 1.1 m (43 in.), 1.7 m (67 in.)) are provided for reference. Though they are expected to differ significantly from adult values, the ISO standard does not state recommended sensor heights applicable to children's ankles, abdomen, and head.

It also specifies the conditions under which an environment is considered homogeneous. Though air temperature, velocity, and humidity are frequently homogeneous, it is rarer for thermal radiation. ISO 7726 describes a method to determine the mean radiant temperature (MRT) from the measurement of black globe temperature, air temperature, and air velocity at the level of the globe and recommends a globe diameter of 0.15 m (5.9 in.). ISO highlights that the use of a black globe thermometer is an approximation due to the difference between the shape of a person and that of a globe. It states that an ellipsoid offers a closer approximation of the shape of the human body but makes no specific reference as to whether this applies to children's bodies as well.

1.3 Methodologies used in the studies

The majority (75%) of the considered papers used the same general methodology: they conducted field studies where environmental factors were measured, personal factors were calculated from adult data, and thermal sensation votes were collected through a questionnaire and compared to the calculated PMV. These studies covered different institution types (25 elementary schools, 3 kindergartens, 2 secondary schools, 2 junior highs, 3 high schools, and 2 nurseries), countries (7 in Europe, 4 in Asia, 2 in South America, 1 in Australia and 1 in the USA), climates, and seasons. Studies included free running, naturally ventilated classrooms (17), heated and/or cooled classrooms with natural ventilation (9), as well as classrooms equipped with mechanical HVAC systems (4). Some studies solely focused on one of the needed factors (Haddad et al., 2013; Nam et al., 2015) but are included because of their impact on the field. Most studies (15) used ASHRAE's 7-point scale to survey the students' thermal sensation. Others adjusted the questionnaire to children's understanding based on assistance from psychologists, doctors, educators, and the children themselves: nine used colors, symbols, and sketches in place or in addition to the questionnaire; four explained the meaning of the words prior to the survey; five adjusted the terminology to match children's vocabulary. Analysis of these alternative surveys methods is beyond the scope of this paper, which instead focuses on the parameters used to calculate PMV.

1.3.1 Environmental factors

Methods used to measure each environmental factor are evaluated as a possible cause for discrepancy between the PMV and TSV. Adherence of sensor characteristics to the previously mentioned standards is verified first, then applicability of the protocols used to children anthropometric characteristics is analyzed.

Air temperature. Around half the considered studies did not specify the measuring range or accuracy of the probes used to measure air temperature. Among those that did, all studies respected the required range criteria, and all but three (De Dear et al., 2015; De Giuli et al., 2012; Martinez-Molina et al., 2017) respected the accuracy requirement. None of the considered studies reported the use of a radiation shield for the air temperature sensor.

Relative humidity. Nearly half the studies did not report the measuring range and accuracy of probes used to measure relative humidity. Among those that did, all respected the accuracy requirement, and only Teli et al., (2016) failed to respect the range requirement.

Air velocity. All the studies that reported these values respected the requirements except for De Dear et al. (2015) and Mors et al. (2011).

Mean radiant temperature. Six of the studies did not measure the mean radiant temperature. Teli et al. (2016) measured the MRT but chose to use the air temperature in their analysis without correction due to its negligible difference from the operative temperature. Conceição & Lúcio (2008) and Alfano et al. (2013) calculated the MRT through the mean value of the compartment's surrounding surface temperatures, as permitted by ISO 7726. None of the considered studies calculated the MRT using angle factors. All of the studies that did measure the MRT used a globe thermometer and respected the diameter requirement of 0.15 m (5.9 in.), except for Fabbri (2013) and Teli et al. (2016) who used a lower accuracy globe of 0.05 m (1.96 in.). None of the studies used an ellipsoid shaped globe.

Occupant posture and location. Occupant posture affects the height of their ankles, abdomen, and head and so dictates the recommended sensor placement heights. It also influences the calculation or measurement of the MRT: black globe shape should be changed between sitting and standing postures as should the angle factors used. In the studies considered, posture ranged between seated (12 of 34), standing (3 studies), reclining (1), and sleeping (1) among those that reported it. Nam et al. (2015) and Yun et al. (2014) reported both standing and seated postures in the classroom but placed the equipment at a single height (1.2 m (47.24 in.) and 1.1 m (43.3 in.), respectively). The location of the occupant inside the space was rarely collected in the considered studies. In addition, none of the studies verified the spatial homogeneity of the classroom. Souza et al. (2020) assumed spatial homogeneity without providing justification. Often, the placement of sensors (in respect to location in the classroom and height from the floor) was chosen based on practicality and protection of the measuring equipment from meddling by the children.

Sensor height. Figure 1.1 presents the heights at which environmental factors were measured in the considered studies. Few measured them at three heights. Most commonly, a single height of 1.1 m (43.3 in.) was used, which is referenced in ISO as both the head height for standing adults and the abdomen height of seated adults. Some studies (Alfano et al., 2013; Haddad et al., 2014) measured at all three ISO recommended heights for seated adults, while Souza et al. (2020) measured at two of them (0.6 and 1.1 m). Though Dijken et al. (2005) and Montazami et al. (2017) reported making measurements at the children's height, no values were specified.

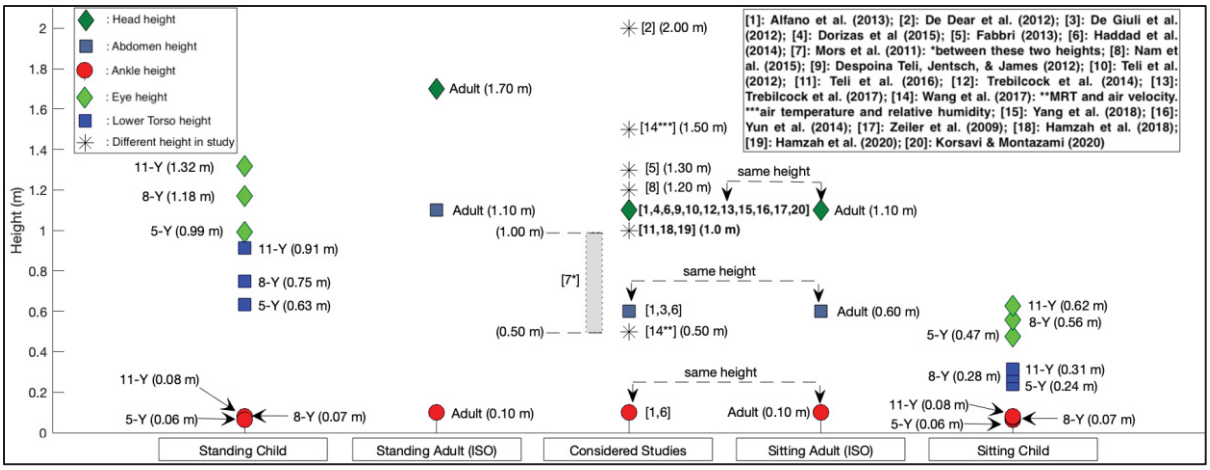

Figure 1.1 Sensor height compared to ankle, abdomen and head height of adults and children aged 5, 8, and 11 years old

Figure 1.1 also shows the ankle, lower torso and eye-level heights of children aged 5, 8 and 11 years old, in the standing and seated position, as collected from CDC data (Mcdowell et al., 2008) and child human body shapes developed by UMTRI (University of Michigan Transportation Research Institute, 2020). These levels are in accordance with Cheng & Brown, (2020) who used a 1 m measurement height to represent the average chest height of children aged 7-12, standing outdoors. Figure 1.1 makes clear that the reference heights presented for children differ significantly from those recommended by ISO for adults, especially in the case of sitting occupants.

1.3.2 Personal factors

Personal factors are those that relate directly to the occupant's personal characteristics. Although studies (Schweiker et al., 2018) suggest that other factors (psychological, sex, fitness, adaptation methods, etc.) have an effect on the perception of thermal comfort, the factors of interest in this paper are metabolic rate and clothing insulation.

Metabolic Rate. In their review on the state of metabolic rate research in the thermal comfort domain, Luo et al. (2018) note that among the six variables in the heat balance equation,

metabolic rate is the parameter whose estimation or prediction is most inaccurate. Havenith (2007) has found that the use of adult metabolic rate data in the assessment of children's thermal comfort results in error. In their experimental study on children aged 8-18 years-old, Harrell et al. (2005) found that the energy expenditure (both at rest and during activity) varies by pubertal stage. Yet almost one fourth of the studies used unchanged adult metabolic rate data in their thermal comfort assessments.

Three studies (Haddad et al., 2013, 2014; Teli et al., 2012) compared TSV to PMV resulting from different children metabolic rate calculation protocols. Haddad et al. (2013, 2014) used novel experimental data to test the sensitivity of the PMV to combinations of RMR values and *met*, obtained through different protocols. Their results underlined the important sensitivity of PMV to both the metabolic rate and RMR and identified potential gaps in methodology. Teli et al. (2012) tested four different approaches to determine the metabolic rate of children and evaluated them based on the resulting level of agreement between PMV and TSV.
The approaches put forward in the considered studies are presented in six groups, based on similarities in their protocol. The protocols and findings of Haddad and Teli, including the agreement of PMV and TSV results, will be discussed.

1. $M_{activity}$ - RMR_{adult}. Very few studies have attempted to use child specific values of metabolic rates in classrooms as an input in the calculation of PVM (Equation (1.1)). Havenith (2007) measured the metabolic rate of children aged 9-16 years old and found values ranging from 52 to 72 W/m^2 (16.48 to 22.82 Btu/h·ft^2) for activities in lecture rooms (lower as an average than those reported from adults doing office work), and from 69 to 80 W/m^2 (21.87 to 25.35 Btu/h·ft^2) for activities in combined lecture-practice rooms. Based on these findings, several studies (Teli et al., 2012; D. Wang et al., 2017; Zeiler & Boxem, 2009) used values in these ranges as the metabolic rate input to the PMV equation without changing the value of RMR_{adult} inherent in the formula.

2. $M_{RMR\text{-}child}$ - RMR_{adult}. Experimental work by Amorim (2007) determined the Energy Expenditure (EE_{child}) of children aged 7-11 years old to range from 4234 to 5941 kJ/day

(4013.25 to 5631.24 Btu/day). Using that value, four studies calculated the RMR of a hypothetical 10-year-old child (RMR_{child}) using Equation (1.3) with a Du Bois & Du Bois (1916) body surface area (A_{DuBois}) of 1.14 m^2 (12.27 ft^2). As shown in Equation (1.4), the metabolic rate of the hypothetical 10-year-old child ($M_{RMR\text{-}child}$) was then calculated by multiplying the child-specific RMR_{child} with the adult *met* value from ASHRAE tabulated data. In this protocol, $M_{RMR\text{-}child}$ is used as an input to the PMV equation without changing the value of RMR_{adult} inherent in the formula. It should be noted that while the Du Bois formula has only been validated for adults, Havenith (2007) verified that its values stayed within 1.5% of those found using J. Wang & Hihara (2004)'s theoretical model, which is validated for children.

$$RMR = EE/A_{DuBois} \tag{1.3}$$

$$M = met \times RMR \tag{1.4}$$

3. $M_{Schofield}$ - RMR_{adult}. A study by Schofield (1985) reviewed 50 years of data on basal metabolism and computed a set of equations to predict the RMR of children from weight (W) or weight and height (WH) for different age groups and genders. Haddad et al. (2014) used the Schofield-WH equations to calculate the $RMR_{Schofield}$. $M_{Schofield}$ was then calculated by multiplying $RMR_{Schofield}$ with the adult *met* value found in ASHRAE tabulated data. In this protocol, $M_{Schofield}$ is used as an input to the PMV equation without changing the value of RMR_{adult} inherent in the formula. This was also the protocol used by (Cheng & Brown, 2020) in their recent outdoor study.

4. M_{BSA} - RMR_{adult}. Five studies adjusted RMR_{adult} to account for the body surface area difference between adults and children. In this protocol, hereafter labelled Body Surface Area (BSA) adjustment**,** an adjusted RMR (RMR_{BSA}) is calculated using Equation (1.5) where $A_{DuBois(adult)}$ is the Du Bois BSA of an adult, and $A_{DuBois(child)}$ that of a 10-year-old child. Some studies (Cheng & Brown, 2020; Haddad et al., 2014) calculated the BSA using Haycock et al. (1978)'s equation which was validated in infants and children, but Haddad et al. (2014) elected to use the Du Bois formula due to its wide use in the field. M_{BSA} was then calculated by

multiplying RMR_{BSA} with the adult *met* value found in ASHRAE tabulated data. This version of the protocol then uses M_{BSA} as an input to the PMV equation without changing the value of RMR_{adult} inherent in the formula. Fabbri (2013) and Martinez-Molina et al. (2017) also used M_{BSA} - RMR_{adult} but adjusted the metabolic rate for the BSA of a 4-5-year-old or 6-7-year-old child, respectively, to better match the occupants concerned.

$$RMR_{BSA} = RMR_{adult} \times \frac{A_{DuBois(adult)}}{A_{DuBois(child)}} \quad (1.5)$$

5. M_{BSA} - RMR_{BSA}. This protocol uses a BSA adjusted metabolic rate as an input to the PMV equation as previously but also replaces the value of RMR_{adult} in the PMV formula with RMR_{BSA}. Teli et al. (2012) and Yang et al. (2018) used this approach in their evaluation.

6. $M_{activity}$ - RMR_{child}. This last protocol uses Havenith's classroom activity metabolic rate, $M_{activity}$, as an input to the PMV equation and replaces the value of RMR_{adult} with RMR_{child} obtained from Amorim's data (see protocol 2, above). Teli et al. (2012) used this approach in their study.

Clothing. In his field study, Havenith (2007) calculated the thermal insulation of students' PE clothing (aged 9-18) based on their BSA and the weight of the clothing but did not consider potential differences in material. He did not find a significant difference between children's (0.9 to 1.0 clo in the winter) and adults' average clothing insulation, implying average adult clothing insulation patterns could reliably be used for children. Similarly, some studies used Standard 55's correlation to determine children's clothing insulation from outdoor temperature or assumed a general insulation value equivalent to those of adults referenced in standards. Alternatively, many studies assumed clothing insulation values tabulated for adult garments could reliably be used for children wearing the same items. Ten studies surveyed the students using a questionnaire of individual garments then calculated the total insulation value using tabulated data from ASHRAE Standard-55 or ISO 9920 (2007) for adult clothing. Some surveyed the students using pre-constructed clothing ensembles using tabulated data from the

aforementioned standards (De Dear et al., 2015) while others only surveyed whether they wore additional garments to these ensembles. Five studies did not survey the children and used their own assumptions on the clothing patterns of the students inspired from average adult clothing insulation. Haddad et al. (2014) also made note of the potential effect of the student's chairs on their clothing insulation value, but few studies reported considering such effects.

1.4 Results and analysis

1.4.1 Measurement of environmental factors

In the thirty-four studies considered, ISO requirements were not always respected, particularly as they relate to the mean radiant temperature. Air temperature sensors were also rarely shielded against radiation effects. Additionally, there was no verification of the vertical homogeneity of classrooms through the criteria presented by ISO even in the three studies where radiant floor heating was used. Most studies measured environmental factors at only one height, and those that employed multiple heights used the ISO recommendations for sitting or standing adults. The few studies that attempted to adjust the measuring heights to fit children's stature failed to specify the heights used or to demonstrate that they corresponded to the anthropometric characteristics of the child occupants concerned. From the references in Figure 1.1, it appears measurements should be made between 0.25 m (9.8 in.) and 0.60 m (23.6 in.) for children in a sitting posture. Knowing most studies reported sitting occupants, the use of a single measurement height of 1.1 m (43.3 in.) is unlikely to provide a representative measurement of the occupant's immediate thermal sensation in all but the most homogeneous environments. Based on the sample of studies considered, inadequate sensor heights could explain part of the discrepancy between PMV and TSV; formal guidance should be provided.

1.4.2 Metabolic rate

There is no consensus in the considered studies on the protocols that should be used to determine the metabolic rate in the evaluation of the thermal comfort of children. Several

studies agreed that the values differed from those of adults performing the same activity, and attributed children's warmer thermal sensation to their high metabolic rate per body weight (Havenith, 2007; Nam et al., 2015; Yun et al., 2014). None of the protocols proposed by the authors succeeded in reconciling the PMV and TSV in their case studies.

The studies that used the first protocol, $M_{activity}$ - RMR_{adult}, reported a deviation between the PMV and TSV, often with PMV underestimating TSV. Teli et al., (2012) also found a poor match between the PPD and the actual number of persons dissatisfied when using that method. The second method, $M_{RMR\text{-}child}$ - RMR_{adult}, was used by Teli et al. (2012), who found it underestimated the TSV. The third protocol, $M_{Schofield}$ - RMR_{adult}, was used in Haddad et al. (2014), who calculated $M_{Schofield}$ for a range of *met* values and found that they all lead to an underestimation of the TSV. The fourth method, M_{BSA} - RMR_{adult}, lead to an underestimation of the TSV in all of the studies that used it, but less so than protocols 1 and 2 according to the comparison made by Teli et al. (2012). The fifth method, M_{BSA} – RMR_{BSA}, lead to the best match among the methods used in Teli et al. (2012) (methods 1, 4, 5, and 6 in the current nomenclature). However, Haddad et al. (2014) found M_{BSA} lead to significant mismatches between the PMV and TSV, while Yang et al. (2018) found the M_{BSA} – RMR_{BSA} method to result in an overestimation of the TSV. The sixth method, $M_{activity}$ - RMR_{child}, showed a larger deviation than all other methods compared in Teli et al. (2012). Haddad et al. (2013) also found that this method led to errors in predicting the TSV. The most thorough studies found on the topic (Haddad et al., 2013, 2014; Teli et al., 2012) did not provide formal conclusions. Instead, they argued for more research to be done, stating fundamental differences in children geometry and physiology (skin temperature, sweat secretion, etc.) would require changes to the assumptions behind the PMV's heat balance equations. Moreover, the experimental data from these studies suffered from the aforementioned issues relating to sensor heights and the following issues relating to clothing insulation, both of which could compromise the accuracy of the PMV calculated.

1.4.3 Clothing insulation

Many studies reported children's clothing insulation values, comparing them to the average clothing insulation expected for adult office workers; 0.5 clo in hot seasons and 1.0 clo in cold seasons. Among the ten studies that surveyed students on the individual garments worn and calculated their insulation value from tabulated adult clothing data, all but two found children's total clothing insulation was lower than typical adult values in office settings, for both warm and cold seasons. Alternatively, the studies which surveyed students using pre-constructed ensembles found children's insulation value to be lower than adults' for the season Fabbri (2013) or similar De Dear et al. (2015). Of the nine studies that surveyed the students on whether they wore an additional garment to a predetermined clothing ensemble, eight found that the value of children's clothing insulation was lower than or equal to that expected for adults. The majority of the studies – especially those that combined surveys and adult clothing insulation – found the clothing insulation of students to be nonuniform and on average different from that expected for adult office workers. None of the studies questioned the applicability of clothing insulation values from tabulated adult data to items worn by children. These results signify that the use of average adult clothing insulation values should not be applied uncritically to children in classrooms.

1.4.4 TSV survey

Doubts cast upon the PMV's applicability to child occupants is partly based upon its failure to match children's TSV gathered through surveys. Yet, the accuracy of children's TSV gathered through current methods is unclear. Several authors demonstrated difficulties in performing such surveys with young children (Martinez-Molina et al., 2017; Mors et al., 2011; Teli et al., 2012). Their difficulty or inability to read, the significant influence of peers, and the intangible nature of the judgment scales prescribed have been highlighted in several studies (Martinez-Molina et al., 2017; Mors et al., 2011; Teli et al., 2012). In Teli et al. (2012), as much as 25% of the responses in a classroom included inconsistencies, such as children expressing a desire for a warmer environment while also reporting they were feeling hot. Response to these

inconsistencies differed; some excluded children's votes which differed too significantly from those of teachers (Nam et al., 2015), others proposed adjustments to the standard survey methodology to adapt it the young participants: adding colors, sketches, and symbols to the questionnaire text, explanations of the terms used or replacing them with simpler words. It is yet unclear whether such adjustments to the survey method would suffice to reconcile PMV and TSV in other circumstances. Until children's self-reported thermal sensations are deemed accurate, the predictive power of the PMV equation should not be judged solely on such a comparison.

1.5 Conclusions

A total of 34 studies implementing thermal comfort assessment of children occupants in indoor spaces were analyzed to provide insight into a methodology for this population. Though no consensual methodology could be identified, several recommendations can be made to help improve the robustness of future field studies.

Better adherence to measurement protocols is needed regarding thermal homogeneity, especially in spaces where radiant heating is present. Recommendations on sensor heights based on children anthropometric data are needed to increase the reliability of environmental parameter measurement.

All methods substituting the RMR in the formulation of the PMV equation with RMR_{Child} produced unreliable results, indicating that attempting to "correct" the PMV equation with real child values is not reliable. Using BSA adjusted values both as an input and inside the PMV equation ($M_{BSA} - RMR_{BSA}$) provided the best match between PMV and TSV. However, the approach needs to be tested in a greater variety of settings before it can be confirmed whether this protocol could serve to scale the equation for children.

Children's clothing habits should not be assumed to match those of adults in an office setting. More research is needed to confirm whether individual children garments offer similar insulation to the equivalent adult item and to better document differences in clothing patterns

between children and adults. Thus, field studies should plan to record children's garments and measure their insulation values until suitable averages can be identified for children.

Several studies found important disparities between PMV and TSV, indicating that current methods fail to aptly assess children's thermal comfort. More research is needed before the cause of this disparity can be identified and corrected.

1.6 Interlude – Discussion on Article 1

In this chapter, an article titled "Evaluating thermal comfort of children: a perspective on commonly used methods" was presented. In it, literature on the evaluation of children's thermal comfort in schools was analyzed, and the reasons for the failure of these methods were explored. One potential source of discrepancy identified are radiant effects, characterized by the mean radiant temperature (MRT), which despite their important contribution to thermal comfort (accounting for 30% of total indoor heat exchange (La Gennusa et al., 2005) were not thoroughly investigated in Article 1. This is because most of the experimental studies considered did not determine nor measure the MRT and elected to use the air temperature alone in their comfort assessment, despite ISO and ASHRAE requirements. Additionally, amongst studies that did consider the MRT, none calculated it using human view factors, electing instead to measure it using a black globe thermometer. The black globe thermometer used (150 mm diameter) was that recommended by ASHRAE for adults, which has not been verified as a reliable tool for the measurement of children's MRT. Additionally, all the measuring equipment, including the globe thermometer, were placed at elevations recommended based on adult standing and/or seated heights. As shown in Figure 1.1, the head and abdomen of seated children are likely to be at significantly lower elevations. These issues suggest that the measurements made are more likely to reflect the MRT felt by an adult rather than that felt by the majority occupants of the classroom (i.e., children).

Article 1 leads to the question: What is the correct way to calculate or measure children's mean radiant temperature? Unlike the wealth of research that can be found on children's metabolic

heat generation, generally stemming from the high interest in children's nutrition and health, research on children's radiant heat exchange is scant, and that on children's view factors is nonexistent. This research topic was thus retained as the main focus of the present thesis.

In the following chapter, a literature review is conducted on the methods available for the determination of the radiation data needed for the accurate calculation of children's MRT. The review will inform the decisions made in the design of the method presented thereafter.

CHAPITRE 2

LITERATURE REVIEW

Following the identification of methodological shortcomings in current thermal comfort evaluations for children, this chapter focuses on the determination of mean radiant temperature and the radiation data required for its calculation. It reviews experimental and numerical approaches used to determine human radiation parameters: the view factors and projected area factors. This chapter provides the theoretical and methodological foundation necessary to develop a rigorous and generalizable approach for calculating human radiative exchange.

2.1 Determining the mean radiant temperature: measurement or calculation?

ISO 7726 defines the mean radiant temperature (MRT) as "the uniform temperature of an imaginary enclosure in which the radiant heat exchange with the human body is equal to that in the actual non-uniform environment" (ISO 7726, 1998). In the context of an indoor enclosure composed of N isothermal surfaces with known temperatures t_1, t_2, …, t_N (expressed in Kelvin), the mean radiant temperature (t_r) can be calculated using Equation (2.1).

$$t_r^4 = t_1^4 F_{P-1} + t_2^4 F_{P-2} + \cdots + t_n^4 F_{P-n} \tag{2.1}$$

This is applicable in situations where surfaces can be assumed to be diffuse and isothermal, and the medium between said surfaces is nonparticipating, assumptions that can be safely made in the indoor environment (ASHRAE-55, 2017). The calculation relies on view factors F_{P-1}, F_{P-2}, …, F_{P-N}, which quantify the fraction of diffuse radiation leaving each surface that directly reaches the person. These view factors are fundamental in radiative heat exchange modeling and are defined based on geometric relationships between the person and the surrounding surfaces (Fanger, 1970; Incropera et al., 2011). ASHRAE Standard 55 (ASHRAE-55, 2017) provides diagrams for the calculation of F of adult humans in the standing and seated postures, which were procured from a 1970 experiment by Fanger (Fanger, 1970).

Equation (2.1) assumes that the occupant is only exchanging long-wave radiation with low temperature surfaces, and only accounts for the long-wave aspect of the human's radiant exchange. In reality, occupants are often exposed to short-wave radiation both in indoor and outdoor environments, mainly from the sun. To account for that heat gain, ASHRAE Standard 55 provides a procedure in its appendix C that is dependent on human projected area factor (f_p). f_p is the ratio between the human's projected area (A_p) and his effective radiation area (A_{eff}, the portion of the total surface area that can exchange radiation with the environment). The f_p arrays provided by ASHRAE for the standing and seated posture are also procured from the same 1970 Fanger experiment.

The MRT can alternatively be approximated using a black globe thermometer (BGT), which is often done in on-site measurements due to its simplicity and low cost (Oliveira et al., 2019). The BGT provides a reading called 'globe temperature' (t_g), and the MRT is then approximated by correcting this reading using air velocity and temperature, as well as globe diameter and emissivity. The shape and size of the globe recommended by ISO 7726 is a 150 mm diameter ellipsoid globe, however a spherical globe is most often used, which overestimates the radiation from the floor and ceiling (Alfano, Dell'isola, et al., 2021; Halawa et al., 2014). The shape and diameter of the recommended globe have been selected based on the f_p of a standing and seated adult. This indicates that the design of a BGT that is appropriate for child occupants is contingent on assessing whether current adult view factors and f_p are applicable to children, and if not, on the determination of child-specific factors. Furthermore, the reliability and convenience of the BGT estimation of the mean radiant temperature has been widely questioned in the literature. While large 150mm globes suffer from a long response time (Fountain, 1987), the smaller globes suffer from important accuracy issues, reaching 10 °C in highly radiant environments (Alfano, Ficco, et al., 2021; Fountain, 1987). Additionally, all globes suffer from a high sensitivity to air velocity that is not accurately corrected in the methodologies established by current standards (Alfano, Dell'isola, et al., 2021; Humphreys, 1977; Oliveira et al., 2019).

In this thesis, we have decided to embark on the necessary first step to determine the needed factors for children (F and f_p). These, along with f_{eff}, will hereafter be referred to as human "radiation data".

2.2 Determination of radiation data: Experimental and numerical methods

2.2.1 View Factor: theoretical basis

Consider the radiation emitted from the differential area dA_1 towards another differential area dA_2 shown in Figure 2.1. The definition of the view factor between the first and second surface is defined as the ratio of the diffuse energy leaving dA_1 directly towards and intercepted by dA_2, to the total diffuse energy leaving dA_1.

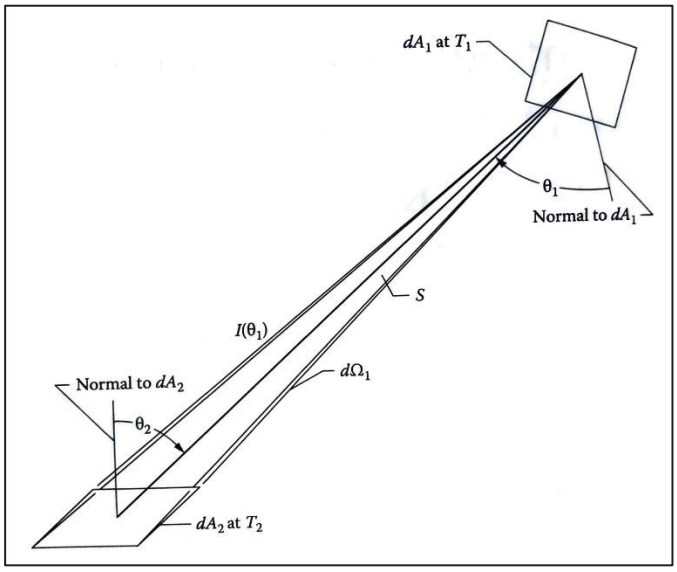

Figure 2.1 Radiative exchange between two infinitesimal surface elements
Taken from Howell et al. (2015)

The view factor between the two can be defined through Equation (2.2), where $d\Omega_1$ is the solid angle subtended by dA_2 when viewed from dA_1 (Fanger, 1970; Howell et al., 2015). As shown, the solid angle $d\Omega_1$, and therefore the view factor, is dependent on the projected area of the

surface dA_2, as well as the distance between the two surfaces S and their orientation from each other, represented by the angles θ_1 and θ_2.

$$dF_{dA_1-dA_2} = \frac{cos\theta_1 d\Omega_1}{\pi} = \frac{cos\theta_1 cos\theta_2}{\pi S^2} dA_2 \tag{2.2}$$

For two finite elements, the view factor can be obtained through the integration of Equation (2.2) as shown in Equation (2.3) (Howell et al., 2015).

$$F_{A_1-A_2} = \frac{1}{A_1} \int_{A_1} \int_{A_2} \frac{cos\theta_1 cos\theta_2}{\pi S^2} dA_2 dA_1 \tag{2.3}$$

For rectangular surfaces in an enclosure, Fanger (1970) derives Equation (2.4) of the view factor between the occupant and a surrounding rectangular surface of dimensions $(a \times b)$ at a distance c from the occupant, expressed in cartesian terms. f_p is the projected area factor, a ratio of the projected area of the human body on the surface, A_p, and the effective radiation area, A_{eff}, of the human body. Therefore, the determination of the projected area (or the projected area factor, f_p) is a necessary step for the determination of the view factor.

$$F_{P-A} = \frac{1}{\pi} \int_{\frac{x}{y}=0}^{\frac{x}{y}=\frac{a}{c}} \int_{\frac{z}{y}=0}^{\frac{z}{y}=\frac{b}{c}} \frac{f_p}{\left[1 + \left(\frac{x}{y}\right)^2 + \left(\frac{z}{y}\right)^2\right]^{\frac{3}{2}}} d\left(\frac{x}{y}\right) d\left(\frac{z}{y}\right) \tag{2.4}$$

2.2.2 View Factors in indoor environment literature

Human view factor literature can be classified into two categories: experimental and numerical. Experimental studies use the photographic method, where a subject is photographed from different azimuth α and altitude β angles to obtain their projected area A_p. Numerical studies use computer programs to determine A_p for numerical models of the human body (which will be referred to in this thesis as "numerical manikins"). Both methods use Equation (2.4), the

cartesian interpretation of Equation (2.3) (Fanger, 1970), to determine the view factor between the subject and a given surface.

Numerical studies often use previous experimental data (usually that of Fanger (1970)) to verify their methods or as a benchmark to demonstrate differences. This attempt offers several advantages. In his 2009 experimental study, Calvino et al. (2009) determined the radiation data of the southern Italian population positing that their body shape and proportions were distinct enough from those of the Scandinavians in Fanger's study to result in different view factors. From the initial 80 participants, individuals with weight and height outside the 10th–90th percentile of the southern Italian population were excluded, resulting in a final representative sample of 20 adults (men and women). This example provides an appreciation for the difficulty of experimentally gathering radiation data. The work required to recruit 60 of these participants and make accurate measurements of their bodies, was in the end useless as they were not retained for the study. In numerical studies, manikins are produced having the desired height and weight. This enables studies to generate "standard" occupants that represent the average of a given population (Kubaha et al., 2004; Park & Tuller, 2011; Tanabe et al., 2000), or to generate several manikins representing different percentiles of a given population to observe the differences amongst them (Rykaczewski et al., 2022). This control over the numerical manikins extends beyond their height and weight: age of the manikins can be changed, as well as their pose and posture, enabling a wide range of variability. Additionally, numerical methods allow for continuous adjustment and recalculations for method refinement, an aspect that is missing from experimental studies. This is an important consideration for the present thesis where child subjects are needed. Experimental work with child participants would require extensive planning of the recruitment and measurement process and evaluation by the university's Research Ethics Committee, without any guarantee that the recruited participants would be representative of the child population studied. For these reasons, we have elected to use a numerical method for the determination of the needed radiation data.

2.3 Numerical methods available

As explained in the previous section, the determination of view factors between an occupant and a surface in its surroundings is contingent on the resolution of the double integration in Equation (2.4). View factor literature provides several methods that can be used to solve the integral, but only a few are applicable to our application: that of a human body with their indoor environment, composed of rectangular surfaces. Analytical methods, such as surface and contour integration, can only be used in situations where both surfaces considered are simple geometrical shapes, thus inapplicable to the complex shape of the human body. To limit our study to methods that are both applicable and commonly used in the field, we put our focus on the following: (1) the hemicube method, which relies on the solid angle definition of view factors presented in Equation (2.2), and (2) the ray tracing method which relies on the parallel ray assumption often made in experimental view factor studies.

The distinction between these two methods was first made by Horikoshi in his 1990 study (Horikoshi et al., 1990), where he challenged the method used by Fanger of placing the camera at a large distance (7 meters) from the occupant. Horikoshi claimed that the large distance violated the solid angle principle and made Fanger's results applicable only to surfaces at large distances from the occupant. Horikoshi's differentiation is illustrated in Figure 2.2: he posits that the f_p viewed from points A, B, C, at a finite small distance from the subject, will be distinct from those viewed from a distance far enough to be considered infinite. He elected to place the camera at a short distance (1 and 2 meters from the occupant) and found significant differences from Fanger's results (up to 40% with the floor), which he attributed deficiencies in Fanger's method (using a camera at a large distance). It should be noted that this large discrepancy was found in the seated posture, and that Fanger's study did not actually determine f_p at the angles used by Horikoshi (i.e., negative elevation angles, where the camera must be placed below the subject's center of mass, as was done by Horikoshi, position C in Figure 2.2). Instead, Fanger assumed the projected area from above to be the same as from below; an assumption labeled the Anterior/Posterior (A/P) symmetry, which is further explained and challenged in Chapter 6. Therefore, it appears possible that this difference between Fanger's

and Horikoshi's results was due to the shading effect of the chair that was neglected in Fanger's work (where the anterior/posterior symmetry was used) and not due to an inherent issue with the use of either the solid angle or parallel ray methods.

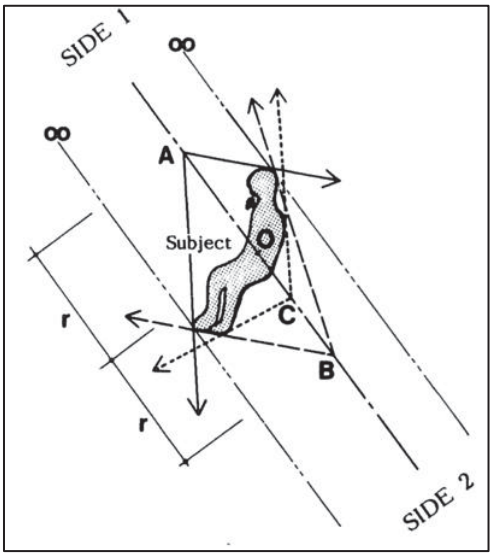

Figure 2.2 Diagram for visible extents of the human body from the viewpoints A, B, and C and an infinite point

Taken from Horikoshi et al. (1990)

Nonetheless, this distinction between the hemicube and ray tracing methods was then repeated by Tanabe et al. (2000) who introduced the terms *parallel ray method* to refer to that used by Fanger, and *solid angle method* to that used by Horikoshi. Tanabe et al. found little difference between the two methods when the distance to the occupant was large (7 meters). In our attempt to create a robust numerical calculation method, we elected to test out both methods and to compare the results to those of Fanger in chapter 3. In the following section we will explain the theoretical basis behind the two numerical methods that were be used in Chapter 5.

2.3.1 Ray tracing: a parallel ray method

Ray tracing is a computer graphics technique that is often used to model light transport in rendering algorithms, particularly for generating digital images. Historically, it has been seen as an accurate but computationally expensive method, but recent development of GPU technology has allowed it to become more accessible in both scientific and engineering applications, as well as real time video game rendering. These developments have allowed for its wider use in radiant heat transfer calculations, particularly for the calculation of view factors (Cumber, 2022; Sönmez et al., 2019; Walker et al., 2010). The method relies on tracing rays from every element of the considered surface (in this case, each mesh of the numerical manikin) and calculating whether those rays reach surfaces that surround it. Essentially, a large number of rays are "fired" from random points on a given object, at random angles into the 3D environment, with the first object that each ray intersects being recorded. The view factor between any two objects is then defined as the fraction of rays leaving one object that reaches the other. The accuracy of the method relies on the number of rays emitted from each surface, which is referred to as the "resolution". Studies have found that having a large enough ray tracing resolution and number of meshes increases the accuracy of view factor calculation (Ansys, 2010; Howell et al., 2015; Modest & Mazumder, 2021; Walker et al., 2010). Ray tracing is also used in solar heat gain software, which several studies have employed for the calculation of human view factors: (Havgaard Vorre et al., 2015; Kubaha et al., 2004; Tanabe et al., 2000) have labeled it as a "parallel ray" method and used it to compare their data to that of Fanger's experiments, which used a photographic method employing the same parallel ray assumption.

2.3.2 Hemicube: a solid angle method

The hemicube method is an adaptation of the unit sphere method, where an hemicube is introduced, housing the hemisphere (Howell et al., 2016), and relies on the solid angle calculation of the view factor as shown in Equation (2.2). As illustrated in Figure 2.3, in this approach, projection B is calculated in place of projection C. The equivalence between the two

methods is based on the fact that the view factor is the same from any object that subtends the same solid angle to the viewer, regardless of the actual shape and orientation of the object. This implies that the view factor between dA_1 and object A is the same as that between dA_1 and the patches B or C. This method is used in computer graphics where it is simpler to calculate the surface B on the hemicube (which is done by dividing the cube into pixels), determining the view factor between each pixel of the cube and the element dA_1 (which is a simple view factor calculation between two small finite squares), and summing the factors for the pixels contained within the area B (Howell et al., 2015). Using this method, sections of a 3D human manikin can be projected onto the hemicube, and the view factor between the body and any element in its surrounding can be determined. In addition, the method was found to be fast and useful for situations that involve blocking and shading by intermediate elements (Kramer et al., 2015), which is likely to be encountered for the human body. These factors make this method very useful for the indoor environment (Rykaczewski et al., 2022).

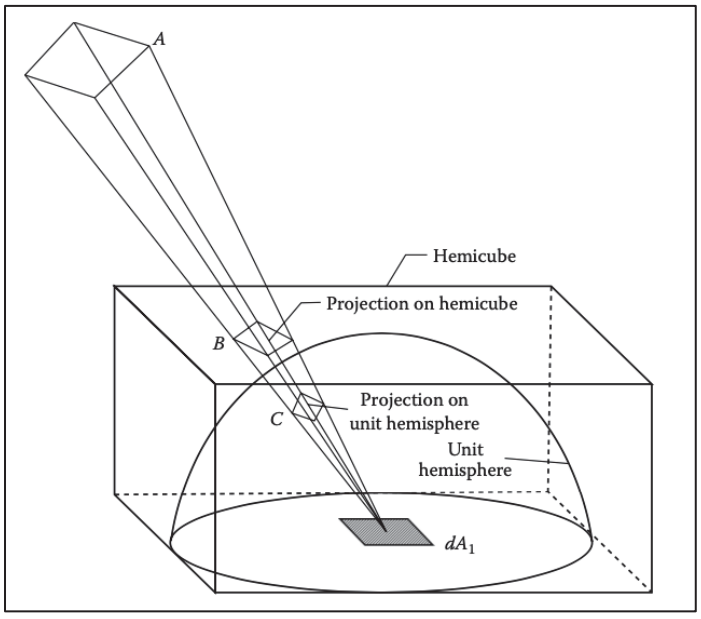

Figure 2.3 Relation between the hemicube and the hemisphere method
Taken from Howell et al. (2015)

In Chapter 3, both methods will be used, and their results will be compared to those in the literature. ANSYS Fluent will be used as it offers both calculation methods in its surface-to-surface radiation model (Ansys, 2010).

2.4 Human body model

Different approaches exist in the literature with regards to the level of detail with which the human body is modelled. Historically, using highly detailed models was too computationally expensive, but recent leaps in computational power allows for more realistic numerical manikins to be used. In fact, every year GPU chips grow in 2.3 times in computational power allowing for more complex calculations (Emberson & Owen, 2025). In human radiation data literature, some studies have elected to simplify the human body to simple geometrical shapes such as cuboids and spheres, allowing for the use of analytical methods for the calculation of its view factors (Chen et al., 2024; Havgaard Vorre et al., 2015; Wei et al., 2004). Others used simplified numerical manikins where each body segment was reduced to a simple geometrical shape (ex. rectangular prism, sphere, etc.), also allowing for a faster and simpler view factor calculation (Francisco et al., 2012; Manabe et al., 2004; Y. Wang et al., 2020; Zeng et al., 2024a). A study by Havgaard Vorre et al. (2015) found that using a detailed numerical manikin resulted in the best match with Fanger's results, as opposed to the use of a sphere, a cube, or a box. In the present thesis, complex human body shape manikins are used, which were procured from the University of Michigan Transportation Research Institute (University of Michigan Transportation Research Institute, 2020). This approach allows for high accuracy and for comparison with other studies in the literature who have elected to use complex models (Havgaard Vorre et al., 2015; Kubaha et al., 2004; Li et al., 2022; Park & Tuller, 2011; Tanabe et al., 2000). Details on the generation and manipulation of the manikins is presented in subsequent chapters.

2.5 Child manikin selection

Children's bodies vary substantially with age, reflecting continuous changes in body size, proportions, and posture throughout growth (Gerber & Pienaar, 2025). Differences between

children become markedly present at the onset of puberty, which introduces rapid and non-linear changes in body shape, mass distribution, and surface area that are not uniform across ethnic backgrounds and between genders (Rusek et al., 2021). In this work, a five-year-old child was selected because this age corresponds to children who are regularly present in both daycares and early school environments. At the same time, children of this age have not yet undergone pubertal development, meaning their anthropometric characteristics remain distinct from those of adolescents and adults while avoiding the large inter-individual variability introduced by puberty. This choice allows the investigation to isolate child-specific differences in radiant heat exchange and to provide radiation data that are representative of that age group across ethnic and gender differences. The body characteristics used correspond to the 50th percentile values reported in NHANES III (1998) for five-year-old children in the United States. The NHANES sample includes participants from all ethnic backgrounds, and at this age, anthropometric differences between boys and girls are negligible.

2.6 Conclusions

This chapter reviewed the theoretical basis and existing methods used to determine human radiation data. While numerical approaches have become increasingly prevalent, the literature reveals persistent disagreements regarding calculation method selection, model assumptions, and the influence of pose and model geometry on results. This highlights the need for a rigorous verification of methodological assumptions.

Building on the methodological foundations established in the previous sections, the following chapter develops and applies a refined numerical method to the calculation of human radiation data. The chapter investigates whether children-specific view factors differ from those of adults in the standing posture and evaluates the significance of these differences on the perceived mean radiant temperature. Through verification against established adult data, and comparisons between adult and child manikins, the chapter addresses core thesis objectives related to both methodological validity and population specificity.

CHAPITRE 3

ARTICLE 2: CONSIDERING CHILD-SPECIFIC VIEW FACTORS IN HUMAN THERMAL BALANCE

Nour Youssef, Katherine D'Avignon

Département de génie de la construction, École de Technologie Supérieure, 1100 Notre-Dame Ouest, Montréal, Québec, Canada H3C 1K3

Paper published in *Science and Technologie for the Built Environment*, June 30 2025

3.1 Introduction

Current thermal balance models rely on both environmental and individual parameters to assess the adequacy of an environment for human occupation. One crucial environmental parameter in these models is the mean radiant temperature (MRT), which can be derived from view factors and the temperatures of adjacent surfaces. View factors serve to weigh the relative impact of each surrounding indoor surface on a person's thermal radiation balance, and are contingent on factors such as surface size, occupant distance from the surface, and their relative orientation. However, currently available standards that provide view factors for the calculation of MRT (ASHRAE, 2017; ASHRAE-55, 2017), accounting for both long-wave and short-wave radiation, rely on the data provided by (Fanger, 1970). This data, which includes the human body's view factors (VF) with surrounding surfaces, projected area factors (f_p), and effective radiation area factors (f_{eff}) in the standing and seated postures, are sourced from experiments that included only adult college-aged subjects. Considering the difference in anthropometric characteristics between adults and children (height, weight, body surface area) (Fredriks et al., 2005; Vignerov, 2009), and the dependence of geometric view factors on these parameters, the question arises: Do these variances impact human body view factors significantly enough to render current values inapplicable to children?

There has been a notable absence of investigation within the literature regarding the suitability of these VF for children. Exploratory work by Youssef & D'Avignon (2023) determined VF

of a 5-year-old child and an adult using a numerical method and found a difference of up to 70% for select surfaces. That work was limited to a small number of surfaces and did not determine the projected area factors (f_p) which can be used to calculate view factors of the human body with any surface at any distance. The present paper aims to verify the conclusions of that work and expand on it by determining f_p of a numerical 5-year-old child model, which will allow us to assess the extent of the effect of VF differences on MRT calculations for various room configurations. The VF data generated for this young child can help inform whether incorporating child-specific radiation data would significantly enhance the precision of thermal balance calculations for this population.

3.2 Literature review

Early seminal works to determine human view factors relied on experimental methods (Fanger, 1970; Jones et al., 1998; Underwood & Ward, 1966). Fanger (1970) determined f_p using the photographic method: he positioned a camera at a distance of 7 meters from his subjects and captured photographs of their shadows from various elevation angles β (0° to 90°, i.e., front of the center of mass to top of the head) and azimuth angles α (0° to 180°, i.e., front to back). Using these f_p values, Fanger produced VF tables for surfaces of different dimensions to distance ratios a/c and b/c, where a and b are the width and length of the surface, and c is the distance between it and the occupant.

Though the photographic method has since further been used to assess human radiation (Calvino et al., 2009; Horikoshi et al., 1990; Kalisperis et al., 1991; La Gennusa et al., 2008; Park & Tuller, 2011), most recent studies have used numerical methods to calculate view factors and projected area factors of humans in indoor environments (Kubaha et al., 2004; Rykaczewski et al., 2022; Tanabe et al., 2000; Yousaf et al., 2008). Significant variations in methodology and objectives are apparent from this literature, and a certain degree of inaccuracy is visible in all works attempting to compare results from studies against one another. Whether the objective is to numerically recreate experimental data, to verify a numerical method against experimental results, or to demonstrate differences from previous

works, no consensus exists on the methodology or metric to use to perform such comparisons. The following considerations have been highlighted as influential: (1) the considered population characteristics, (2) the numerical method used and its effects on the determined data, (3) the effect of pose and posture, and (4) statistical metrics used. Each is discussed in detail over the next sections.

3.2.1 Considered population

A majority of papers have concentrated on reaffirming the human thermal radiation data (mainly f_p and f_{eff}) found for the demographic examined in the influential 1970 Fanger study (i.e. young, healthy adults), albeit employing diverse methodologies (Horikoshi et al., 1990; Jones et al., 1998; Kubaha et al., 2004; La Gennusa et al., 2008; Tanabe et al., 2000). Anthropometric characteristics of the manikins or subjects used in those studies for comparison with past literature are tabulated in Table 3.1. In all cases listed, Fanger's data was the basis used for comparison. Though 10 female and 10 male adult subjects participated in Fanger's study, he presented the resulting f_p data as an average of those of his male and female subjects, both nude and clothed, due to the small effect he found sex and clothes to have on the f_p values (within 8%). All literature found use these average f_p values as basis of comparison, regardless of the population characteristics studied (body size, gender, etc.).

Some have broadened the populations considered, examining the effect of anthropometric differences between people of different nationalities or body characteristics (BMI, height) on their view factors (VF). Calvino et al. (2009) considered the southern Italian population and examined whether anthropometric differences between them and the Scandinavian participants in Fanger's study would affect *VF*. From 80 available participants, they excluded those whose weight and height fell outside the 10^{th} to 90^{th} percentile of the southern Italian population, to ensure the participants retained (20 adult men and women) represented it accurately. They found variances from Fanger's f_p (ie. the average of his male and female participants, both clothed and nude) of up to 8% for the standing posture and 52% for the seated posture, which they attributed to the anthropometric variations between the populations: average height and

weight of examined Italian subjects were 1.67 m and 64.27 kg, whereas those studied by Fanger were 1.72 m and 62.2 kg. The paper also notes a difference in Sitting-Height-to-Stature ratio (SHS) between the two populations, which reflects a difference in body shape, but provides no value.

Rykaczewski et al. (2022) investigated the impact of BMI and height variations among the American adult population on their f_p and f_{eff}. For the same height, they found that BMI and gender have mostly little effect on f_p. Yet, for low elevation angles ($\beta = 0°$ to $20°$) they observed significant differences ($\Delta f_p \approx 42\%$) for manikins with a BMI above the 80^{th} percentile compared to those of the 50^{th}; implying that for a Body Surface Area (BSA) difference of around 8%, the radiative influence of the floor could be significantly different. When verifying their method, they compared f_p of their "average" male manikin (50^{th} percentile height and BMI of American males) to Fanger's average results. However, as indicated in Table 3.1, the manikin BSA of 1.9 m^2 is closer to that of only Fanger's male subjects (1.86 m^2) but with a height (1.76m) closer to the average of both his male and female subjects (1.74 m). Tanabe et al. (2000), after having validated his method using Fanger's average results, conducted a comparison between a "standard" (height of 1.75 m, unspecified weight) and a "10% wider" adult male manikin, revealing a maximum difference in f_p of 7%. Kubaha et al. (2004) compared a sample of normal- and over-weight Canadian adult men and women participants and found only a small difference in their f_p (maximum absolute difference of 0.017) and f_{eff}. They used the data of their average, normal weight males to compare against Fanger's average results.

Kubaha et al. (2004) focused on determining local projected area factors rather than examining effects of population variations on radiation data. To validate their method, they created an "average" male manikin with a BSA (1.83 m^2) on par with Fanger's male subjects (1.86 m^2), but with a height (1.75 m) comparable to the average of Fanger's men and women participants (1.76m). They compared this male manikin's results against Fanger's average results. La Gennusa et al. (2008) focused on calculating view factors for occupants in spaces with complex geometries (e.g., inclined walls) but did not report the anthropometric characteristics of the

subjects whose results were compared to Fanger's. Overall, most studies in the literature used male manikins or predominantly male subjects and compared their results to Fanger's data, which represents an average of both male and female participants. When examining the impact of diversity within the adult population—such as differences in sex, weight, height, and nationality—the largest deviations from Fanger's averaged f_p results were: 52% for nationality (Calvino et al., 2009), 42% for BMI (Rykaczewski et al., 2022), and 8% for sex (Fanger, 1970). Given the greater physical differences between adults and children—ex. the difference in BSA between an average adult man and an average 5-year-old boy is 55% (Table 3.1)—the discrepancies in radiation data between these two groups are likely to be even more pronounced. Besides the work of Youssef & D'Avignon (2023), no other literature was found that attempted to determine children's radiation data.

3.2.2 Numerical methods

Two commonly employed experimental approaches to determine radiation data are the parallel ray and solid angle methods. The difference between the two approaches is shown in Figure 3.1.

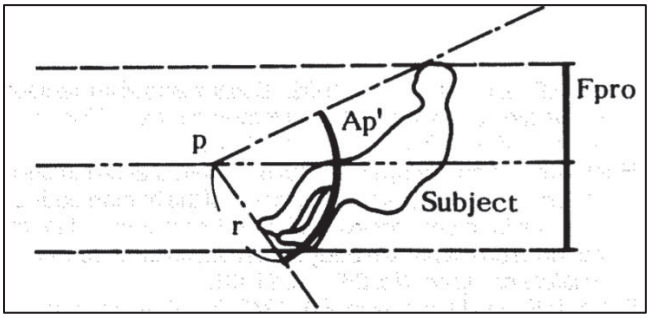

Figure 3.1 Diagram for comparison between parallel ray projected area (F_{pro}) and hemispherical projected area (A'_p)

Taken from Horikoshi et al. (1990)

The first assumes that thermal radiation travels in parallel rays between surfaces, making it suitable to determine solar gains and view factors between occupants and surfaces at a considerable distance (Tanabe et al., 2000). This aligns with the Fanger (1970) experiment,

where participants were positioned 7 meters away from the camera. For that reason, most studies attempting to verify their numerical values using Fanger's data have used solar heat gain software that rely on the parallel ray assumption (Kubaha et al., 2004; Tanabe et al., 2000). In contrast, Horikoshi et al. (1990) introduced the solid angle method, which uses closer distances (1 and 2 meters) between subjects and the camera. They noted this method is more appropriate to determine view factors in the indoor environment as surfaces are at closer distances to occupants and observed variations from Fanger's values reaching up to 40% for the floor. Tanabe et al. (2000) discussed the difference between the two methods and demonstrated that VF determined using both methods meet quite well when the distance between the occupant and surface is 7 m. They did not quantify the difference nor discuss whether the effect could become important for surfaces at smaller distances, such as the floor. VF used in the calculation of MRT in the indoor environment are defined on the assumption that the human body is an infinitesimal point exchanging radiation with surrounding surfaces without self-radiation. This includes Fanger's VF and consequently, VF appearing in standards (ASHRAE-55, 2017; ISO 7726, 1998). Most software, including Ansys Fluent, do not make that assumption, and self-radiation is present in the view factors they calculate. To account for this difference, Youssef & D'Avignon (2023) used a correction factor (f_c) to ensure the sum of view factors between the manikin and all surrounding surfaces was unity.

3.2.3 Effect of pose and posture

It is clear from the literature that the posture of an occupant has an effect on radiation exchanges with their environment (Kurazumi et al. 2008). Though most literature focuses on the standing and seated postures (Calvino et al., 2005, 2009; Horikoshi et al., 1990; Jones et al., 1998; Kubaha et al., 2004; La Gennusa et al., 2007, 2008; Rykaczewski et al., 2022; Underwood & Ward, 1966), some studies have investigated other pertinent postures such as seated cross-legged on the floor (Tanabe et al., 2000) or other floor seating postures (Kurazumi et al., 2008) and found considerable differences in f_{eff}, compared to the usual standing and seated postures.

Pose, referring to a particular way of standing or sitting (crouched, straight-back, etc.), though not as widely investigated, has also been demonstrated to influence f_{eff} (Rykaczewski et al., 2022; Yousaf et al., 2008). Studies reporting the effect of pose on f_{eff} are detailed in Table 3.1. In Fanger's study, the standing subjects were described as having their arms touching their torso (see 3.2a) and it can be noted from Table 3.1 that the f_{eff} obtained is the lowest in the literature, having only been confirmed by Tanabe. Rykaczewski et al. (2022) and Yousaf et al. (2008) found that raising the arms away from the vertical by 35° (see Figure 3.2c) increased the value of f_{eff} for the standing posture by 7 and 6% respectively. Yousaf et al. (2007) found that having arms that are vertical but not touching the torso resulted in an increase of 4% in f_{eff}. The effect of pose has also been noted by Kubaha et al. (2004) who found an f_{eff} value which matched well (within 5%) with those of Bedford (1935), Horikoshi et al. (1990), and Miyazaki (1995) but differed significantly from those of Fanger (1970) and Tanabe et al. (2000) (~ 13%). They attributed this variation to the difference in the "relaxation" of the model; whereas Kubaha's model (Figure 3.2b) adopted a "relaxed" pose, those presented in Fanger's and Tanabe's studies (Figure 3.2a) had "compact" poses, with extremities close to the body, resulting in a lower value of effective body surface area.

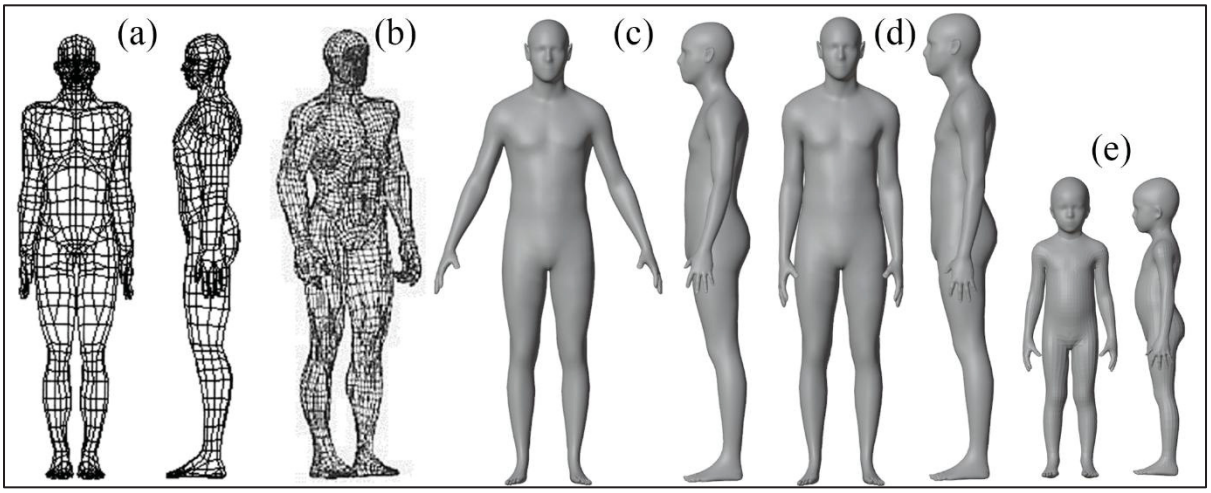

Figure 3.2 Numerical manikins used in (a) Tanabe et al. (2000), (b) Kubaha et al. (2004), (c) Present - Adult with arms raised, (d) Present – Adult with arms lowered, (e) Present – Child with arms lowered

Taken and adapted from Tanabe et al. (2000) and Kubaha et al. (2004)

Table 3.1 Comparison of effective radiation area factor from the literature for the standing posture

Study	Height (m)	A_t[1](m^2)	A_{Du}[2](m^2)	Pose[3]	f_{eff} Nude	f_{eff} Clothed
Fanger (1970) (M+F)	1.72	-	1.74	Arms along torso	0.725	0.87
Fanger (1970) (M)	1.78	-	1.86	Arms along torso	0.725	0.87
Fanger (1970) (F)	1.66	-	1.61	Arms along torso	0.725	0.87
Horikoshi (1990)	1.70	-	1.69	Arms along torso	0.803	0.91
Tanabe et al. (2000)	1.75	1.72	-	Arms along torso	0.744	-
Kubaha et al. (2004)	1.75	-	1.83	Arms lowered	0.840	-
Yousaf et al. (2007)	-	-	-	Arms raised 35º	0.830	-
				Arms lowered	0.810	-
				Arms along torso	0.780	-
Kurazumi et al. (2008)	1.75	1.76	1.81	Arms along torso	0.773	-
Calvino et al. (2009)	1.68	1.71	-	Arms along torso	0.840	0.910

[1] Total body surface area, reported by the software used in the case of numerical manikins, or averaged measured body surface areas of the subjects in the case of experimental studies.

[2] Approximated body surface area using DuBois and DuBois's (1916) formula: $A_{Du} = 0.007184 \times (H \times 100)^{0.725} \times W^{0.425} (m^2)$, where H: height (m), W: weight (kg).

[3] Angles indicated refer to arm position relative to the torso, with arms along the torso equivalent to 0º.

Table 3.1 - Comparison of effective radiation area factor from the literature for the standing posture (continued)

Study	Height (m)	A_t[1](m^2)	A_{Du}[2](m^2)	Pose[3]	f_{eff} Nude	f_{eff} Clothed
Rykaczewski et al. (2022)[4]	1.76	1.9	2	Arms raised 35º	0.801	0.910
				Arms along torso	0.748[5]	0.850
Park & Tuller (2010)	1.74	1.85	1.90	Arms lowered	0.826	-
Youssef & D'Avignon (2023): Adult	1.71	1.61	1.69	Arms raised 35º	0.827	-
Youssef & D'Avignon (2023): 5-year-old boy	1.13	0.76	0.78	Arms raised 35º	0.847	-
Present: Adult	1.78	1.73	1.86	Arms lowered	0.779	-
Present: 5-B	1.13	0.78	0.78	Arms lowered	0.844	-

Rykaczewski et al. (2022) sought to quantify the effect of arm pose on f_p by changing the arm position (i.e. arms along and away from the trunk) on their manikin. They found that raising the arms only affects the value of f_p significantly for a β of 90°, corresponding to the top-down angle, where the value of f_p increased from 0.08 to 0.1 (20%). Due to the particularity of this vantage point, used to determine view factors of both the floor and ceiling, and the absence of detailed information regarding Fanger's subjects' poses, it is worthwhile to investigate whether variations in arm pose significantly contribute to deviations from Fanger's f_p.

[1] Total body surface area, reported by the software used in the case of numerical manikins, or averaged measured body surface areas of the subjects in the case of experimental studies.

[2] Approximated body surface area using DuBois and DuBois's (1916) formula: $A_{Du} = 0.007184 \times (H \times 100)^{0.725} \times W^{0.425} (m^2)$, where H: height (m), W: weight (kg).

[3] Angles indicated refer to arm position relative to the torso, with arms along the torso equivalent to 0º.

[4] Data reported is for a male subject of 50th percentile in height and BMI. The study reported f_{eff} of the clothed manikin. Value of f_{eff} for the nude body was calculated using $f_{eff,nude} = f_{eff,clothes}/f_{cl}$, where f_{cl} is the clothing area factor reported in the study as 1.12 - 1.15.

[5] Calculated from the reported value of $f_{eff,clothed}$ using $f_{eff,clothed} = f_{cl} \cdot f_{eff,nude}$, where f_{cl} = 1.135, an average of value for summer clothing.

3.2.4 Statistical comparison method

In the studies considered, there was no consensus on the statistical method used to compare f_p values across the literature. Some studies used comparison plots with (Tanabe et al., 2000) or without (Calvino et al., 2009) regression analysis. In these plots, the abscissa represented the authors' f_p, while the ordinate displayed the reference f_p (ex. Fanger's). Most of the studies relied on descriptive statistics. Some provided detailed information, including mean, minimum, maximum, and standard deviation of relative and absolute errors (La Gennusa et al., 2008; Park & Tuller, 2010). However, the majority only reported typical or average errors (Kubaha et al., 2004; Rykaczewski et al., 2022; Yousaf et al., 2007) and noted instances where certain data showed larger discrepancies. Some studies compared the "shape" of their f_p plots to others found in the literature, usually Fanger's, relying on the graphs to declare that the "curve behavior" showed a "general agreement" with those of Fanger (Calvino et al., 2009; Kubaha et al., 2004; Rykaczewski et al., 2022; Tanabe et al., 2000). None of the studies provided quantitative statistical data to support this claim; instead, they relied on qualitative comparisons of the shapes of the curves. Park & Tuller (2010) sought to assess the significance of differences between various body types on f_p. They compared the variations found across different studies and used the magnitude of the maximum absolute differences (0.173) to argue against the significance of body type differences within the same study. According to this approach, the degree of variation observed between studies for the same body type or population can serve as a benchmark for determining whether differences between body types within a single study are significant.

Very few papers calculated or compared VF results to those of Fanger or other past literature. Horikoshi (1990), who determined VF without determining f_p, relied on visual comparison between his graphs and Fanger's, reporting the typical and maximum differences. Tanabe et al. (2000) used visual comparison and provided the maximum relative error found (3%), but only for values of a/c lower than 1. La Gennusa et al. (2008) compared their results to those of Kalisperis et al. (1991) who determined VF for inclined surfaces, by visually comparing the curves for different a/c values and analyzing apparent discrepancies.

This paper aims to fill the gap in thermal balance literature by providing radiation data for a 5-year-old numerical child manikin. An adult manikin will be used first and its results compared to literature to verify various method assumptions; both parallel ray and hemicubes methods will be compared and the effect of manikin pose will be tested. In the absence of clear consensus in the literature, both qualitative and quantitative comparison methods will be used to assess the differences in the projected area factors, effective radiation area factors and view factors calculated, with the variations found between the adults in the literature used as a benchmark for significance. Finally, test cases will be used to evaluate the influence of view factor differences found on the mean radiant temperature calculated for both adult and child occupants in two test scenarios.

3.3 Methodology

3.3.1 Human shape manikins

Human-shaped manikins were created using UMTRI's HumanShape™ (University of Michigan Transportation Research Institute, 2020), a modeling tool which generates realistic 3D human shapes based on anthropometric parameters. The modeler requires specific information about the occupant, namely their age, gender, height, body mass index BMI, and SHS. For the adult male manikin (labelled A-M, shown in Figures 3.2c and 3.2d), we used the average anthropometric measurements from the 10 male participants in Fanger's study (1970) as the aim was to create a numerical manikin that most resembled these participants. By using the data of only the male participants, we were able to use UMTRI's standing adult male model. The resulting manikin had a BSA of 1.86 m^2, which matches that of Fanger's male subjects, and is close in value to the BSA of the male manikins used by Rykaczewski et al. (2022) and Kubaha et al. (2004) (see Table 3.1). The child manikin was created using UMTRI's child-specific modeling tool, representing an average 5-year-old boy (labelled 5-B, shown in Figure 3.2e). We used statistical data representing the 50^{th} percentile boy aged 5 years old from

Frisancho (2008) which was based on sampling from NHANES III (1998) and includes data from diverse ethnic groups in the United States.

Table 3.2 provides the average anthropometric measurements of the male participants in Fanger's study, as well as those of the numerical manikins generated. The SHS depends on the sitting height, i.e. the length from head to foot when seated, which was not provided in Fanger's study. Instead, we utilized the average sitting height of men aged 20 to 29.9 years old, sourced from Frisancho (2008).

Table 3.2 Anthropometric data used for the generation of the numerical manikins

Study	Age (years)	Stature (m)	Weight (kg)	BMI (kg/m^2)	SHS	A_t[1] (m^2)	A_{DuBois} (m^2)
Fanger (M)	N/S[2]	1.78 ± 0.07	68.7 ± 6.6	22	-	-	1.86 ± 0.11
A-M	22	1.78	-	22	0.51	1.7296	1.8600
5 y.o., 50^{th} perc	5	1.128	19.2	15.48	0.53	-	0.7757
5-B	5	1.128	19.2	16	0.54	0.7806	0.7757

The UMTRI HumanShape™ generator, for both child and adult manikins, produces models with raised arms at an angle of ~ 35° from the vertical. The models' pose was rectified using Blender (2025), lowering them by ~ 18° until they were aligned with, but not touching, the torso. This correction was carried out to match figures and descriptions provided in Fanger (1970) and the pictures (Figure 3.2a) provided in Tanabe et al. (2000) which closely matched Fanger's results. To test the effect of pose on radiation results, two adult manikins were considered: the one initially produced by the generator with arms raised at ~ 35° from the vertical (labeled A-M-R), and the one with rectified with arms at ~ 17° from the vertical (labeled A-M-L).

[1] Total manikin body surface area measured by the Ansys software, including the area under the feet.

[2] N/S: Not specified. Age in Fanger's study was not disclosed but the 20 participants were assumed to be "college aged" and therefore the adult numerical manikin was generated for a 22-year-old male.

The HumanShape™ generator creates meshed bodies that often result in a body surface area lower than that predicted by the DuBois formula A_{Du}. To calculate the total body surface area of each manikin (A_t), we applied the methodology described by Rykaczewski et al. (2022). Table 3.2 shows A_t is 7% lower than A_{Du} for the adult manikin, and 0.6% for the 5-B manikin. As discussed by Looney et al. (2020), this divergence can be partly attributed to UMTRI participants wearing undergarments during measurements, while DuBois participants were measured in a completely nude state. Importantly, these variances are on par with the 5% estimated error range reported for the DuBois equation (DuBois & DuBois, 1916) and are akin to the difference found by Rykaczewski et al. (2022) for their average male manikin (6.3%). Since solely A_{Du} is used in the literature for calculating f_{eff}, it will also be used in this work.

3.3.2 Geometry and Meshing

The manikins were uploaded into Ansys SpaceClaim (2010), where the faceted bodies were reduced by 90% (from 28,850 to 2,876 faces for adult manikin). Because the manikins used are highly detailed, especially around the fingers, toes, and face, this reduction was necessary to fix mesh defects such as self-intersecting elements and contact mismatches, as was done by Rykaczewski et al. (2022).

The method of Rykaczewski et al. (2022) was employed, positioning the manikins within a sphere centered on their center of mass, as illustrated in Figure 3.3. Each sphere section (*ss*) was identified by the elevation (β) and azimuth (α) angle of its center point. Considering the anterior-posterior and left-right symmetry of the human body assumed by Fanger (see Figure 3.3), and to enable comparison with his results, only one fourth of the sphere sections were considered. Illustrated in yellow on Figure 3.3, the 79 sphere sections considered were those whose center is at α between 0° and 180°, and β between 0° and 90°. Given that radiation calculations pertain exclusively to sections of the body capable of exchanging radiation with their surroundings, we excluded the bottom surface of the feet (A_{feet}) from the total manikin surface area (A_t) considered as they primarily exchange heat with the floor through conduction. For the adult manikin, the value of A_{feet} was determined to be 288 cm², which closely aligns

with the 230 cm² value reported by Kurazumi et al. (2008) for the standing posture. In the case of the child manikin 5-B, A_{feet} was 188 cm². This resulted in value A_b which is the manikin surface area considered in all further radiation calculations.

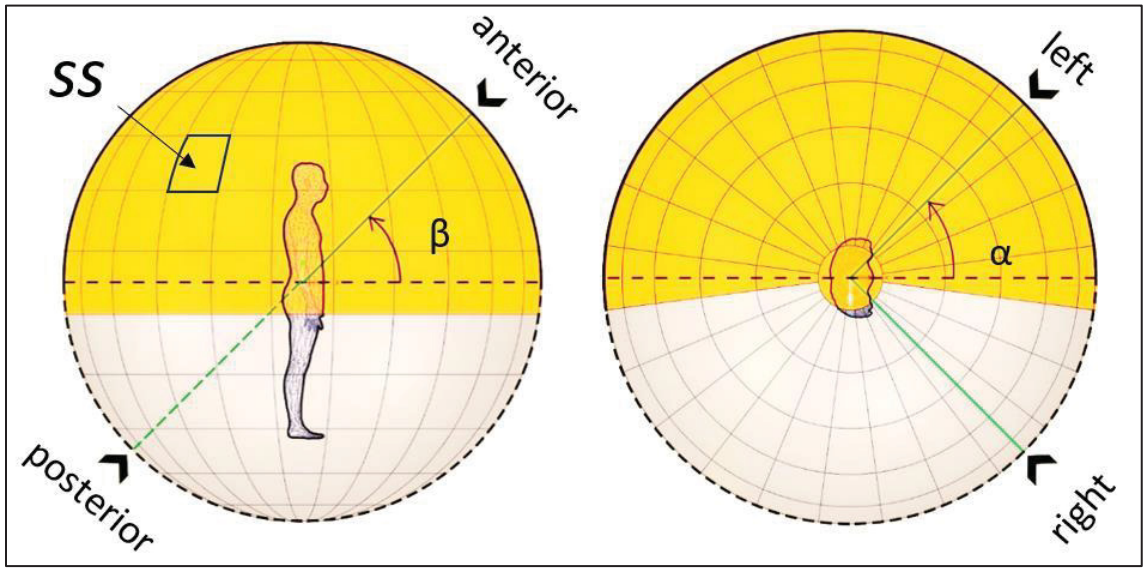

Figure 3.3 Side and top views of the adult manikin in the sphere. The sphere radius illustrated was reduced for clarity and does not reflect that used in the calculations (7 meters)

The geometry was then meshed using the patch-independent tetrahedron method, a recommended approach for meshing intricate geometries like the human body (Ansys, 2010). This process yielded a total element count ranging between 1.2 and 3.1 million, depending on the manikin. Additional mesh refinement attempts did not yield any significant alterations in VF calculations.

3.3.3 Calculation method

The meshed model was sent to Ansys Fluent where the surface-to-surface radiation model was used to calculate the view factors through the ray tracing method (a parallel ray method), and the hemicube method (a solid angle method) and compared to those of Fanger. For both methods, the resolution was increased to reduce the effect of aliasing. An analysis of the effect of the resolution on the calculation results was conducted, and a resolution of 100 pixels per

surface element was found to be sufficient. All calculation steps using the numerical modelling results to obtain VF are shown in Figure 3.4 and detailed in the following sections.

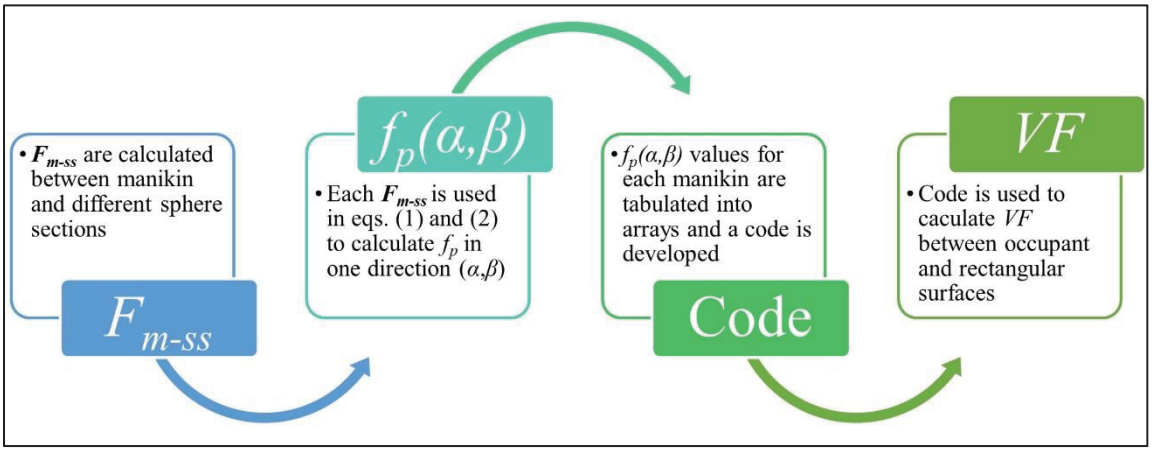

Figure 3.4 Calculation steps for each manikin

Hereafter, $F_{m\text{-}ss}$ is used to refer to the view factor determined by Ansys Fluent between the manikin (m) and each sphere section (ss), while VF is used to refer to the view factor between the occupant and a surrounding rectangular surface, used for the calculation of the MRT.

3.3.4 Projected Area Factors, f_p

Ansys Fluent calculated the view factors (F_{m-ss}) between the manikin and each of the 79 sphere sections (ss) shown in yellow on Figure 3.3. A correction factor (f_c) was applied as per Equation (3.1) to eliminate self-radiation (Youssef & D'Avignon, 2023). Using the corrected view factors ($F'_{m\text{-}ss}$), the f_p of each ss was calculated using Equation (3.2) where r_s is the sphere radius (7 meters) and A_{ss} is the area of the sphere section. A_{ss} is uniform for all sections at the same β and was provided by Ansys.

$$F'_{m-ss} = f_c \cdot F_{m-ss} \tag{3.1}$$

$$f_p = \frac{\pi \times r_s^2 \times F\prime_{m-ss}}{A_{ss}} \quad (3.2)$$

f_p values were determined from Ansys for all three manikins, A-M-L, A-M-R and 5-B, and their values were compared.

3.3.5 View Factors, VF

We developed a code, adapted from the MRT tool developed by the Center for the Built Environment (CBE) (Tartarini et al., 2020), that uses a matrix of f_p values to determine the VF of an occupant with a rectangular surface. The code uses as an input a rectangular surface A of dimensions a×b, whose corner is at a distance c_A from the occupant's center and divides it into differential surfaces of dimensions 0.02×0.02 m. For each differential surface (dA), based on its angular orientation from the occupant (α_{dA} and β_{dA}, measured from the center of dA), f_p is determined using bilinear interpolation from a matrix of f_p values. This matrix changes according to the manikin considered. One such matrix includes Fanger's f_p values as provided in Appendix C of ASHRAE 55 for various α and β. From the f_p value calculated for each dA, the code calculates a differential view factor dVF between the considered occupant and dA through Equation (3.3), where c_{dA} is the distance from the occupant's center of mass to the center of dA. The VF between the occupant and the entire surface (*A*) is calculated by summing the differential view factors (dVF).

$$dVF = \frac{f_p \times c_A \times dA}{\pi \times {c_{dA}}^3} \quad (3.3)$$

To verify the code, we used it to generate VF for different surface dimensions (a, b) and distance ratios (a/c_A, b/c_A), using the matrix of Fanger f_p retrieved from Appendix C of ASHRAE Standard 55. VF were then retrieved from the graphs presented by Fanger (1970) for the same surfaces and compared. VF generated using the code matched well those read from the graphs, the maximum absolute difference was 0.003, with most absolute differences

remaining between 0 and 0.001. This allowed us to verify that the code functions correctly and provides correct values of VF using f_p.

3.3.6 Effective Radiation Area Factor, f_{eff}

Based on the work of Rykaczewski et al., (2022), the view factor between the sphere and the manikin ($F_{s\text{-}m}$) was calculated using the Ansys Fluent software. From Fanger's definition, A_{eff} was calculated using the view factor between the sphere and the manikin ($F_{s\text{-}m}$) and the numerical manikin surface area considered for radiative heat exchange (A_b) through Equation (3.4). f_{eff} was then calculated by dividing A_{eff} by A_{DuBois}. $F_{s\text{-}m}$ were produced from Ansys for both poses, 'A-M-R' and 'A-M-L', as well for the child manikin 5-B, and the resulting f_{eff} values were compared.

$$F_{s-m} \times A_s = A_b \times F_{m-s} = A_{eff} \tag{3.4}$$

3.3.7 Verification and comparison

To verify and compare our f_p results to the literature, we used a mixture of regression analysis, descriptive analysis, and shape comparison, for both the adult and child manikins. We contrasted our errors (i.e. differences to Fanger's average results) to those found in the literature. For VF, we documented the absolute errors (between A-M and Fanger's average data) and the differences (between A-M and 5-B). As suggested by the work of Park & Tuller (2010), the magnitude of the differences found between results for our adult manikin and those of adults in the literature was used as a benchmark to assess the significance of the differences between the adult and child manikins within this study. To analyze the impact of VF differences between adults and children, we examined two test cases: a radiant floor heating

case and a chilled ceiling case. VF and MRT calculated for an adult and a child in various locations within the same classroom were compared.

3.4 Results and Discussions

3.4.1 Verification of Adult Manikin results against Fanger's data

Projected area factors

Calculated values of f_p for manikin A-M-L using both the parallel ray and solid angle methods are compared to those of Fanger's experiments in Figure 3.5. The values can be found in Table A A-1 and A A-2 in Appendix A. For the sphere radius tested, both methods produce values that match well with those of Fanger (relative error < 10% and absolute error < 0.023), and to each other (relative and absolute difference = 0). The lack of difference between parallel ray and solid angle results is likely due to the large distance (7 meters) between the manikin and the surface. This mirrors the findings of Tanabe et al. (2000) who found no significant difference between the two methods when the distance between the occupant and the surface is large. Consequently, for the rest of the calculations in this paper, the parallel ray method was used, and the sphere radius was maintained at 7 meters.

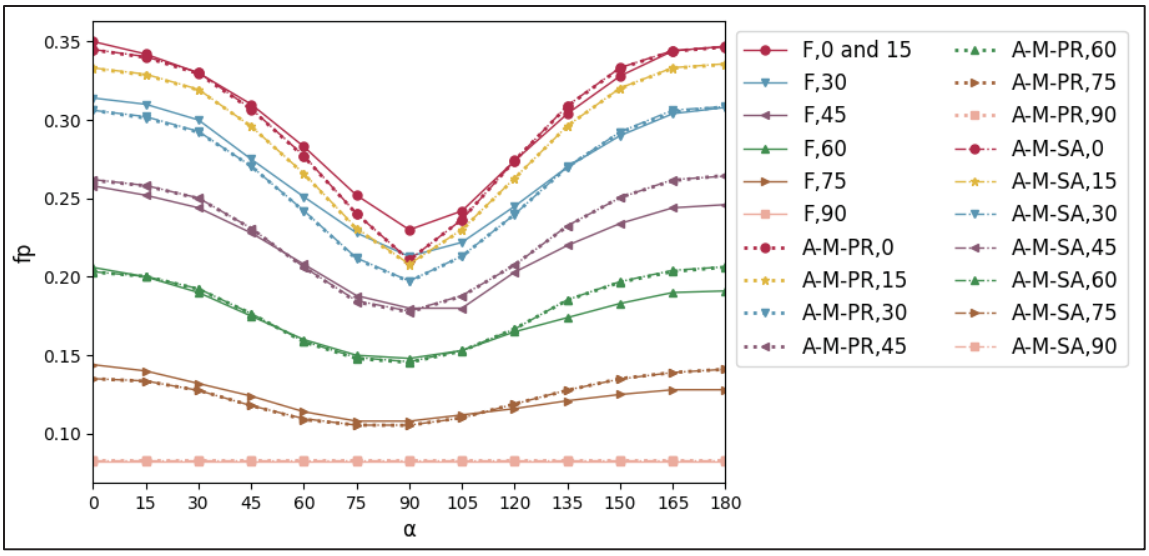

Figure 3.5 f_p as a function of α for each test case. Legend includes three components: data source (F: Fanger's experimental results or A-M: adult manikin); numerical method (SA: solid angle or PR: parallel ray method); value of β

The mean and maximum of error between our results and those of Fanger are presented in Table 3.3 and contrasted against relative and absolute errors found in the literature.

Table 3.3 Relative f_p error between studies in the literature and Fanger

		Present	*Rykaczewski et al. (2022)*	*La Gennusa et al. (2008)*	*Kubaha et al. (2004)*	*Park and Tuller (2010)*
Relative error	**Mean**	0%	2.43%	0%	13%	-
	Maximum	10%	10%	7.5%	-	9.1%
Absolute error	**Mean**	0.001	-	0.0016	-	-
	Maximum	0.022	-	0.0175	-	0.02

The highest relative error of -10% is found for β = 75° and α = 180°, but due to the small values of f_p at the high values of β, the difference in absolute terms is only 0.013. The highest absolute differences are found for β = 15°, where our results underestimate those of Fanger by up to 0.022 for α = 75° and 90°. Fanger's f_p for β=15° and α = 90° is underestimated at a similar

magnitude in other studies (Kubaha et al., 2004; Park & Tuller, 2011; Rykaczewski et al., 2022; Tanabe et al., 2000). For β = 0° and 15°, Fanger reports the same curve for both angles. Our results show a good match for β = 0°, with the exception of α = 90°, where the difference reaches 0.019, comparable with results of Park & Tuller (2010) who reported absolute errors of up to 0.019 for β = 45° and high values of α (>135°). As shown in Figure 3.2, the shoulders, upper back, and chest areas of the Tanabe et al. (2000) numerical manikin (Figure 3.2a) are much rounder and more muscular than those of the manikin used in the present study (Figure 3.2d). Tanabe et al. (2000) is also the numerical study that matched best with Fanger's data. This difference can explain our underestimation of Fanger's f_p for angles where these body sections are most prominent; sideways angle α = 90° (which can be seen in Figure 3.2a and 3.2d) shows the considerable chest size difference between the two manikins. Similar to the present study, Rykaczewski et al. (2022) have found a maximum difference from Fanger of 10% at α = 45°, 90°and 135°, which they attributed to the difference in pose; their manikins had their arms lowered but not touching the torso, whereas the subjects of Fanger are assumed to have had their arms touching their torso. The effect of pose will be further analyzed in the next section. La Gennusa et al. (2008) found a mean error from Fanger of around 0%, and a maximum error of + 7.5% which is on par with our results. Kubaha et al. (2004) reported a "typical" error from Fanger of about 5% for most α and β angles, but they did not report the value of the largest discrepancy. Overall, the relative errors found in this study are comparable with those found by others in the literature who compared their data to Fanger's.

Figure 3.6 presents f_p of manikin A-M-L (shown in Figure 3.2d), compared to values of Fanger (1970) and Rykaczewski et al. (2022). Due to the difference in angle increments used, we can only compare 28 individual values, while 79 can be compared with Fanger. The figure shows our numerical results match well with those of both studies.

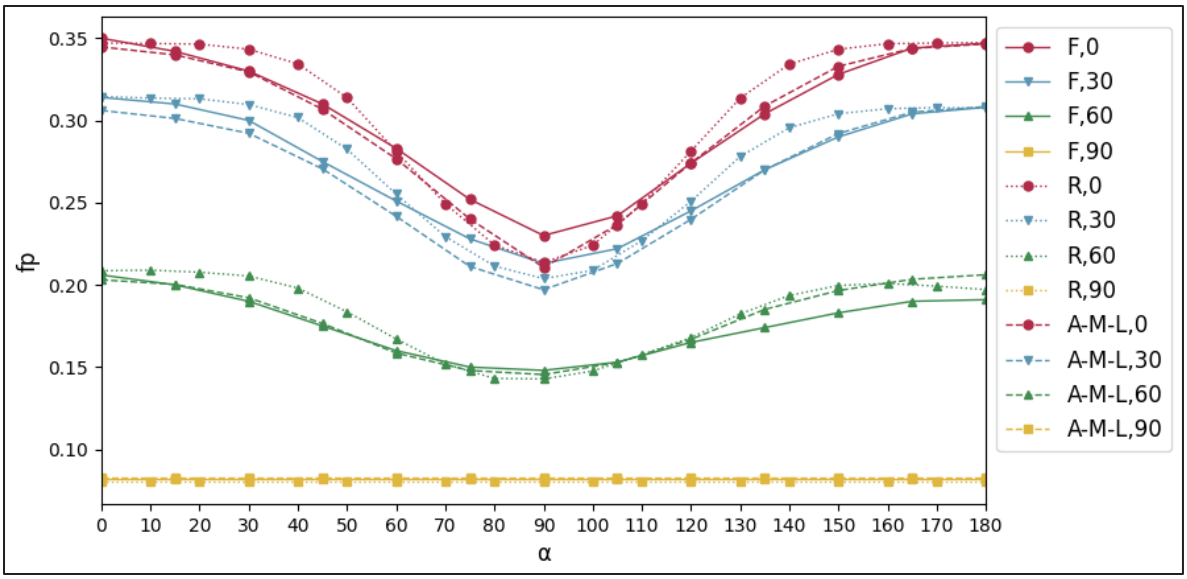

Figure 3.6 f_p of Fanger's (F) experimental results, Rykaczewski's (R) numerical results, and adult manikin with lowered arms (A-M-L). Number indicates the value of β

Results from regression analysis conducted to determine the significance of the difference with Fanger's f_p are presented in Table 3.4. Overall, f_p values found in the present study slightly underestimated those found by Fanger, but the regression analysis reveals a good correlation. The overall regression coefficient is found to be 1.01, with a coefficient of determination at 0.99. Considering each elevation angle separately, the regression coefficient is the best at 0.993 for $\beta = 75°$, and the worst at 1.045 for $\beta = 15°$, where the highest discrepancies are found. Comparing our regression analysis to that performed by Tanabe et al. (2000), we find that our overall and individual regression coefficients are lower (overall 1.003), but our coefficients of determination are consistently higher (Tanabe's 0.931 to 0.979, versus our 0.99). This indicates that our regression model is more robust than that presented by Tanabe.

Table 3.4 Correlation of projected area factors between Fanger and Adult manikin with lowered arms (A-M-L), for various elevation angles

Study	Elevation ($\boldsymbol{\beta}$)	0°	15°	30°	45°	60°	75°	total
Present study	Regression coefficient	1.009	1.045	1.021	0.968	0.976	0.993	1.01
	Coefficient of determination	0.99	0.99	0.99	0.99	0.99	0.99	0.99
Tanabe (2000)	Regression coefficient	1.004	1.025	0.998	0.954	0.982	1.054	1.003
	Coefficient of determination	0.961	0.974	0.966	0.979	0.961	0.931	0.987

The effect of pose on the calculation of f_p is examined in Figure 3.7, where f_p is compared for A-M-R (arms as Figure 3.2c), A-M-L (arms as Figure 3.2d), and Fanger's data (arm angle not specified, but assumed to be vertical touching the torso based on illustrations). The values of f_p for A-M-R and A-M-L can be found in Tables A A-3 and A A-1, respectively, in Appendix A. As can be observed, lowering the arms reduces the difference between the numerical manikin values and those of Fanger, particularly for β of 90° (top view). For β = 90°, A-M-R deviated from Fanger's f_p value by -17%. Therefore, it is evident that lowering the arms of the manikins improves the match with Fanger's data, which reflects the findings of Rykaczewski et al. (2022) and Yousaf et al. (2008). Considering A-M-R did not have its arms touching the torso as Tanabe (2000)'s model did, and Fanger's subjects are assumed to have, it is possible that this difference contributes to the remaining discrepancy found, in addition to the minor differences in body mass and muscle distribution discussed above.

Comparing the two poses, the differences in f_p observed is highest at -15% for the top-down view ($\beta = 90°$) which is close to that found by Rykaczewski et al. (2022) (-20%). The noticeable difference between the two poses lies in the shape of the graphs: as shown in Figure 3.7, the curves representing A-M-L exhibit a behavior more similar to Fanger's compared to A-M-R. This is especially noticeable for shallow and high azimuth angles, despite sometimes having larger individual point differences. This difference is understandable since, at these

angles, the position of the arms greatly alters the projected area of the body. In contrast, at middle angles (side view), the arm position does not affect the projected area of the body.

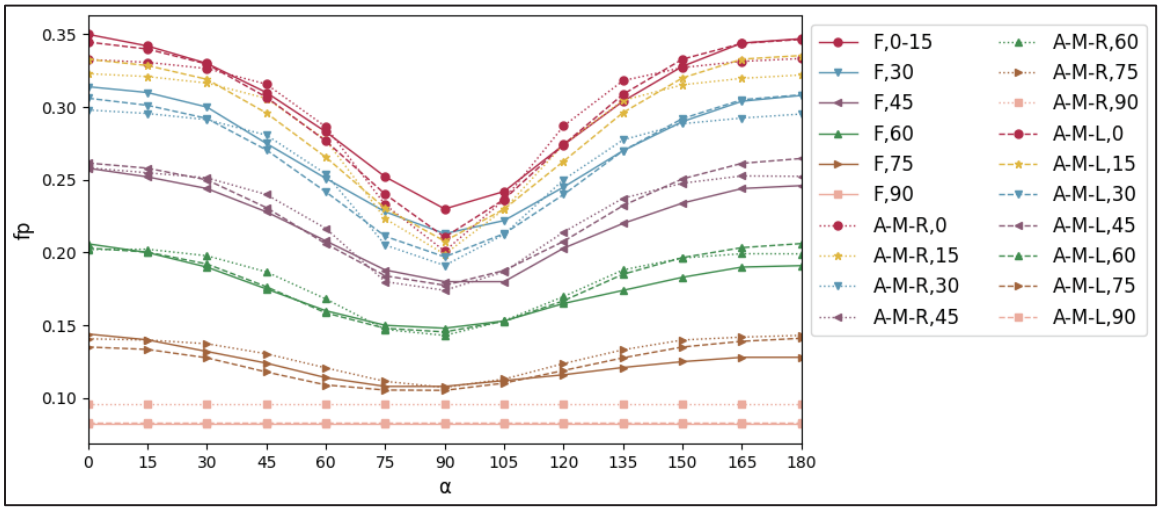

Figure 3.7 Effect of pose on f_p: Fanger's data (F) adult manikin with raised arms (A-M-R), adult manikin with lowered arms (A-M-L) at varying β

Effective radiation area factor

An important parameter commonly used to quantify the effect of pose and posture on radiation exchange with the environment is the effective radiation area factor (f_{eff}). As tabulated in Table 3.1, we found that lowering the arms of the manikin (A-M-R versus A-M-L) decreased the value of f_{eff} from 0.827 to 0.779, a difference of 5.8%. It is likely that lowering them further until they touch the torso would further decrease this value, as found by Rykaczewski et al. (2022) and Yousaf et al. (2008). This was not feasible with the current numerical manikin without causing severe model body distortion. Nonetheless, the value of f_{eff} for 'A-M-L' was still 7.5% higher than that determined by Fanger, but within 5% of past studies (Calvino et al., 2009; Horikoshi et al., 1990; Kubaha et al., 2004; Kurazumi et al., 2008), and within 2% of other research with lowered arms not touching the torso (Rykaczewski et al., 2022; Yousaf et al., 2008). For the remainder of the paper, the adult manikin considered will be that with lowered arms and it will be referred to as "A-M". The child manikin 5-B also has its arms lowered.

View Factors

View factors of A-M for the different cases defined by Fanger are shown in Figure 3.8. The view factors match well with those of Fanger: For all cases, the absolute error was mostly null or 0.001, with the maximum error at 0.003 only occurring 23 times among the 486 values calculated (4.73% of total points). This error is on par with the discrepancy between the graphically interpreted values from Fanger's diagram (Fanger, 1970) and the values generated by the code.

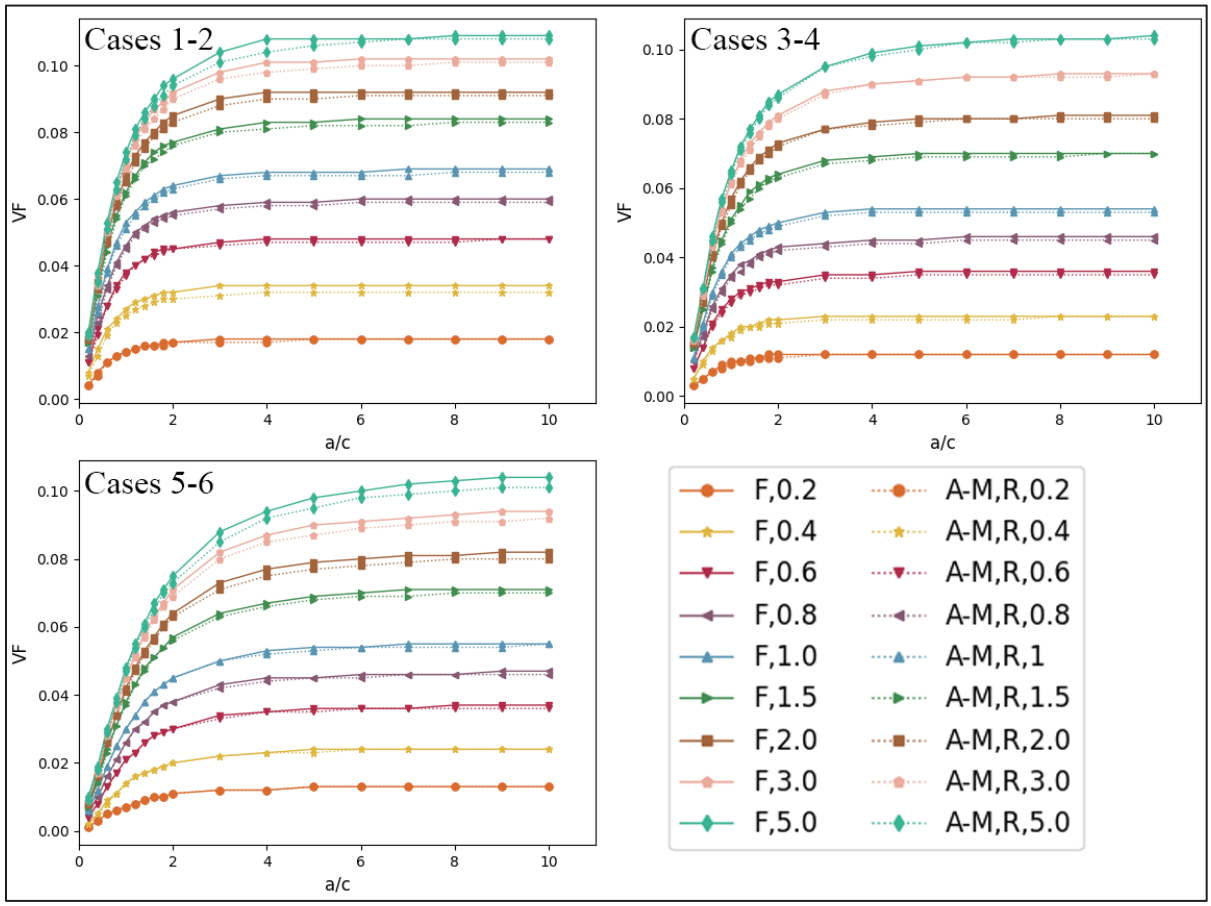

Figure 3.8 View factors comparison between Fanger and A-M for the cases defined by Fanger. Cases 1-2: with a vertical rectangle in front or behind, above or below center of mass, Cases 3-4: with a rectangle on the side wall, forward or behind, above or below center of mass

3.4.2 Children Manikins

Projected area factor

The f_p curves of the 5-year-old boy manikin (5-B) are compared to those of the adult manikin (A-M) in Figure 3.9. The values of f_p for 5-B can be found in Table A A-4 in Appendix A. For elevation angles 0°, 15°, and 30°, the difference between the adult and child f_p values is present, but lower than 15%. For higher elevations, 45°, 60°, 75°, and 90°, the difference becomes more noticeable, reaching values of 22%.

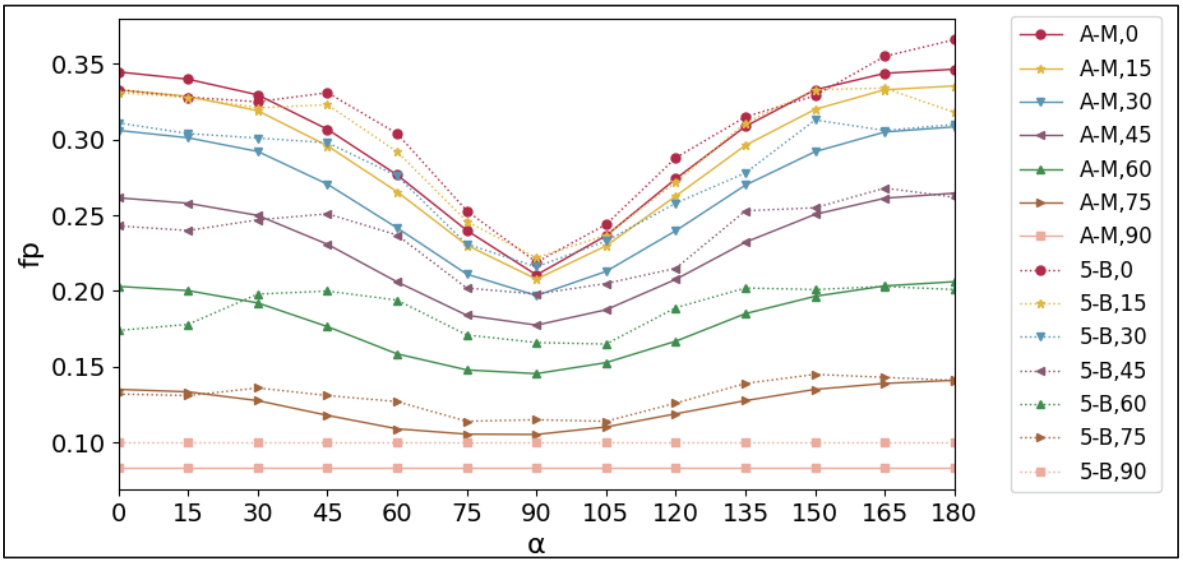

Figure 3.9 f_p of the adult manikin A-M and 5-B manikin, at various α and β

Figure 3.9 reveals a distinct difference in the curve shapes between the child and adult manikins that was not present between the adult manikin and curves from the literature depicted in Figures 3.5 and 3.6. While there are differences in individual points between A-M-L, Fanger's, and Rykaczewski's data, they consistently exhibit a similar overall "shape": as illustrated on Figure 3.6, f_p curves begin with high values for low azimuth angles, gradually decreasing until they reach a minimum at α = 90°, then ascend again in a quasi-symmetrical fashion until they peak once more at α = 180°. For the 5-B child manikin, this pattern, characteristic to all adult

f_p curves found in the literature, is not observed. For elevation angles $\beta = 0°$, 15°, and 30°, the curves appear relatively flat for $\alpha \leq 45°$, before descending to a minimum at $\alpha = 90°$. They then ascend again, albeit without displaying the same uniformity as the adult curves: while the $\beta = 0°$ curve ascends to another maximum at $\alpha = 180°$ as the adult's does, the $\beta = 15°$ and 30° curves reach their maximum earlier — at $\alpha = 165°$ and 150°, respectively — before marginally declining again. For $\beta = 45°$ and 60°, the curves start from a significantly lower value at $\alpha = 0°$ than their adult counterparts, they rise to a maximum at $\alpha = 45°$, drop to a minimum at $\alpha = 90°$ and 105°, respectively, then climb again to a secondary peak at $\alpha = 165°$. For $\beta = 75°$, the 5-B curve roughly mirrors the shape of the adult's.

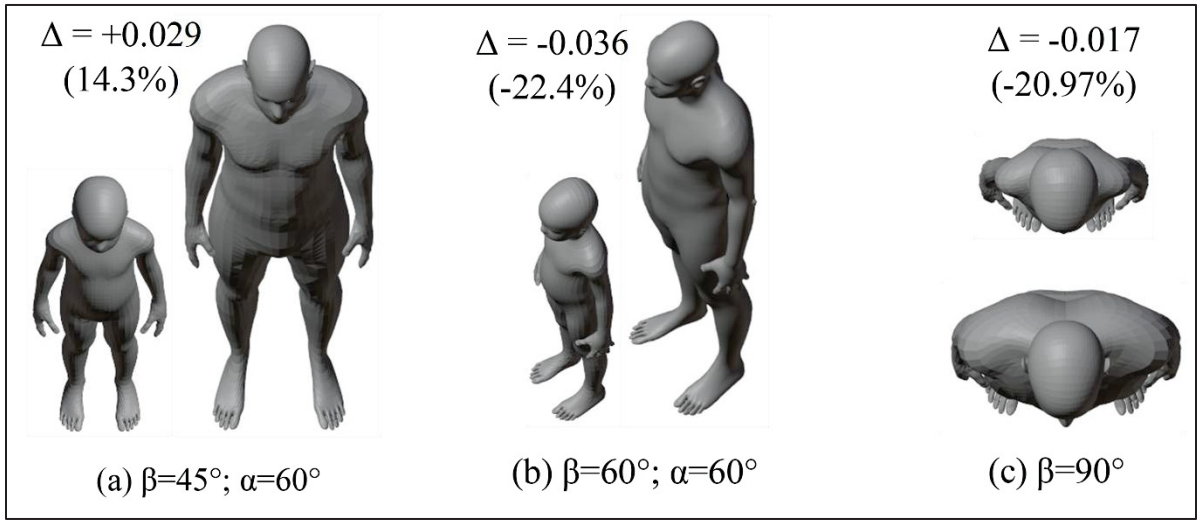

Figure 3.10 Different angle views of the A-M and 5-B manikins

Figure 3.10 shows the A-M and 5-B manikins from the azimuth and elevation angles which showed the most significant differences. Δ represents the absolute difference in f_p between A-M and 5-B, with the value indicated in parenthesis representing the relative difference (with A-M as the reference). Overall, the differences in f_p between the adult and child manikins stem from their distinct body shapes. The adult is taller, broader, and leaner, with the greatest bulk concentrated in the chest, back, and shoulders. In contrast, the child is shorter and rounder, with more volume concentrated in the head and abdominal area, while having a narrower chest, slimmer arms and shoulders, and shorter legs.

For nearly all front-facing angles ($\alpha = 0°$ and 15°), the A-M manikin exhibits a higher f_p value. Figure 3.10a illustrates one such angle and makes apparent this is likely a result of the adult's broader shoulders, chest, and hips in proportion to his size. Conversely, the other angles shown in Figure 3.10 display a significant negative Δ, indicating the child has larger f_p than the adult. Among all elevation angles, $\beta = 60°$ (Figure 3.10b) exhibits the greatest negative difference, with statistically significant differences across $0° \leq \alpha \leq 120°$. At this high elevation angle, the upper body obscures the legs, reducing the projected area—which particularly impacts the adult manikin, whose longer legs (SHS of 0.51 vs. the child's 0.54) make up a larger portion of total body area. For the other elevation angles, the most notable differences typically occur at azimuth angle of 60°, and occasionally at 45°. At $\beta = 90°$, the top-down view illustrated in Figure 3.10c, the child manikin shows a higher f_p value, likely due to its large head-to-body ratio. From this angle, the adult's broader features—such as the chest, back, and longer legs—are largely obscured. In contrast, the child's more prominent head remain visible, resulting in a greater f_p.

View Factors

Figure 3.11 presents a comparison of VF between A-M and 5-B. The absolute difference in VF between the manikins is notably more pronounced and evident than that found between Fanger and A-M in Figure 3.8; out of a total 486 data points, 73 have an absolute difference of 0.003 (15%), for 66 it is 0.004 (13.5%), and for 6 it is of 0.005 (6.5%). These absolute differences are greatest for higher values of a/c, where the absolute VF values are also greater. Since the graphs presented only represent one-fourth of any wall surrounding the occupant, the difference in VF between the adult and the child will be greater for the entire surface. As detailed above, these absolute differences are greater in magnitude and frequency than those found between A-M and Fanger.

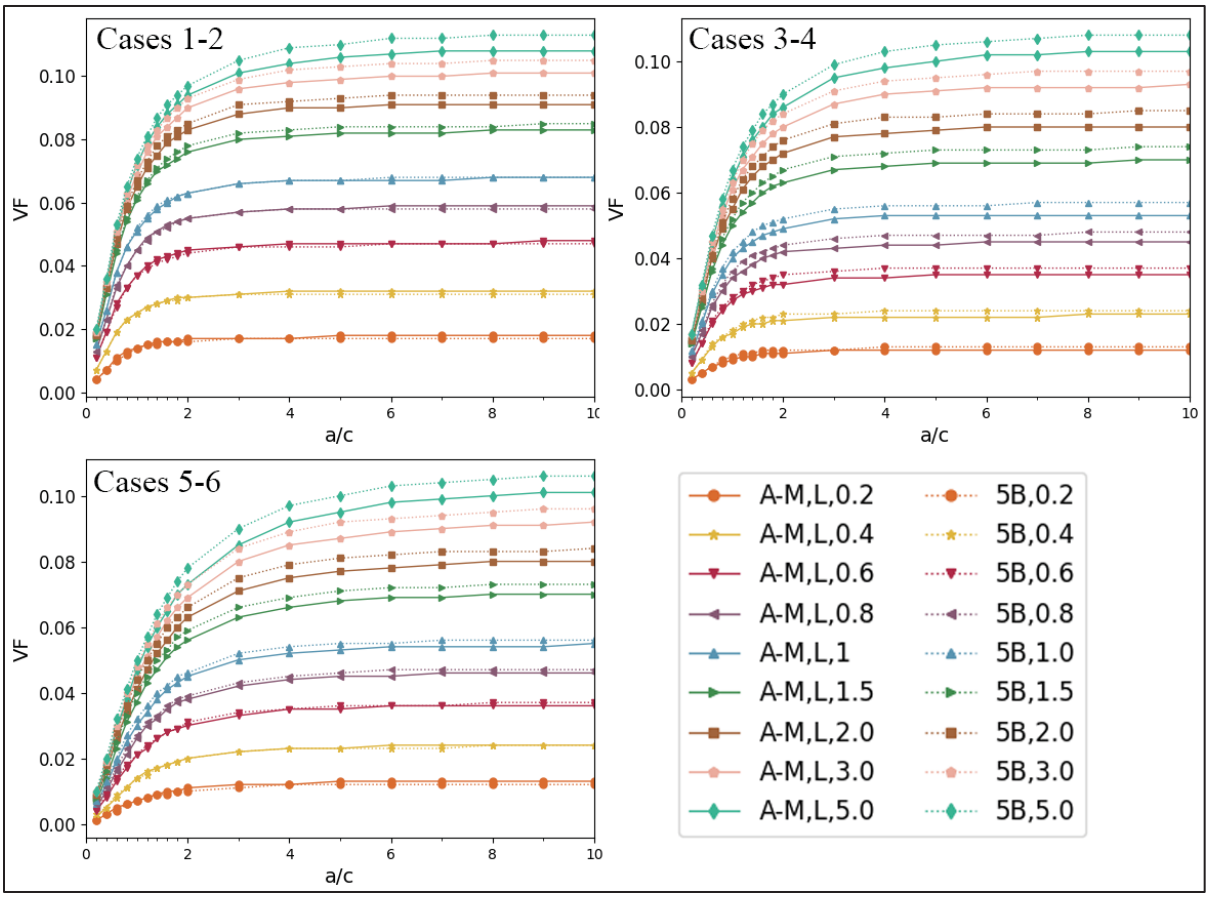

Figure 3.11 Comparison of *VF* for A-M-L and 5-B for the cases proposed by Fanger. Cases 1-2: with a vertical rectangle in front or behind, above or below center of mass, Cases 3-4: with a rectangle on the side wall, forward or behind, above or below center of mass, Cases 5-6: a rectangle on the ceiling or on the floor, forward or behind centre of mass

3.5 Test scenarios

A classroom of dimensions 8.8×8×3.965 m is considered based on the architectural plans of an existing preschool classroom in Quebec, Canada. The classroom features three internal walls (right, left, and rear), while the external front wall is predominantly a large window covering 72% of its total area. Two scenarios are considered, as detailed in Table 3.5.

Table 3.5 Temperature of surfaces in Celsius for the test scenarios considered

Surface	Front	Rear	Left	Right	Ceiling	Floor	Window
Scenario 1: Hot Floor	19.5	20.5	20.5	20.5	18.5	26	18
Scenario 2: Cool Ceiling	24.5	22	23	23	17	21	22

In the first scenario, the room floor is heated using a radiant heating system. The chosen floor temperature aligns with the design floor temperature of the existing classroom. This temperature is slightly below the maximum recommended by ASHRAE (ASHRAE-55, 2017) of 28 °C. In the second scenario, the room is equipped with a chilled ceiling system and temperatures were selected based on a classroom design example from ASHRAE Handbook (ASHRAE, 2017). The ceiling temperature of 17 °C was chosen to be well above the dew point temperature.

Difference in MRT calculated for the adult and child (MRT_{child} - MRT_{adult}) at 9 different positions in the room are presented in Figure 3.12. For the hot floor scenario, the mean difference is 0.92 °C with a small SD (0.06 °C), whereas for the cold ceiling scenario, the mean difference is lower (0.64 °C) but with the same SD of 0.06 °C.

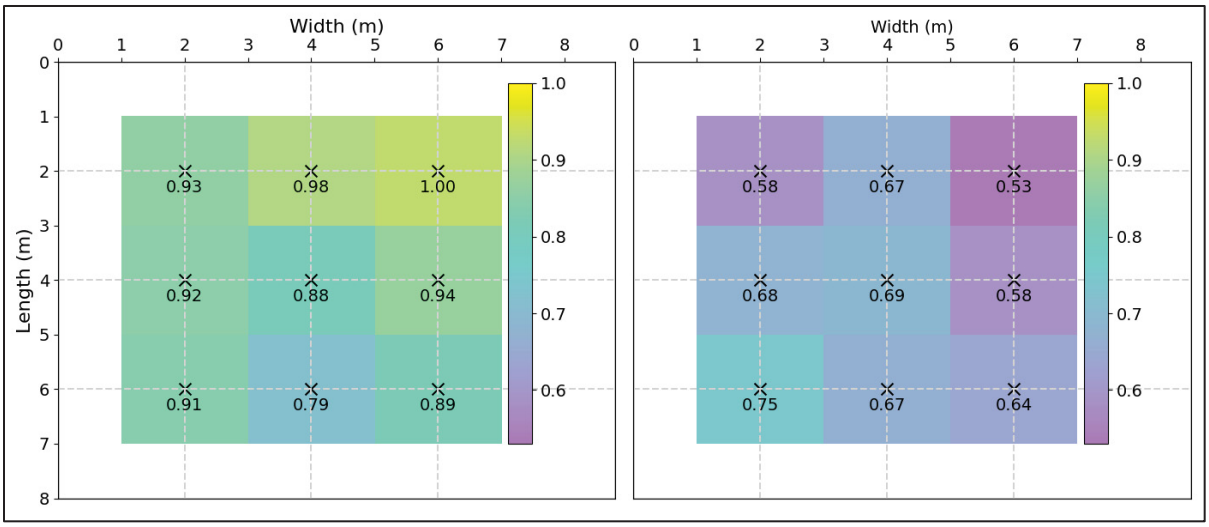

Figure 3.12 Difference in MRT (°C) between the adult and child occupants for (a) Hot floor scenario, and (b) Cold ceiling scenario

As shown in Figure 3.12, the largest difference occurs in the hot floor scenario, likely due to the smaller distance between the floor and the occupant's center of mass. For this scenario, the child's center of mass is assumed to be 0.6 m from the floor, the median abdomen height of a 5-year-old child (Youssef & D'Avignon, 2021), while the adult's center of mass is assumed to be at 1 m from the floor (Fanger, 1970; ISO 7726, 1998). If we consider the point with the highest difference (width = 6 m, length = 2 m) and assume both the adult and child's center of mass are 1 m above the ground, the difference in MRT reduces to 0.6 °C. Given that the actual abdomen elevation of standing children in a preschool classroom is closer to 0.6 m rather than 1 m, we can confidently state that they are likely to experience a mean radiant temperature that is up to 1 °C higher than that experienced by adults when high floor temperatures are present. The difference in elevation between the child and the adult also likely contributes to the *MRT* difference.

The impact of this 1°C difference on occupants' thermal comfort represented by the Predicted Mean Vote (*PMV*) depends on various environmental parameters and individual factors. Using Fanger's (1970) tables on PMV sensitivity, a 0.5–1°C difference in MRT would correspond to a *PMV* variation of ±0.06 to ±0.12 between adults and children. Similarly, Alfano et al. (2008) analyzed the PMV equation's sensitivity to MRT and found that a ±0.2°C change in MRT

resulted in a PMV variation of ±0.16 to ±0.25. Such a difference in PMV is likely to produce differences in perceived comfort between an adult and child in identical environmental conditions such as those documented in past literature relating to classrooms, where children represent the majority of occupants in the space (Teli et al., 2012, 2016).

3.6 Conclusions

The study presented a numerical method for the calculation of f_p and VF which was verified using Fanger's experimental data. The minimal relative differences (<10%) between our results and Fanger's resembles values found in the literature and confirms the accuracy of our method. Our analysis of the effect of arm positions, and comparison with other studies in the literature, support our claim that these differences are due to body shape and pose differences between manikin and occupant.

The parallel ray method was found to produce similar results to the solid angle method when a large distance of 7 meters is considered between the occupants and the surfaces that surround them. In the literature of human view factors in the indoor environment, Fanger's data (f_{eff}, f_p, and VF) is considered as reference, and is used to determine the human body's radiant exchange with the environment as well as his solar heat gains. Considering the significantly smaller distances that are likely to be found in indoor environments, exploring whether Fanger's data, which uses a parallel ray method at a large distance, is applicable to all radiant exchange calculations should be considered in future works.

The study reveals significant differences in f_p between adults and small children, particularly at higher elevation angles (45°, 60°, 75°, and 90°), where the differences reached up to 22% for the standard 5-year-old. Distinct variations in the curve shapes of f_p were observed, indicating that young children cannot be assumed to have the same f_p as those used in standards.

View factor analysis showed significant absolute differences between the adult and the 5-year-old, especially at higher values of a/c. In the two scenarios used, these differences were shown to significantly impact their mean radiant temperature (MRT). A hot floor scenario showed a mean difference of + 0.92 °C and a cold ceiling scenario showing + 0.64 °C, with the child consistently having a higher MRT than that of the adult under identical conditions. This finding aligns with the result of thermal comfort studies, which have shown that children often feel warmer than predicted by the Predicted Mean Vote (PMV) method (Teli et al., 2012, 2016). These results suggest that in some cases, the discrepancy could be due to differences in *MRT* and incorrect elevation of environmental sensors. Addressing these differences could help reduce the inconsistency in *PMV* calculations applied to children.

This study was limited to investigating the difference in VF between young children (5 years old) and adults. Further investigations are needed to determine if this difference also applies to older children and to identify the age at which children's VF become similar to those of adults. Overall, the findings underscore the importance of accounting for the effect of height and body shape differences when analyzing thermal comfort and radiation exchange. Utilizing view factors specifically determined for children is likely to reduce inaccuracies currently present in assessments of their thermal comfort.

3.7 Interlude – Discussion on Article 2

This chapter introduced a rigorous numerical approach for calculating radiation data and applied it to both adult and child manikins in the standing posture. It confirms the necessity of child-specific radiation data in this posture, with differences of particular significance being found for the ceiling and floor. Knowing the occupants' closer proximity to the floor in the seated posture, leads us to investigate differences in radiation data between seated adults and child occupants. The seated posture brings about its' own methodological considerations which must be investigated, notably the anterior/posterior symmetry assumption, widely in use in view factor literature. These considerations are the topic of the next chapter.

CHAPITRE 4

ARTICLE 3: ARE WE OVERESTIMATING RADIANT EFFECTS? RE-EXAMINING VIEW FACTORS IN THE SEATED POSTURE

Nour Youssef, Katherine D'Avignon

Département de génie de la construction, École de Technologie Supérieure, 1100 Notre-Dame Ouest, Montréal, Québec, Canada H3C 1K3

Paper published in *Building and Environment*, October 14 2025

4.1 Introduction

The determination of view factors (F) and projected area factors (f_p) is an important endeavor in thermal comfort literature due to the significant role of radiation in occupant comfort in both indoor and outdoor environments (Flouris et al., 2018; Kántor & Unger, 2011). Outdoors, research shows that radiation from the ground can increase the risk of heat stress (Fan & McColl, 2024; Habibi et al., 2024; Imhoff et al., 2010). In the indoor environment, radiant heated floors and chilled ceilings have gained traction due to their superior performance in both delivering thermal comfort with reduced energy consumption (Hooshmand et al., 2023; Liu et al., 2025), increasing their deployment in office and institutional buildings (Hu & Niu, 2012; Natural Resources Canada, 2024; Rhee & Kim, 2015). Yet, the effect of radiation on occupant comfort is still evaluated from data determined in long-dating experiments which few have been able to replicate, and relied on assumptions which have never been verified.

Humans spend 90% of their time indoors (United States Environmental Protection Agency, 2025) and 40-55% of that time sitting down (Colley et al., 2022; Matthews et al., 2008). Though research on occupant radiation in the standing posture has expanded from the early methods and populations studied (Horikoshi et al., 1990; Kurazumi et al., 2008; Rykaczewski et al., 2022), very little literature can be found on the seated posture. This paper seeks to address these lacunas by determining the radiation data of an adult and child numerical manikin in the

seated posture under various scenarios, addressing several of the calculation assumptions held in the literature.

4.2 Literature Review

When an occupant is in a moderate indoor environment, ASHRAE-55 recommends the calculation of the Mean Radiant Temperature ($\overline{t_r}$) using Equation (4.1). In those circumstances, the dominant form of radiation present is the long wave emissions of the surrounding surfaces, which are assumed to be grey, diffuse, isothermal, and at a low temperature so view factors are used. $\overline{t_r}$ is defined as the uniform temperature of a hypothetical black-body enclosure that would produce the same net radiative heat exchange with the subject as the actual, more complex radiative environment, t_i is the temperature of each surrounding surface, and $F_{p\rightarrow i}$ is the view factor between the occupant and that surface (ASHRAE-55, 2017). On the other hand, direct solar-beam radiation can be characterized by a small area, high temperature, and high directional radiant emission at a large distance, so the projected area factor f_p is used for the calculation of solar radiation effects on occupants. Therefore, knowledge of f_p and $\overline{t_r}$ enables us to derive an expression of the total net thermal radiation leaving the body (R), as shown in Equation (4.2), expressed as the difference between the long-wave emission of the body (R_{lw}) and absorbed short-wave radiation from the sun (R_{sw}) where σ is the Stefan-Boltzmann constant, ε is the emissivity of the human body, α_{ir} is the absorptivity of the skin/clothing for the short-wave band considered (in this case the sun), A_{eff} is the effective radiation area of the human body in m^2, and q_{ir} is the intensity of radiation emitted by the sun in watts.

$$\overline{t_r} = \sqrt[4]{\sum_{i=1}^{N} {t_i}^4 F_{p\rightarrow i}} \tag{4.1}$$

$$R = R_{lw} - R_{sw} = \sigma \varepsilon A_{eff}\left[{t_{cl}}^4 - {\bar{t}_r}^4\right] - \alpha_{ir} f_p A_{eff} q_{ir} \tag{4.2}$$

The view factor (F) is a mathematical geometrical property that depends on the location of the occupant (i.e. their distance and orientation from surrounding surfaces), the size of the considered surface (variables a, b, and c in Figure 4.1), as well as the occupant's posture, meaning view factors are different for seated and standing persons. The projected area factor (f_p) is dependent on the orientation of the radiating surface with respect to the person, as expressed through the azimuth and altitude of the surface with respect to the occupant (variables α and β in Figure 4.1), as well as the occupant's posture. Despite the presence of other measurement tools for the assessment of the mean radiant temperature, calculation through view factors remains the most reliable method (Alfano, Dell'isola, et al., 2021; Alfano et al., 2023).

Fanger (1970) provides diagrams illustrating view factors for a nominal occupant in either the standing or seated posture with various rectangular surfaces in its surrounding for the purpose of direct mean radiant temperature calculations. Computer codes have recently been developed (Arens et al., 2015; ASHRAE-55, 2017; Tartarini et al., 2020) that instead determine F for a specific surface using Fanger's f_p arrays in Equation (4.3). Therefore, f_p is the single parameter needed to determine the total radiant exchange of the occupant with his environment, taking into account both the long-wave R_{lw} and short-wave R_{sw} component of that exchange.

$$F_{P-A} = \frac{1}{\pi} \int_{\frac{x}{y}=0}^{\frac{x}{y}=\frac{a}{c}} \int_{\frac{z}{y}=0}^{\frac{z}{y}=\frac{b}{c}} \frac{f_p}{[1 + \left(\frac{x}{y}\right)^2 + \left(\frac{z}{y}\right)^2]^{3/2}} d\left(\frac{x}{y}\right) d\left(\frac{z}{y}\right) \tag{4.3}$$

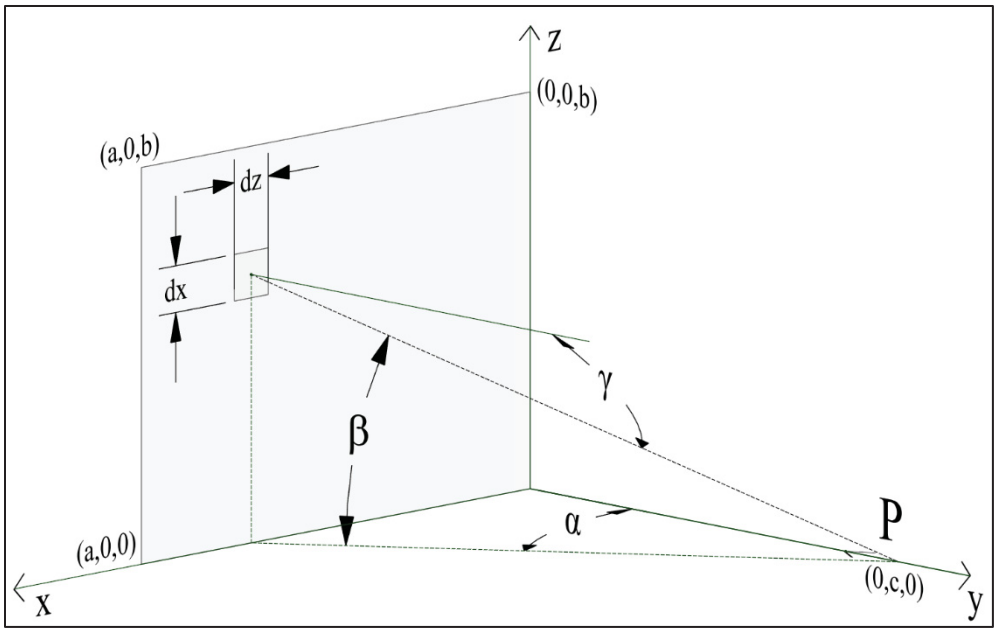

Figure 4.1 Diagram of the basis for the evaluation of the view factor between a person (P) and a rectangular surface

Adapted from Fanger (1970)

The values of F and f_p provided by standards (ASHRAE-55, 2017; ISO, 1994) and used by professionals (Tartarini et al., 2020) are those extracted from the Fanger study (Fanger, 1970) where adult participants were photographed in the standing and seated posture using an orthographic projection camera rotated front to back ($0° \leq \alpha \leq 180°$ on Figure 4.1) and front to top ($0° \leq \beta \leq 90°$) in fifteen-degree increments. Only one fourth of the sphere was considered, as left-right L/R and anterior-posterior A/P symmetry was assumed. As shown in Figure 4.2a, L/R refers to vertical axis symmetry of the left and right side of the human body, so a person's f_p at the same angle β from their left side and right side (meaning at (α,β) and (-α, β)) are presumed equal. Literature has demonstrated this to be a reasonable assumption in healthy non-disabled adults and children (Hope et al., 2013) provided pose is also symmetrical across the vertical axis. A/P symmetry refers to the point symmetry of the front and back side of the human body with respect to the centre of volume, where a surface that is in front of and above the occupant's centre of volume is assumed to have the same f_p as that of a surface behind and

below, as shown in Figure 4.2b. This assumption is illustrated in Fanger's cases one to six (Fanger, 1970). Following this assumption, the f_p values for surfaces that are below the occupant's center of volume were never measured in Fanger's experiments but were instead determined through Equation (4.4) (Tartarini et al., 2020).

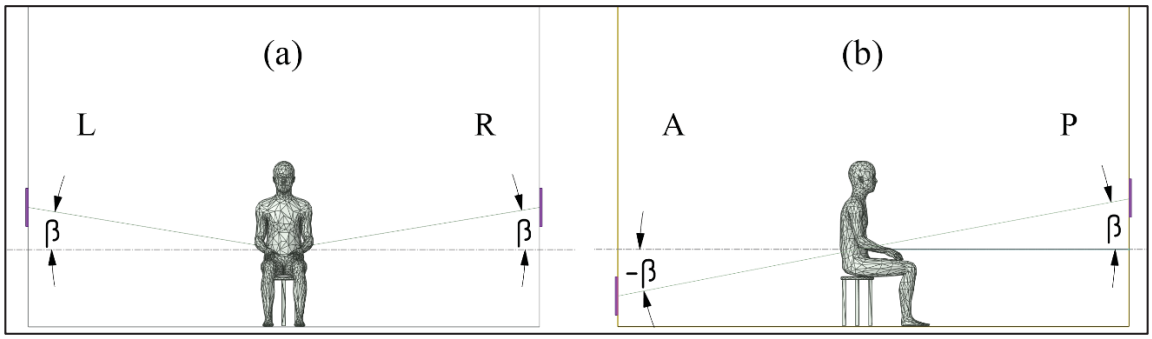

Figure 4.2 Illustrations of the (a) Left/Right (L/R) symmetry as seen from α = 0°, and (b) Anterior/Posterior (A/P) symmetry as seen from α = 90°

$$if\ \beta < 0\ \Rightarrow\ f_p(\alpha, \beta) = f_p(180 - \alpha, -\beta) \tag{4.4}$$

Using such f_p for the calculation of F between the occupant and the floor is only applicable if no objects intercept the line of sight between the two. For the seated posture, the object upon which the occupant sits would effectively shade parts of the occupant's body from certain sections of the floor. Knowing Fanger's participants were most likely seated on a stool during his experiments; this would have affected the projected areas photographed for values of α > 90° (i.e. shading the back of the occupant's legs). The most significant shading effect of the seat would only be appreciated for negative values of β, which were not considered in the Fanger experiment. Other studies that used Fanger's data (whether his f_p arrays or his F diagrams), either to reproduce them using a numerical algorithm (Cannistraro et al., 1992; Rizzo et al., 1991) or to expand their applicability to complex room shapes (Kalisperis et al., 1991), inherently make those same assumptions.

Horikoshi et al. (1990) conducted a study using the photographic method with four adult male subjects. They set themselves apart from the Fanger study by taking photographs at close distances from the subjects: 1 and 2 meters. They hypothesized the large distance between subject and camera in Fanger's work (7 meters) made their data inapplicable to calculations where surfaces are at a close distance from occupants, such as floors. In addition, they did not assume A/P symmetry and determined F (but not f_p) for floor surfaces. In the seated posture, their findings were largely different from Fanger's, reaching a 40% difference in F for the floor. The study did not describe nor address the presence of any seat in the experiment, nor the shading ensued. Instead, they concluded differing results were born out of the distinct photographic methods used, which would be exacerbated at short distances. A recent numerical investigation that replicated Horikoshi's experiment at close distances found differing results and posited that this discrepancy was born out of methodological issues in Horikoshi's work (Youssef & D'Avignon, 2023).

La Gennusa et al. (2007, 2008) and Calvino et al. (2009) conducted experimental studies on subjects representative of the southern Italian population, based on the method proposed by Calvino et al. (2005). In the original photographic experiment of Calvino et al. (2005), occupants were seated on a backless chair (i.e. a stool) which researchers stated strongly interfered with the visibility of the subjects' legs. They considered this interference to be unwanted, and so the images were "treated" to eliminate the stool from the photographs. None of these studies discussed the shading effect of the chair in possibly reducing the real radiant exchange of the body with the floor. All three studies determined f_p from the same altitude angles used by Fanger, effectively assuming A/P symmetry.

Lo Curcio FP (2009), as reported by Nucara et al. (2012), determined f_p numerically using adult numerical manikins of men and women both in the standing and seated postures. In the seated posture, the study claims a "significant agreement" with Fanger's data, except at $\beta = 30°$ where the difference reached 0.08 (45%). The study also assumed A/P symmetry, opting to only determine f_p for positive values of β. They did not model a seat, and the effect of seat shading was not discussed.

Tanabe et al. (2000) and Kubaha et al. (2004) used floating seated numerical manikins and compared their f_p results to Fanger's. Despite both having found a good match when comparing their results in the standing posture, Tanabe found some discrepancy for the seated posture. Havgaard Vorre et al. (2015) determined the F of a floating manikin, using a ray tracing method in Ansys CFD, and found a good match with those determined using Fanger's F diagrams. The absence of a chair was noted as a limitation by the authors.

Overall, A/P symmetry is a widely used assumption in view factor literature, and consequently most studies opt to only determined f_p for positive values of β. Despite several researchers noting the large effect seat shading should have on this data, seats are rarely modelled in numerical studies, and the effect of seat shading on the photographs taken is rarely addressed in experimental studies.

Some studies have focussed on the shading caused by furniture and/or other occupants. Manabe et al. (2004) studied the effect of room occupancy density on F of seated manikins due to shading by other occupants. They did not discuss the effect of seat shading and modelled their manikins "floating" in the air with no seats beneath them. The study notes F found between the seated occupant and the floor surpassed that of the standing occupant, without making note of the unrealistic floating configuration. In all the cases considered, the view factor between the studied occupant and other occupants increases as occupant intensity increases, reaching a maximum of 0.27 in the seated posture when surrounded by 49 occupants. In all cases, the reported full body view factor with the floor is the highest due to the unrealistic "floating" configuration. Other studies acknowledged the effect of seat shading without treating the data accordingly (Li et al., 2022; Zeng et al., 2024b). Only Francisco et al. (2012) determined the view factors between a simplified human manikin and surrounding surfaces that included a small seat, table, drawer unit, computer and screen. They found F between occupant and chair to be the highest (F_{chair} = 0.08) out of all the surrounding furniture, indicating the importance of shading by this specific piece of furniture. As a result, F found between the occupant and floor was much smaller (ΔF = 0.111) than in Vorre's study which

considered occupants to be floating (Havgaard Vorre et al., 2015). These findings indicate the magnitude of the effect of shading from surrounding objects (seats, desks, tables, other occupants, etc.) is highly contextual. For the seated posture however, a seat of some form will indubitably be present, raising the question as to whether it may be wiser to systematically include minimal shading from a stool, than to generalize the use of view factors which neglect it altogether.

Fanger's data (both f_p and F) are used by standards such as ASHRAE-55 (ASHRAE-55, 2017), ISO 7730 (ISO 7730, 2005), and ISO 7726 (ISO 7726, 1998) for the calculation of $\overline{t_r}$ for any occupants regardless of their anthropomorphic characteristics. Several researchers have sought to confirm whether the radiation data obtained by Fanger for young Scandinavian adult males, applies to other populations. Nucara et al., (2012) reports that Lo Curcio FP (2009) studied adult models of men and women with anthropometric data characteristic of different nationalities (Italian, Australian and British, Chinese, Japanese, German, and American) and found absolute differences in f_p ($\Delta f_p < \pm 0.017$ for standing and $\Delta f_p < \pm 0.018$ for seated) between the populations considered in both the standing and seated cases. Similarly, Calvino et al., (2009) considered the southern Italian population and found differences in f_p of up to ±0.018 (8%) in the standing posture, and up to 0.081 (52%) in the seated posture when comparing to Fanger's Scandinavian subjects. Rykaczewski et al. (2022) investigated the impact of BMI and height variations among the American adult population on their f_p and f_{eff} in the standing posture and found that differences <10%, apart from extreme cases (BMI > 80th percentile) where Δf_p reached 42%. Similarly, Tanabe et al. (2000) found differences of 7% in f_p when comparing a "standard" to a "10% wider" adult male manikin. Park & Tuller (2011) compared a normal- and over-weight Canadian adult men and women in the standing and walking postures and found absolute differences in $f_p < 0.017$. Children on the other hand, constitute a larger proportion of every population (TheGlobalEconomy.com, 2025) and have larger anthropometric and body surface area differences from adults than differences found amongst adults (Frisancho, 2008), and recent investigations indicate adult radiation data does not always apply to them (Youssef & D'Avignon, 2023, 2025). Youssef & D'Avignon (2025) found a difference in f_p reaching 23% and 0.036 when comparing a 5-y.o. child manikin in the

standing posture to an adult. As the standing child's F with the floor was found to bear the greatest difference to the adult's F (up to 23%), an investigation into the underestimation of floor F for children in the seated posture appears warranted.

Across human view factor literature, the general method used to quantify differences in radiation data stemming from one's methodological approach relies on comparing results to established literature, mainly the experimental results of Fanger. Thus, a manikin or sample of participants resembling the average anthropometric characteristics of participants in the Fanger study are used, their f_p or F are determined and compared to Fanger's resulting f_p or F values. Comparison of f_p curve shapes (Calvino et al., 2009; Kubaha et al., 2004; Rykaczewski et al., 2022; Tanabe et al., 2000), relative and absolute differences (Kubaha et al., 2004; La Gennusa et al., 2005; Park & Tuller, 2011; Rykaczewski et al., 2022), as well as regression models (Tanabe et al., 2000) are the most common methods used. The significance of differences found across different populations can then be judge relative to differences due to the methodological approach employed (Park & Tuller, 2011).

This paper aims to make a thorough investigation of radiation data for seated occupants. First, the effect of long-held assumptions for this posture, particularly anterior-posterior symmetry and the disregard for the effect of seat shading, on F and f_p are investigated. Then, the particularity of child occupants is examined for the seated posture. Finally, a test case is used to evaluate the influence of these assumptions on view factors in a sample room under two scenarios, one employing radiant floor heating and one employing a chilled ceiling.

4.3 Methodology

The approach used in this study is inspired by the method outlined in Youssef & D'Avignon (2025), which was used to determine radiation data for occupants in the standing posture. Numerical models for two seated adults and one seated child were created using the UMTRI human body shape generator (University of Michigan Transportation Research Institute, 2020) and parameters listed in Table 4.1. Anthropometric characteristics of the male manikin,

"Youssef", represent the average of the 10 men in Fanger's 1970 study (Fanger, 1970), while the female manikin, "Nour", is based on the mean of the 10 women in said study. As the sitting-height-to-stature (SHS) ratio of the subjects was not specified in the original work, average SHS data for northern European young adult men and women (Fredriks et al., 2005) were used, as shown in Table 4.1. The child manikin, "Adam", was created based on the anthropometric characteristics of the 50th percentile 5 y.o. American boy from the CDC (Frisancho, 2008).

Table 4.1 Anthropometric data of numerical manikins

Manikin	Age [years]	Gender	Height [m]	BMI	SHS
Youssef	22	Male	1.78	22	0.51
Nour	22	Female	1.66	22	0.53
Adam	5	Male	1.125	16	0.53

The manikin postures produced by the UMTRI generator are typical of car seat occupants (i.e., inclined seatback, inclined seat cushion, raised arms, etc.) and were adjusted in Blender (2025) towards more typical postures associated with indoor seating: manikins were adjusted so that their knee angle was at 90 degrees from the thighs, their torso recline and neck angles were at zero degrees from the vertical axis, their arms as vertical as the manikin adjustment allowed, and their elbows close to a 90 degree angle from the arm. Although the exact posture of seated subjects was not detailed in Fanger's book (Fanger, 1970), Figures 42 to 47 suggest occupants rested their arms on their thighs, which was also the pose adopted by Tanabe et al. (2000). Additional adjustments were made to position the chest slightly forward and the neck slightly back to achieve the desired torso flex angle. Manikin poses used are shown in Figures 4.3, 4.4, and 4.5.

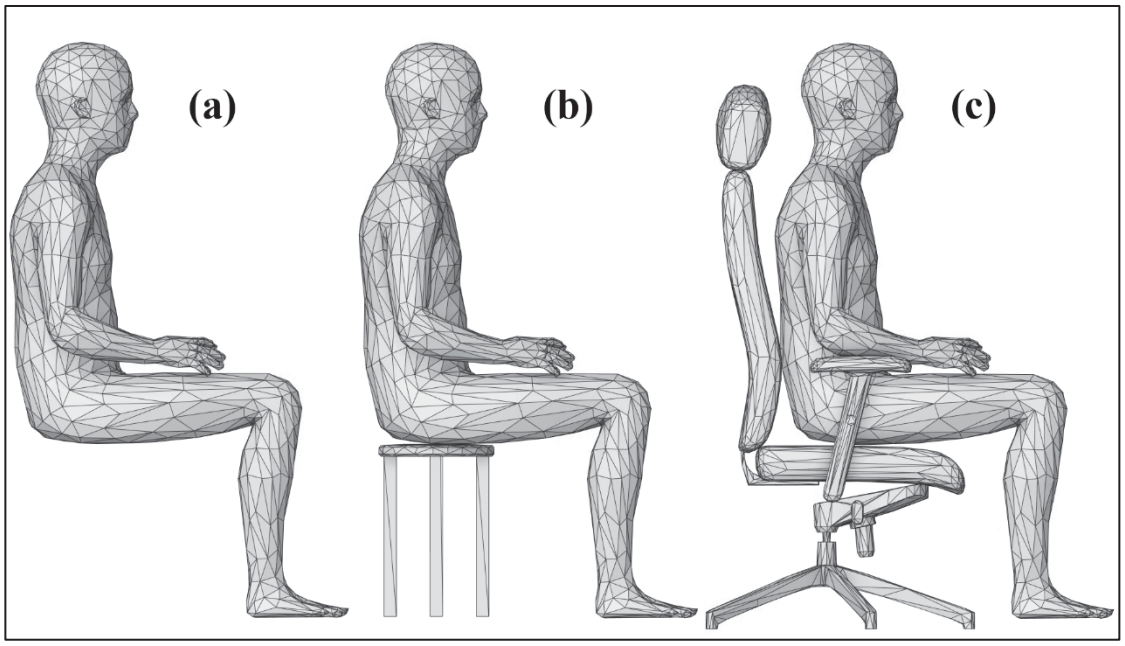

Figure 4.3 Youssef in the three seated configurations considered: (a) *float* (b) *stool* (c) *chair*

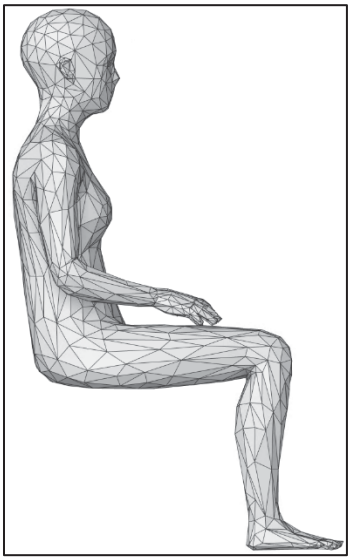

Figure 4.4 Nour in the *float* configuration

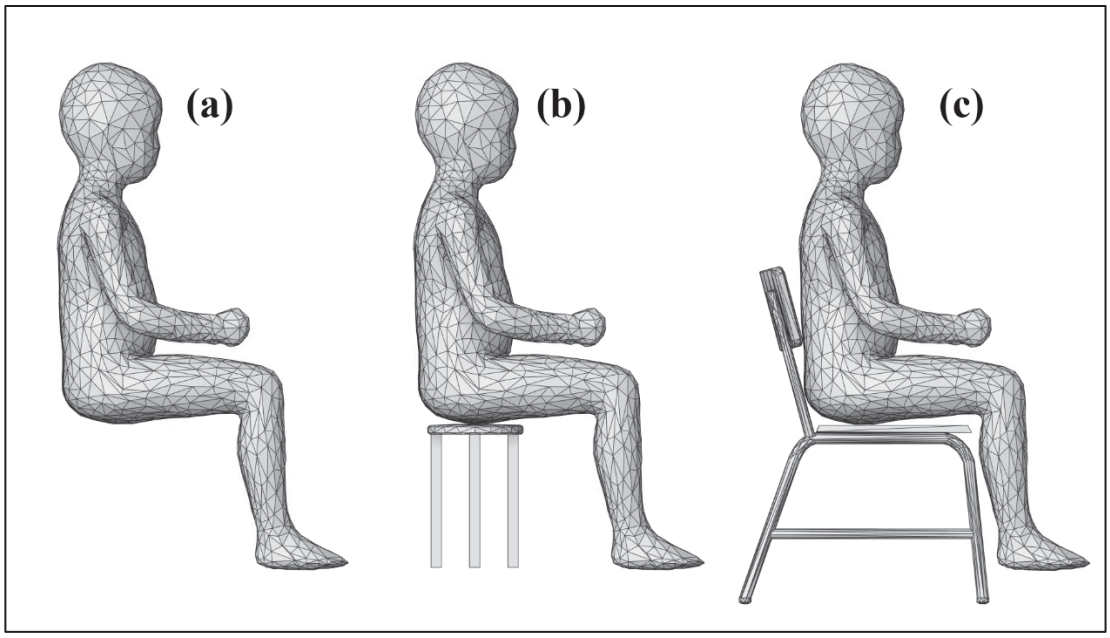

Figure 4.5 Adam in the three seated configurations considered: (a) *float* (b) *stool* (c) *chair*

The manikins were imported into Ansys Spaceclaim (ANSYS, 2010) and positioned at the center of a 7-meter radius sphere to remove any impact from the parallel ray assumption used in the ray-tracing method (Horikoshi et al., 1990; Youssef & D'Avignon, 2025), whose surface was divided into segments of 15-degree increments. Each manikin was aligned such that its center of mass coincided with the sphere's center, facing α and β of zero. Each section was identified by the spherical angle of its center with respect to the sphere center, with α representing the azimuth and β the altitude.

Manikins Youssef and Adam were modeled in three configurations: *float*, *stool*, and *chair*, as shown in Figures 4.3 and 4.5, while the Nour manikin was only modeled in the *float* configuration, shown in Figure 4.4. The *float* configuration had all three manikins "floating in the air", meaning no chair or supporting object was simulated beneath their thighs.

Seat selection was made to present the breadth of possible shading, from the most minimal amount represented by the *stool*, to the large and highly shading office *chair*. The stool (*stool*

configuration) had a height of 0.3817 m for the Youssef manikin and 0.246 m for the Adam manikin. It was retrieved from a free 3D model website (free3d.com user ksalk3d, 2019), adjusted to remove structural parts that did not pertain to the radiation calculations (truss, screws), sized and positioned so the bottom of the manikin's feet was level with the base of the stool legs, and the contact area between the manikin and stool seat was proportionally equal between the two manikins.

The Youssef manikin was analyzed seated on an office chair equipped with back and neck support (*chair* configuration), measuring 1.3 m from top to bottom (free3d.com user printable_models, 2019). The backrest, headrest, and seat dimensions were 2650 cm^2, 694 cm^2, and 2135 cm^2, respectively. The Adam manikin was evaluated seated on a school chair (*chair* configuration) from (cgtrader.com user Rafor, 2023), measuring 0.58 m from top to bottom, with backrest and seat dimensions of 401 cm^2 and 751 cm^2, respectively. For all cases, only one-half of the sphere was considered ($0 \leq \alpha \leq 180°$ and $-90 \leq \beta \leq 90°$), assuming L/R symmetry but not A/P symmetry. All manikins had their feet areas deselected from radiation calculations as they are assumed to be in contact with the floor.

The manikins were meshed in Ansys using the patch-independent tetrahedron method, resulting in a total element count ranging from 1.3 to 6.4 million, depending on the configuration. The meshed model was then imported into Ansys Fluent, where the surface-to-surface radiation model was applied. View factors (F_{m-ss}) between the manikin (m) and each selected surface (ss) were computed using the ray-tracing method, employing a resolution of 100 to minimize aliasing effects. The determined view factors were post processed to minimize the row sum error of the view factor matrix using the least square method (Larsen & Howell, 1986).

The computed view factor values (F_{m-ss}) were used to determine f_p for manikin m with respect to each considered sphere surface section ss at an angle (α, β) relative to the manikin's center of volume, following Equations (4.5) and (4.6). A correction factor (f_c) was applied to account

for the self-radiation effect of the human body, shown in Equation (4.5) where r_S refers to the sphere radius (7 m), and A_{ss} refers to the sphere section surface area in m^2.

$$F'_{m-ss} = f_c \cdot F_{m-ss} \tag{4.5}$$

$$f_p = \frac{\pi \times r_s^2 \times F'_{m-ss}}{A_{ss}} \tag{4.6}$$

A custom code was employed to calculate the view factor (F) between the occupant and any rectangular surface from the arrays of f_p determined, using Equation (4.3) and the summation law.

A theoretical test case from literature was considered to quantify the impact of f_p differences on $\overline{t_r}$. The view factors between an occupant and each surrounding surface was calculated and compared using the f_p data derived from the configurations described above: Youssef and Adam in the three configurations (*float*, *stool*, and *chair*), as well as the view factors derived from Fanger's data.

4.4 Results and Discussions

4.4.1 Verification of adult manikin results against literature

The f_p data of the adult manikins Youssef and Nour, in the *float* configuration, are compared to those of Fanger's nude male and female subjects in Figures 4.6 and 4.7, respectively. The f_p values can be found in Tables A B-1 and A B-2 in the Appendix B. The f_p curves display the same behavior as those found in the Fanger study (Figures 4.6 and 4.7, (a), (b) and (c)).

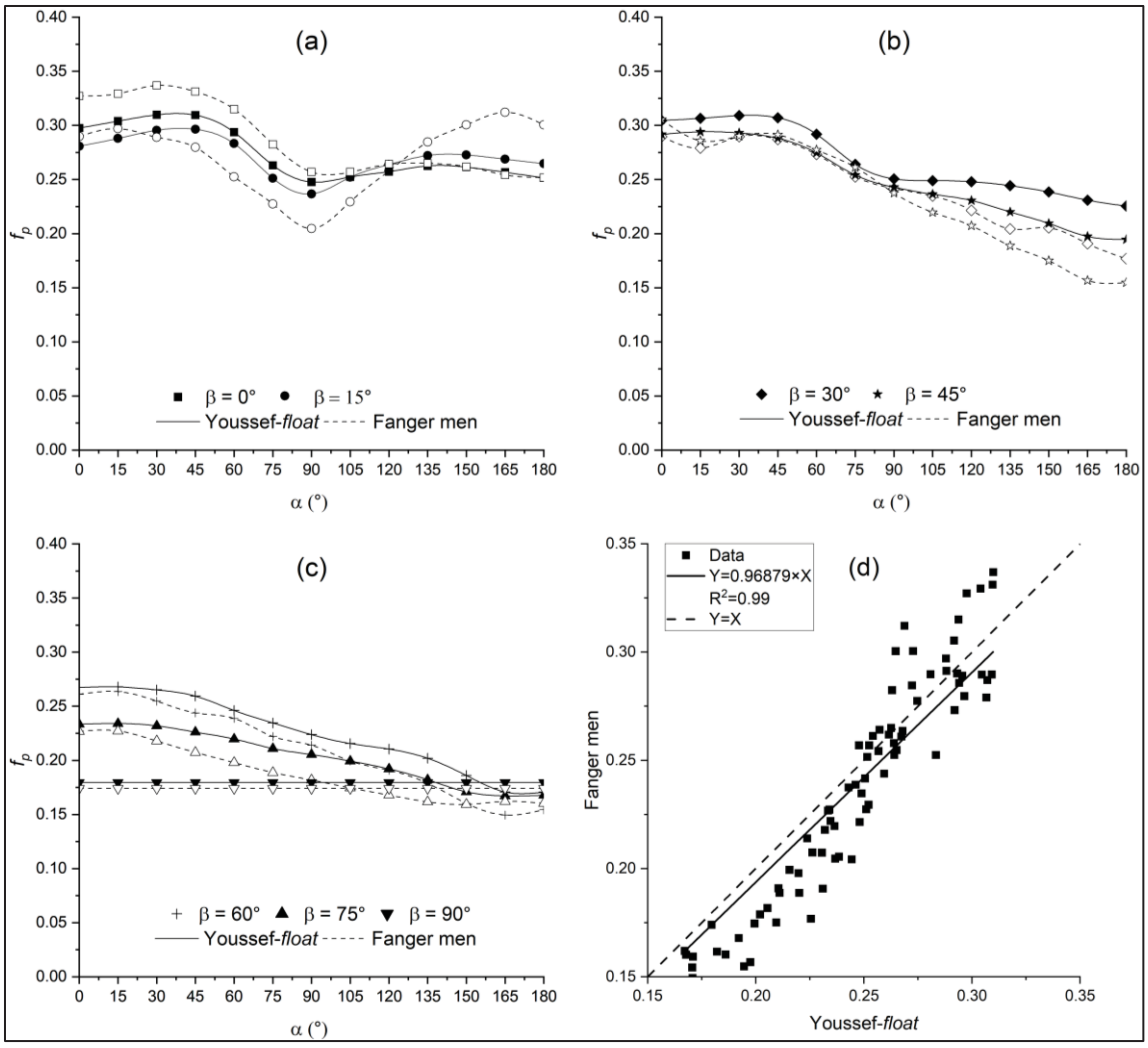

Figure 4.6 Comparison of f_p between Youssef-*float* and Fanger's nude male subjects: (a) altitude 0°, 15°; (b) altitude 30°, 45°; (c) altitude 60°, 75°, 90°; (d) correlation of f_p between Youssef-*float* and Fanger's men

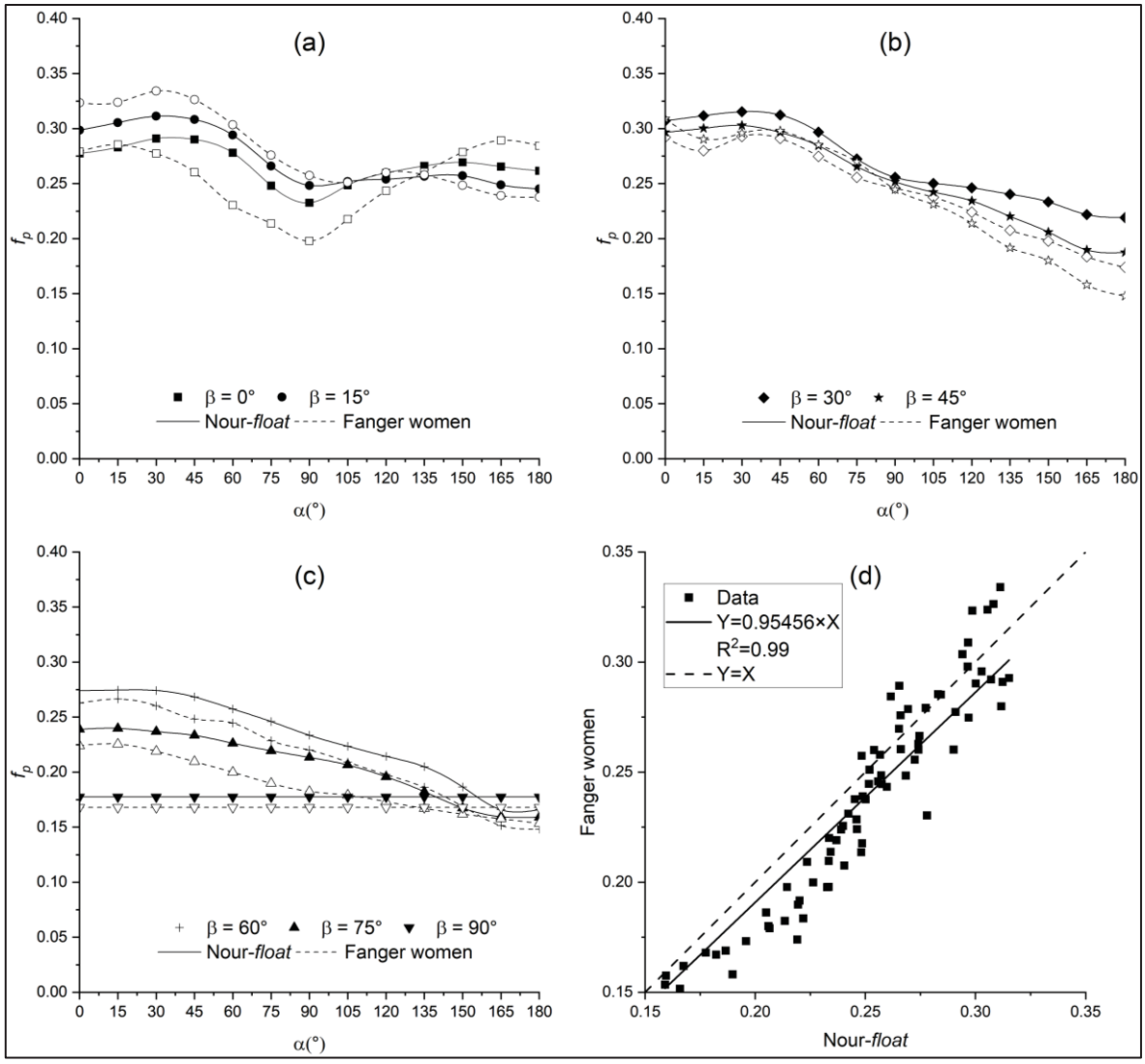

Figure 4.7 Comparison of f_p between Nour-*float* and Fanger's nude female subjects: (a) altitude 0°, 15°; (b) altitude 30°, 45°; (c) altitude 60°, 75°, 90°; (d) correlation of f_p between Nour-*float* and Fanger's women

For the Youssef manikin, the maximum difference found was -27.50% (Δf_p=-0.0486), with a mean of -5.11% (Δf_p= -0.0088). For the Nour manikin, the maximum difference found was -26.80% (Δf_p= -0.0476), with the mean being -6.35% (Δf_p= -0.0121). The difference is least prominent (<16% and Δf_p< -0.031) in the higher altitude angles (β = 60°, 75°, and 90°) where the curves display similar patterns. For shallow altitude angles (β = 0° and 15°), the relative difference is lower than 15% except for the Nour manikin at the middle azimuth angles (60°

$\leq \alpha \leq 90°$) where it is higher than 16%. The highest differences (>16%) were found for β = 30° and 45° and $\alpha \geq 135°$, where the manikins overestimate the values of f_p provided by Fanger. The reduction of the error at higher altitude angles can be attributed to the uniformity of the shape of the manikins and subjects at these angles, where individual differences in body shape and pose are less influential. The magnitude of both absolute and relative differences found is on par with that found in the literature which, as shown in Table 4.2, are as high as +52% ($\Delta f_p = 0.081$).

Table 4.2 Absolute and relative error between literature and Fanger's experimental results for f_p

Error / **Study**	**Minimum**		**Maximum**		**Mean**	
	Abs.	Rel.	Abs.	Rel.	Abs.	Rel.
Tanabe et al.	-	-21%	-	+20%	-	0%
La Gennusa et al.	-0.0401	-23%	0.081	+52%	-0.001	0%
Lo Curcio	-	N/S	0.08	45%	-	N/S
Present: Youssef-*float*	-0.0486	-27.5%	0.0434	+13.9	-0.0088	-5.1%
Present: Nour-*float*	-0.0476	-26.8%	0.0248	+8.2	-0.0121	-6.3%

A regression analysis of the significance of the difference with Fanger's data is conducted and presented in Figures 4.6d and 4.7d, as well as Table 4.3, where it is compared to the regression performed by Tanabe et al. (2000) for each β curve. Overall, the present data slightly overestimates Fanger's results, except at β=15° where Youssef-*float* and Nour-*float* slightly underestimates Fanger's. The Youssef manikin shows a better match with Fanger's men than the Nour manikin with Fanger's women, but the differences found are consistent with those found by Tanabe. Comparing our regression analysis to that of Tanabe, we find that our overall and individual regression coefficients are lower than Tanabe's (overall 1.002), but our

coefficients of determination are consistently higher (Tanabe's 0.397 to 0.93, versus our 0.99), indicating our differences from Fanger have smaller variations than the differences between Tanabe and Fanger.

Table 4.3 Correlation of f_p with Fanger's results

Study	***β*** / Metric	0°	15°	30°	45°	60°	75°	total
Youssef-*float*	Regression coefficient	1.000	1.049	0.911	0.956	0.940	0.922	0.969
	Coefficient of determination	0.99	0.99	0.99	0.99	0.99	0.99	0.99
Nour-*float*	Regression coefficient	0.957	1.029	0.91	0.96	0.937	0.910	0.955
	Coefficient of determination	0.99	0.99	0.99	0.99	0.99	0.99	0.99
Tanabe (2000)	Regression coefficient	0.99	1.04	0.944	0.979	1.016	1.042	1.002
	Coefficient of determination	0.397	0.739	0.846	0.93	0.964	0.796	0.891

Figure 4.8 presents f_p of the Youssef-*float* manikin compared to the numerical results of Tanabe et al. (2000). For all β curves, there is a good match between our results and those of Tanabe, and the regression coefficient found is better than that found with the Fanger data (0.973). Based on this comparison with literature, the proposed method is deemed valid to determine the radiation data of the various numerical manikins and configurations studied.

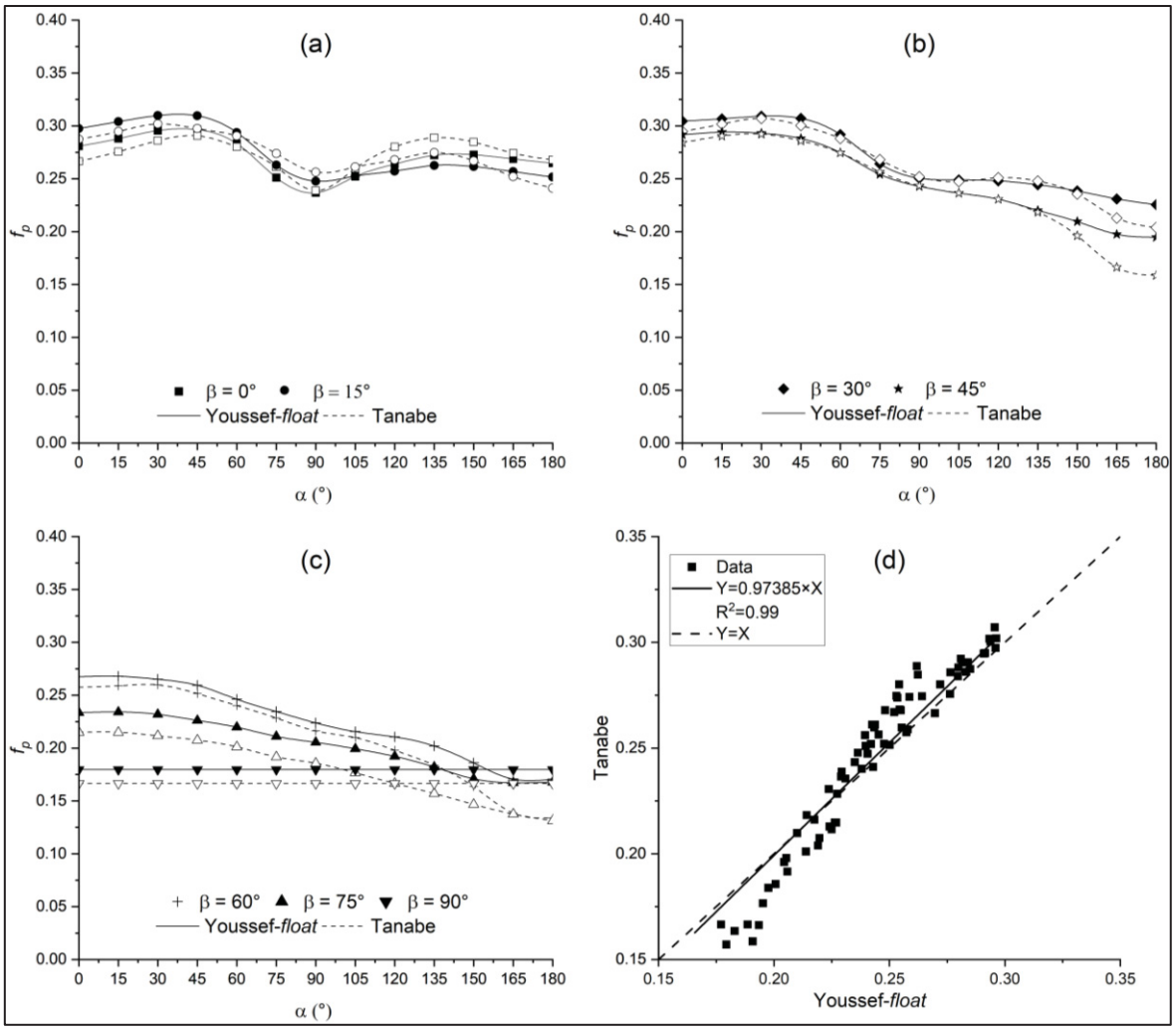

Figure 4.8 Comparison of f_p between Youssef-*float* and Tanabe et al. (2000): (a) altitude 0°, 15°; (b) altitude 30°, 45°; (c) altitude 60°, 75°, 90°; (d) correlation of f_p between Youssef-*float* and Tanabe

4.4.2 Anterior-posterior symmetry in the seated posture and effect of seating

Figure 4.9 shows the f_p curves for the Youssef manikin in the three considered configurations: *float*, *stool*, and *chair*. The tabulated data can be found in Tables A B-1, A B-4, and A B-6 of Appendix B. To analyze the anterior-posterior symmetry assumption, each subfigure shows the curve for both the positive and negative altitude as well as the vertical line of symmetry that applies under the A/P symmetry assumption. This assumption implies, for example in Figure 4.9a, that the β = -15° curve would be symmetrical with the β=15° curve with respect

to the vertical symmetry line (highlighted), as deduced from Equation (4.4) and Figure 4.2b (Tartarini et al., 2020).

Looking at the curves of the *float* configuration (dash line for positive β, solid line for the corresponding negative β), the symmetry is present though not perfect. In addition, as Figure 4.9f shows, the top-down (β = 90°) and down-top (β = -90°) f_p values are comparable when the manikin is floating. This mirrors the findings of past studies (Havgaard Vorre et al., 2015; Kubaha et al., 2004; Manabe et al., 2004; Tanabe et al., 2000) which simulated manikins in the floating configuration, did not consider negative β and assumed A/P symmetry, which found similar results to those of Fanger. This can lead us to conclude that if the manikin is floating, the A/P symmetry assumption is acceptable.

Analysing Figure 4.9 for the *stool* configuration, we find that the symmetry is no longer in place. Comparing the positive β curves of the *stool* configuration (short-dash line) with those of the *float* configuration (dash line), we can see that these configurations are almost identical for positive values of β (difference less than 4% and 0.006). On the other hand, comparing the negative β curves of the *stool* configuration (dash-dot-dot line) with those of the *float* configuration (solid line), we can see evident difference, where the *stool* configuration has visibly lower values of f_p, due to the blocking effect of the stool. The gap between the two lines is small for the lower values of β = -15° and -30° (1%-12%, 0.0024-0.0348) and becomes clearly larger as the altitude increases, reaching 28% and 0.0575 for β = -75°, and 26% and 0.0488 for β = -90°. As a result, the positive (short-dash line) and negative (dash-dot-dot line) β curves for the *stool* configuration do not display symmetry with respect to the vertical symmetry line, and the A/P assumption is not valid.

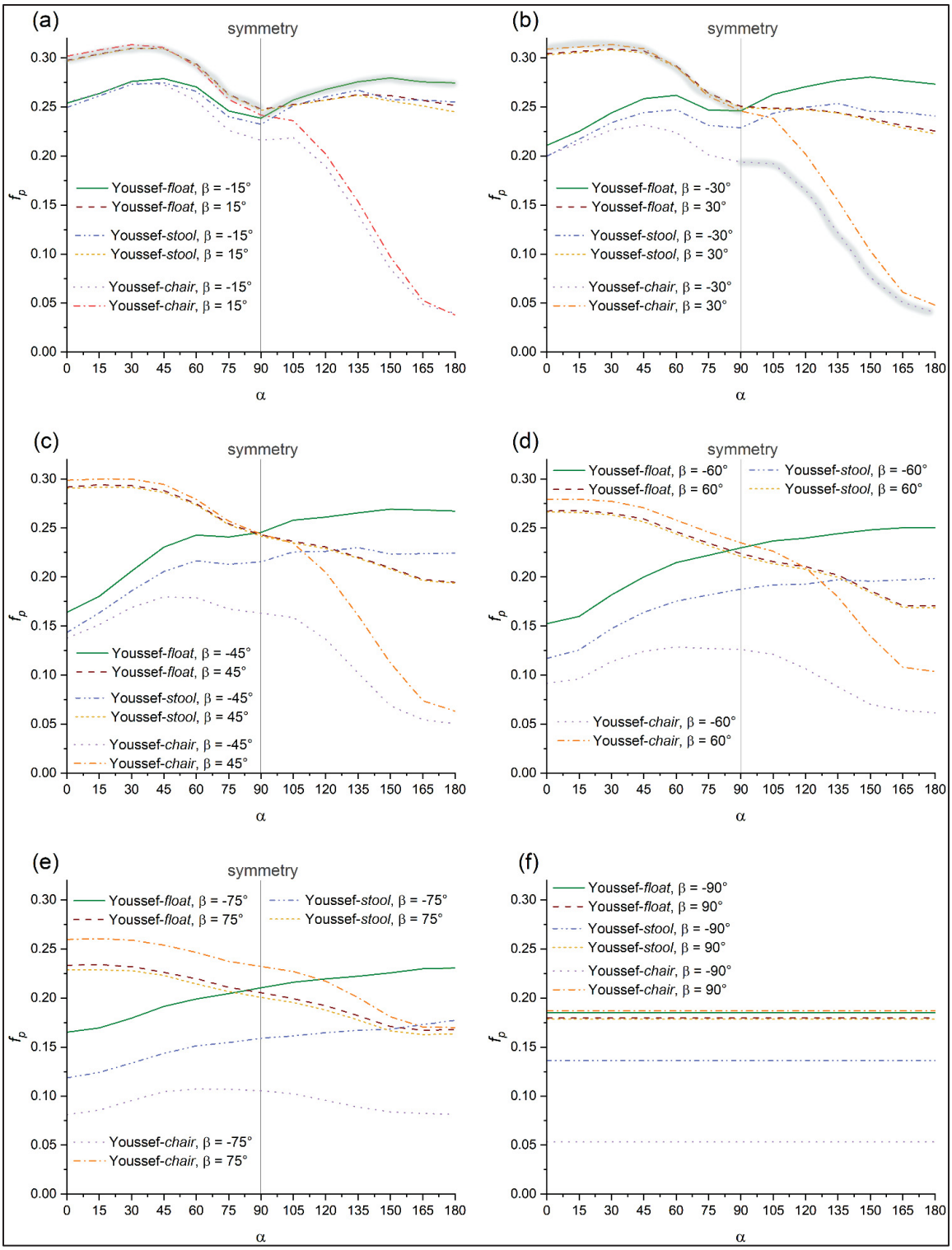

Figure 4.9 f_p comparison of the Youssef manikin in different configurations

The *chair* configuration displays even larger differences from both the *float* and *stool* configurations. Comparing the negative β curves of the *chair* configuration (dot line) with those of the *float* configuration (solid line), we can see a very large difference, where the *chair* configuration has visibly lower values of f_p, due to the blocking effect of the chair. The gap between the two lines is remarkable for both low and high values of β, reaching a maximum of 86% and 0.235. The largest difference is observed for azimuth angles α >90°, where the blocking effect of the chair back is most influential. Comparing the positive β curves of the *chair* configuration (dash-dot line) with those of the *float* configuration (dash line), it can be observed that for high azimuth ($\alpha \geq 45°$) and low altitude ($\beta \leq 60°$), the chair configuration has a lower f_p value than that of the float configuration due to the shading effect of the chair back and seat. For low azimuth ($\alpha \leq 30°$), the difference is marginal (<5%), except for $\beta = +75°$ where the chair configuration has a higher value than that of the float configuration (average of 10%). This difference can be explained by A_p being equal between the two configurations for that angle, and A_{eff} being much smaller for the *chair* configuration, making the f_p value of the *chair* configuration larger. Similarly, the A/P symmetry for the *chair* configuration is not valid, as shown in the blue highlight in Figure 4.9b.

Comparing the chair and stool configurations, the same observations can be made, alas to a smaller degree for higher negative altitudes ($\beta \leq -60°$) but comparably for high azimuth angles ($\alpha \geq 90°$) where the shading effect of chair back is noticeable, reaching a difference of 85% and 0.092 for $\alpha = 180°$. These relative and absolute differences between seat configurations are much larger than the methodological differences with the literature (27% and 0.048) and can thus be deemed significant.

4.4.3 Children manikin in different configurations, comparison with adult

The f_p curves of the Adam-*float* manikin are compared to those of the adult Youssef-*float* manikin in Figure 4.10. The tabulated data for the Adam manikin in the different configurations are presented in Tables A B-3, A B-5, and A B-7 of Appendix B. As can be seen in Figures 4.10a, 4.10b, and 4.10c, the curves display a similar shape and there are no

distinct patterns like those observed between the adult and child manikins in the standing posture (Youssef & D'Avignon, 2025). In addition, the regression analysis shown in Figure 4.10d shows that the difference between the two sets of data is insignificant. The largest difference observed is 12.63% and 0.022 for $\beta = -90°$, whereas for the positive values of β, the difference is lower than 8% and 0.018, much smaller than the methodological differences found with the literature (27% and 0.048). A comparison between the same adult and child manikins in the standing posture resulted in different curve shapes and a consistent difference that reached 22% and 0.036 (Youssef & D'Avignon, 2025). It is likely that the shape and size of the occupant in the seated posture has a smaller effect on their f_p than that observed in the standing posture due to the compact shape of the body in that posture. Though investigations into the seated posture in the literature are scant, comparing the observed population differences in that literature ($\Delta f_p \approx 0.017$), we can conclude differences between children and adults are insignificant in this posture.

Figure 4.11 shows the f_p curves of the Adam manikin in the three configurations: *float*, *stool*, and *chair*. Similar observations to those made for the Youssef manikin can be made here. The blocking effect of the chair for Adam-*chair* configuration is remarkable (up to 76% and 0.143) but less than that observed for the Youssef-*chair* configuration (86% and 0.235). This is because the school chair (shown in Figure 4.5c) is significantly smaller compared to the size of the child than the office chair (shown in Figure 4.4c) compared to the size of the adult. This results in the school chair having a smaller shading effect, particularly with respect to the back where the Youssef-*chair* manikin has the entire back and head shaded by the chair, whereas the Adam-*chair* manikin's back is only partially shaded.

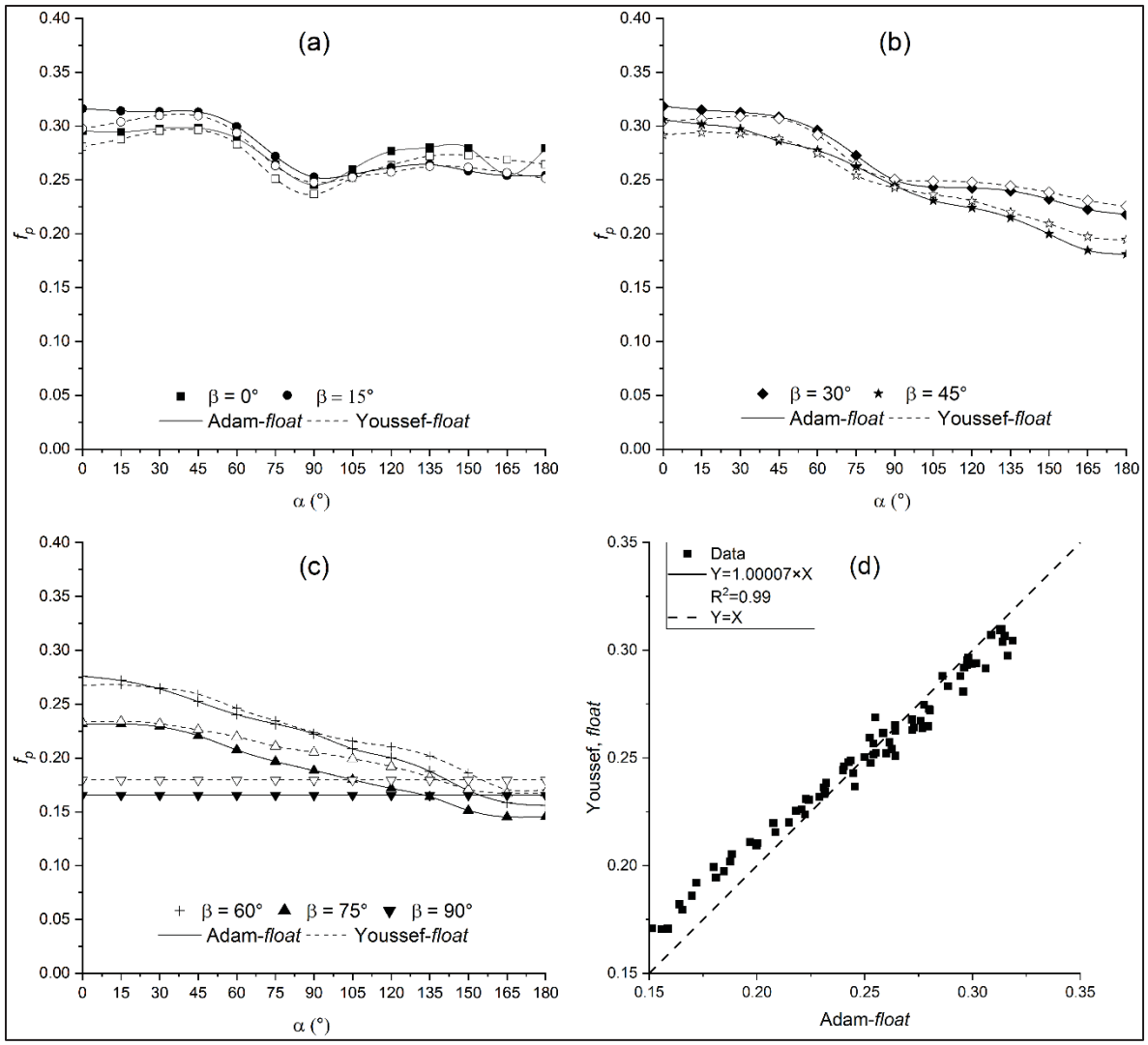

Figure 4.10 Comparison of f_p between Adam-*float* and Youssef-*float* (a) altitude 0°, 15°; (b) altitude 30°, 45°; (c) altitude 60°, 75°, 90°; (d) correlation of f_p between Adam-*float* and Youssef-*float*

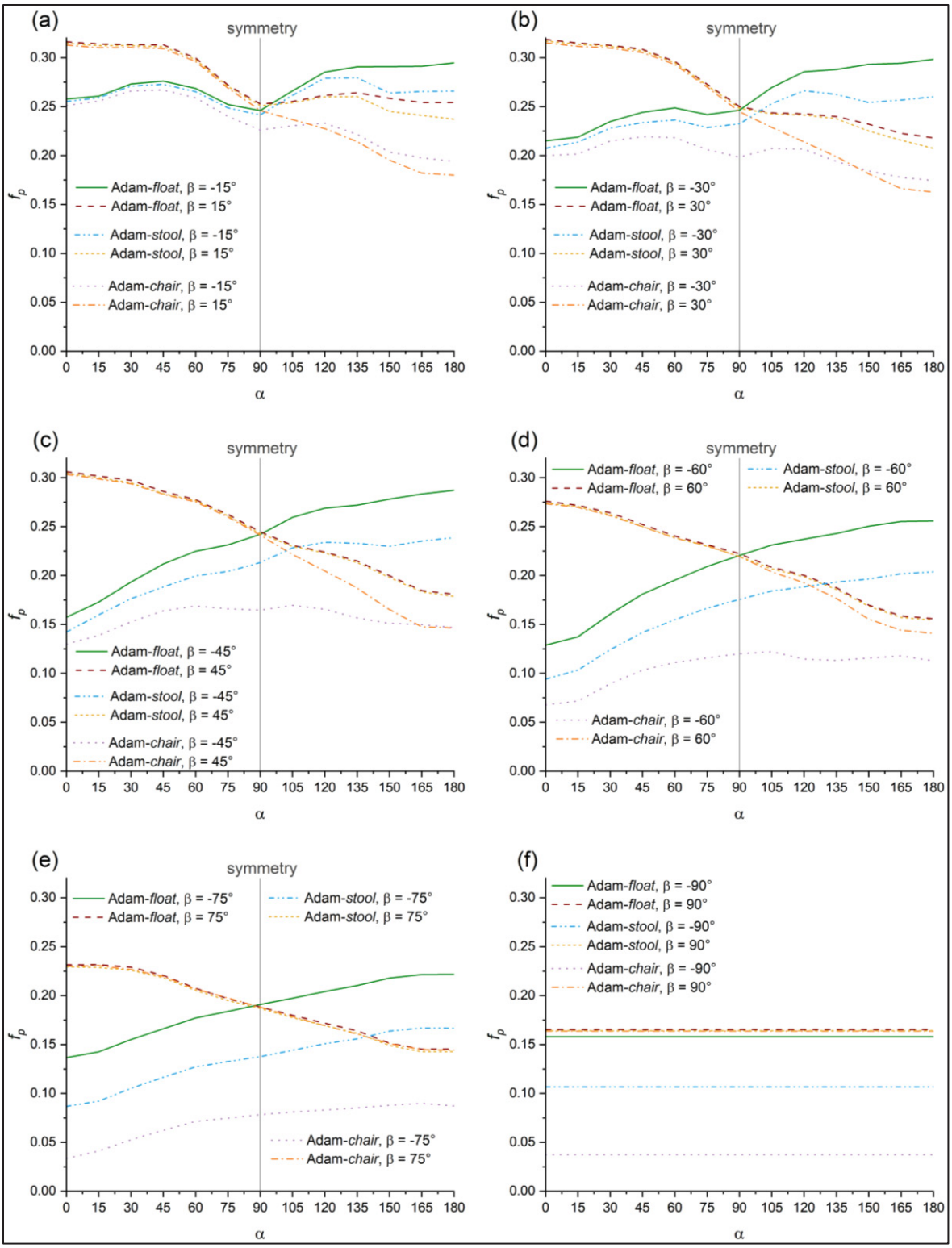

Figure 4.11 f_p comparison of the Adam manikin in different configurations

4.4.4 Test scenarios

Two theoretical test scenarios are presented to analyze the effect of the differences between adults and children, as well as the effect of seat configuration on the mean radiant temperature. In both scenarios, a room of dimensions 8×8×4 m, with the occupant seated in the middle, is considered. The adult occupant's center of mass is assumed to be at an altitude of 0.6 m from the floor, based on the recommendations made by ASHRAE (ASHRAE-55, 2017) and Fanger (Fanger, 1970) for the seated posture. The child's center of mass is assumed to be at an altitude of 0.24 m based on the abdomen altitude of seated standard 5-year-old (Youssef & D'Avignon, 2021). In the first scenario, a "hot floor" with radiant floor heating is used, while in the second, a "cool ceiling" with a chilled ceiling is implemented. The temperature of each surface presented in Table 4.4 was selected based on the classroom design example from ASHRAE Handbook (ASHRAE, 2017), used by Youssef & D'Avignon (2025).

Table 4.4 Temperature of surfaces in Celsius for the test scenarios considered

Surface	Front	Rear	Left	Right	Ceiling	Floor	Window
Scenario 1: Hot Floor	19.5	20.5	20.5	20.5	18.5	26	18
Scenario 2: Cool Ceiling	24.5	22	23	23	17	21	22

Figure 4.12 shows the view factors of the considered occupant with each surface. "Fanger diagrams" refers to the values determined using the view factor diagrams presented by Fanger (Fanger, 1970); "Fanger code" refers to the values calculated using Fanger's f_p arrays and the code developed based on Equation (4.3). The values for each manikin configuration were calculated using their corresponding f_p arrays presented previously (tabulated in Appendix B) and the code.

There is a good match between the “Fanger diagrams” and “Fanger code” values (within 2%) and between the Youssef-*float* and “Fanger code” (within 3%). Both Youssef and Adam manikins in the *stool* configuration have similar values to those in the *float* configuration for the walls and ceiling (within 3%) but show a difference of 9% for the floor. The Adam-*chair* manikin shows a significantly lower F for the rear wall (22%) and floor (25%) than the *float* configuration, while the Youssef-*chair* manikin shows an even larger difference for the rear wall (67%) and the floor (36%), due to the larger shading of the office chair. Comparing the adult and child manikins, the differences in F are present but less significant than the effect of seating. For the float configuration, Youssef has a lower F than Adam for the floor (by 10%), and a higher *F* for the ceiling (by 13%) and rear wall (8%). This is likely due to the larger altitude (0.6 m) of Youssef than Adam (0.24 m). For the stool configuration, the same variations are found (10% for the floor, 13% for the ceiling, and 10% for the rear wall). For the *chair* configuration, the difference between the two manikins is large, due to the larger shading of the office chair: Youssef’s F with the rear wall is half that of Adam’s, and his F with the floor is 30% lower.

Table 4.5 shows the mean radiant temperature calculated for each configuration using Equation (4.1). For both scenarios, the Fanger diagram and code produce the same temperature as both the Youssef-*float* and Adam-*float* manikin. This leads us to conclude that whereas differences of up to 1 °C were reported in similar circumstances in the standing posture between adults and children (Youssef & D’Avignon, 2025), the differences in the seated posture are negligible. Remarkable differences are found between seat configurations. For Youssef, introducing the stool decreases $\overline{t_r}$ by 0.4 °C in the hot floor scenario and 0.2 °C in the cold ceiling scenario, while introducing the chair decreases it by 2.0 °C and 1.3 °C, respectively. This is due to the chair shading the body from the radiant effect of both the floor and rear wall. For Adam, introducing the stool decreases $\overline{t_r}$ by 0.3 °C in the hot floor scenario and 0.2 °C in the cold ceiling scenario, while the chair decreases it by 1.2 °C and 0.8 °C, respectively.

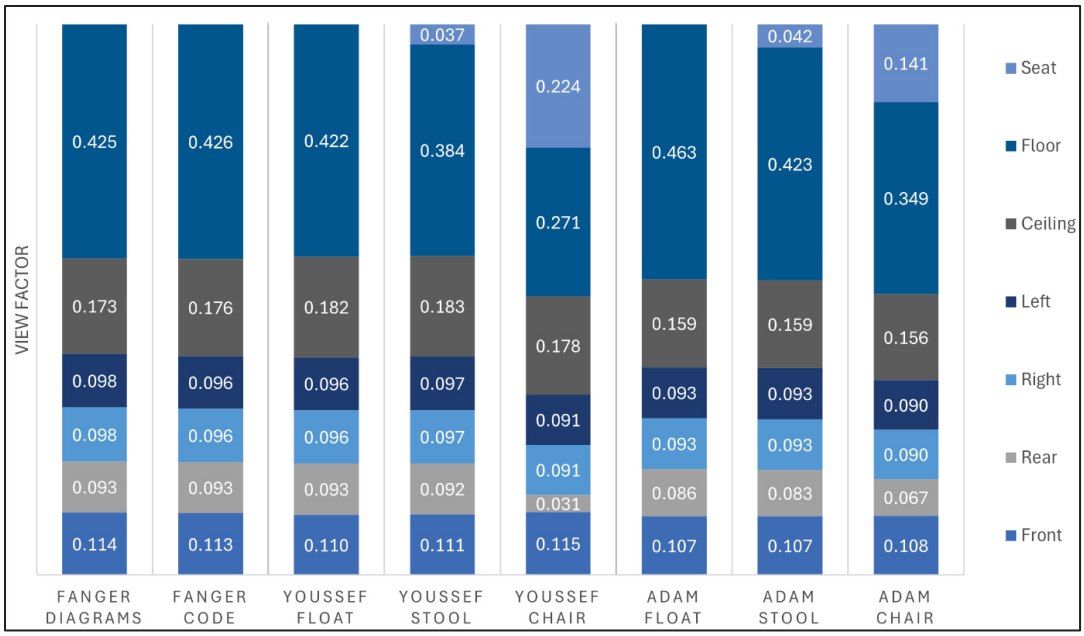

Figure 4.12 View factors calculated for each method and configuration

The effect of a 2 °C difference on occupants' thermal comfort, expressed through the Predicted Mean Vote (PMV), varies according to both environmental conditions and individual characteristics. Several studies have challenged the use of the PMV equation for the prediction of children's thermal comfort as the applicability of several of its terms is limited to adults (Gao et al., 2024; Youssef & D'Avignon, 2021). But the effect of a difference in $\bar{t}_r$ can be propagated to PMV, based on Fanger (1970)'s PMV sensitivity tables; a 0.5–2 °C shift in $\bar{t}_r$ corresponds to a PMV change of approximately ±0.06 to ±0.24. Alfano et al. (2013), who also analyzed the sensitivity of the PMV equation to $\bar{t}_r$ found that a variation of ±0.2 ºC resulted in a difference of ±0.16 to ±0.25 in the PMV. These PMV differences (up to 0.2) can result in uncertainty in attribution to a thermal comfort category (ISO, 1994), and can cause failure in predicting real thermal comfort conditions.

Table 4.5 Mean radiant temperature calculated for each method and configuration

Source	**Fanger**		**Youssef**			**Adam**		
	Diagrams	**Code**	***float***	***stool***	***chair***	***float***	***stool***	***chair***
	Hot Floor							
$\bar{t_r}$ **(°C)**	23.0	23.1	23.0	22.7	21.1	23.0	22.6	21.8
	Cold Ceiling							
	21.5	21.5	21.5	21.3	20.2	21.5	21.3	20.8

4.5 Conclusions

The study explored the calculation of f_p for an adult and child manikin in the seated posture. The anterior-posterior symmetry commonly assumed in seated literature was investigated and found to be valid only if the occupants are assumed to be floating in the air. The presence of a seat, even one as nonintrusive as a stool, makes that assumption invalid, and requires the use of negative β values for all realistic scenarios in a seated posture. These findings indicate current view factors F used in the design and evaluation of indoor and outdoor spaces should be revised for the seated posture and dispense of that assumption.

We found seat shading had significant effect on f_p regardless of the seat type considered. The presence of the stool, the most minimalist seat deemed realistic, was found to decrease f_p by up to 28% ($\Delta f_p = 0.0575$) for the adult manikin and by up to 36% ($\Delta f_p = 0.055$) for the child manikin. The presence of an office chair decreased f_p by up to 86% ($\Delta f_p = 0.235$) for the adult manikin due to its large obstruction of radiation, while a school chair decreased the child's f_p by up to 76% ($\Delta f_p = 0.143$). The significant differences between chair configurations indicate that chair type may have to be considered in the most severe cases. Generally, it is our recommendation that a minimum chair blocking effect be systematically considered, through the use of appropriate f_p values, when designing radiant systems for spaces where prolonged seating occurs, such as offices and schools.

Differences between the adult and child manikins in the seated posture were found to be minimal (<12% and <0.022), paling in comparison to differences found between the same standing adult and child manikins (up to 22% and 0.036) (Youssef & D'Avignon, 2025).
Two test scenarios were used to investigate the effect of occupant age and chair type on mean radiant temperature. It was found that age effects mean radiant temperature only marginally (less than 0.04 °C), while the presence of a stool, an example of minimalist seating, impacted $\bar{t}_r$ by 0.37 °C for the adult and 0.3 °C for the child. A standard executive office chair resulted in a decrease of 2.0 °C for the adult, while a school chair decreased $\bar{t}_r$ by 1.2 °C for the child. It appears using f_p values in current standards for the calculation of $\bar{t}_r$ may result in a gross overestimation of the effect of radiant surfaces for seated occupants which could impact their thermal comfort in spaces with large radiant surfaces.

This paper clearly establishes the significant effect of the assumptions studied (i.e. no seat shading and A/P symmetry) on radiant heat transfer between the body and its environment. In both theoretical test cases considered, correcting these undue assumptions significantly reduced the mean radiant temperature experienced by the occupant from surrounding building surfaces. To confirm their net effect on the occupant's heat balance and thermal comfort, several other important aspects should also be considered such as the relative importance of local discomfort on the back and thighs, clothing insulation increase brought about by the chair presence and type, as well as potential reradiation by the chair to the occupant. Further research is needed to establish the full effect of correcting these radiation assumptions in the seated posture.

CONCLUSION AND CONTRIBUTIONS

The thesis addressed the objectives and sub-objectives laid out in the introduction in the following manner:

Development of a rigorous method for the determination of radiation data

The development of the method (objective 1) was laid out in the two journal papers presented in Chapters 3 and 4. Chapter 3 focused only on the standing posture and addressed the first two methodology issues presented: a. the calculation method and b. the effect of pose. We found that using the ray tracing method, that employs the parallel ray assumption, for the determination of radiation data is adequate and provides almost identical results to the hemicube method, which employs the solid angle assumption, provided a high resolution and a high distance is used. The paper's conclusions were then carried into the following paper where solely ray tracing was used due to its high computational speed. Additionally, the effect of pose was investigated in Chapter 3, where we found that pose will affect the match with established literature significantly. Similarly, in the subsequent Chapter 4, the pose was adjusted to match that assumed by the subjects in compared literature to minimize its effect on the results.

Chapter 4 focused on the seated posture and addressed the two remaining methodological issues presented: c. the Anterior/Posterior (A/P) symmetry assumption and d. the effect of seat shading. We found that the A/P symmetry assumption is only applicable when the seated occupants are "floating" in the air without any seat beneath them, which is an unrealistic situation. The inevitable presence of a seat will impact the projected area factors and render the A/P symmetry assumption void. This finding indicates that the use of only positive values of β is inadequate for this posture and will result in a false assessment of radiation exchange. The effect of seat shading (d.) was investigated by considering a large breadth of seats: a minimally shading stool and a highly shading office chair. We found that the type of seating used will vary the impact of shading, particularly affecting the view factors with the floor and rear walls. The stool was found to lower f_p by up to 28% for the child and 36% for the adult, a

school chair by 76% and an office chair by 86%. In the two test case scenarios investigated, we found that this lowered the perceived mean radiant temperature by 0.3 °C in the case of the stool, 1.2 °C in the case of the school chair, and 2 °C in the case of an office chair. This difference implies that the PMV of the seated child occupant in a classroom would be different than that of a seated adult in an office, partially due to the difference in shading of the office chair than that of a school chair.

Assessment of radiation data differences between adults and children

The particularity of thermal comfort assessment of children (objective 2) was addressed in the first chapter. Several lacunae were identified and suggestions on measurement elevations based on age were presented. In the third chapter, the mean radiant temperature was calculated for a standing adult and child occupant based on the elevations suggested in Figure 2.1, which was found to affect the calculated temperature by up to 0.4 °C. Thus, it is recommended that the appropriate elevations are used for the assessment of radiant effects on child occupants both in calculations and measurements, especially in spaces with radiating surfaces.

The difference between adult and child radiation data in the standing posture was addressed in Chapter 3 where it was found to be significant: the f_p curves for the two manikins had distinct shapes, f_p was different by up to 22%, and in the test case the mean radiant temperature perceived by the child was found to be up to 1 °C higher than that perceived by the adult. It is recommended to use child-specific radiation data in thermal comfort assessment of spaces occupied by children where they are likely to be standing.

The difference between adult and child radiation data in the seated posture was addressed in Chapter 4 where it was found to be insignificant: the f_p curves for the two manikins had a similar shape, f_p differences were lower than 12%, and both the calculated view factors and mean radiant temperature were found to match closely for the adult and child. It is then sufficient to use adult radiation data in the assessment of spaces where child occupants are likely to be seated, albeit after addressing the issues with the adult seated data discussed earlier.

Provision of radiation data

The radiation data procured from the second and third article (Chapters 3 and 4, respectively) are presented in Appendix A (standing posture) and B (seated posture) of the thesis. This data includes the projected area factors representative of a 5-year-old child in the standing and seated posture, on a stool and a school chair, as well as data representative of an adult male in the standing and seated posture, on a stool and an office chair (objective 3). The data provided can be used for both the calculation of the mean radiant temperature in the indoor environment, as well as human solar heat gains both in the indoor and outdoor environment. Additionally, this data lends itself for use in cabin thermal comfort assessments such as automobiles, trains, and airplane cabins, where thermal radiation is important.

Contributions and originality

This research addresses an important gap in thermal comfort literature and standards: child occupants. The measurement heights recommended in Chapter 1 can be used in thermal comfort assessments to reflect children's thermal environment accurately. The radiation data provided in the appendices can be used in standards for the accurate calculation of children's radiant thermal exchange with their environment, which can have consequences on the design of classrooms, particularly those where radiant effects are important (spaces with radiant floors or chilled ceilings, spaces with large windows, etc.). Presently there are no studies that provide such data, and current standards use data that is only applicable to adults.

In addition, this research provides radiation data of adults in the seated posture that consider the shading effects of their seats, with two types of seats considered (stool, chair). One of the main contributions of the study of the seated posture in Chapter 4 is the debunking of the Anterior/Posterior symmetry assumption, which has been widely held in human view factor literature. This can have important ramifications on the design of radiant systems in office spaces where occupants will likely receive less radiation than designed or predicted. The radiation data provided in this thesis (those of children in both postures, as well as those of adults in the seated posture where seat shading is accounted for) can be used in thermal comfort

assessment tools such as the CBE 3D mean radiant temperature tool (Arens et al., 2015), or their thermal comfort tool for ASHRAE-55 (Tartarini et al., 2020) (that currently does not calculate the mean radiant temperature). The projected area factor tables can also be used to determine solar heat gain (ASHRAE-55, 2017) in both the indoor and outdoor environment.

Limitations and future work

Although the radiation data provided in this thesis is limited to 12 manikin configurations, the method developed is generalizable and can be used for the determination of radiation data of occupants of any age, gender, shape, pose, or posture. In this thesis, a manikin representing a 5-year-old boy was retained to assess whether radiation effects on children's bodies could be reasonably assessed from adult radiation data. The choice of the gender and age of the child manikin retained for this purpose does not allow us to generalize the results to all children but suffices to warrant further studies to establish until what age the differences found remain significant. The two types of seating studied (stool and chair) were selected as two extremes of the range likely to be found in the settings of interest, an office and classroom. Literature or experimental documentation could help to confirm the validity of the specific seat shape and size modelled and minor adjustments made, such as the seat elevation from the ground and whether the child's feet should be supported or left hanging. Additionally, radiation data could be determined for other pertinent cases such as for children in the supine posture, adults and children in different seating and sleeping configurations (regular beds, hospital beds, a variety of seating options).

As stated in the literature review, the black globe thermometers currently in use are designed based on adult data and have not been verified for children. This verification has been so far impossible as it is contingent on having child specific radiation data. The data provided in this thesis can be used to calculate and verify the measurements in studies aiming to design BGTs suitable for the child population.

The current study investigated the effect of seat shading on the radiant heat exchange in the indoor environment. Though a significant reduction in the radiant heat exchange between the

occupant and floor is found, the present work does not allow us to make a final conclusion on the net effect this would have on the occupant's overall heat balance. A holistic study should be conducted that considers the total effect of the seat on the occupant's thermal comfort by including the conductive and convective heat exchanges.

The first chapter of the thesis highlights several areas in which children's thermal comfort differs from that of adults and proposes suggestions for improvement. While this work specifically focuses on radiant heat exchange, other components of children's thermal balance remain insufficiently explored. Differences in heat loss through sweating, convective heat transfer coefficients, and metabolic heat generation are all likely to influence both children's thermal comfort and the design of HVAC systems in classrooms. The development of a novel thermal comfort evaluation protocol, specifically adapted to children, is a logical next step in improving the comfort and health of this occupant group.

Finally, the full implications of the radiation data generated as part of this thesis on HVAC system design practices remains to be determined. The implications of using child-specific radiation data for HVAC system design in classrooms, particularly in the case of radiant heating and cooling systems, warrant investigation. Similarly, the impact of seat shading on radiant heat exchange warrants a review of radiant system design practices for both classroom and office spaces. The insights provided by this thesis could be useful in a review of HVAC design practices for all spaces with important radiant effects whether it be those equipped with radiant floors or chilled ceilings, or even large windows.

APPENDIX A
PROJECTED AREA FACTORS OF STANDING OCCUPANTS – CHAPTER 3

Table A A-1 - f_p values of the adult manikin with its arms lowered, calculated using the parallel ray method

A-M-PR Lowered arms								
f_p		β(°)						
		0	**15**	**30**	**45**	**60**	**75**	**90**
α(°)	**0**	0.344698	0.332821	0.306086	0.261548	0.203074	0.135078	0.083
	15	0.339881	0.328554	0.301205	0.257989	0.200290	0.133423	0.083
	30	0.329551	0.319078	0.292184	0.249962	0.192149	0.127631	0.083
	45	0.306803	0.295915	0.270559	0.230880	0.176512	0.117909	0.083
	60	0.276669	0.265548	0.241705	0.206043	0.158518	0.109014	0.083
	75	0.240058	0.230304	0.211183	0.184007	0.147914	0.105497	0.083
	90	0.210619	0.207861	0.197034	0.177495	0.145451	0.105290	0.083
	105	0.236579	0.229861	0.212975	0.187642	0.152734	0.110255	0.083
	120	0.274153	0.262721	0.239852	0.207708	0.166872	0.118943	0.083
	135	0.308730	0.296192	0.269941	0.232243	0.185080	0.127631	0.083
	150	0.332923	0.320020	0.292061	0.250644	0.196541	0.135078	0.083
	165	0.343789	0.332932	0.305036	0.261320	0.203396	0.139008	0.083
	180	0.346518	0.335426	0.308434	0.264652	0.206180	0.141077	0.083

Table A A-2 - f_p values of the adult manikin with its arms lowered, calculated using the solid angle method

A-M-SA Lowered arms								
f_p		β(°)						
		0	**15**	**30**	**45**	**60**	**75**	**90**
α(°)	**0**	0.344944	0.333206	0.306171	0.262013	0.20327	0.135072	0.082875
	15	0.340388	0.329155	0.302087	0.258222	0.200266	0.133622	0.082875
	30	0.330257	0.319498	0.292682	0.250259	0.192436	0.127614	0.082875
	45	0.307153	0.295912	0.270591	0.230996	0.17656	0.117877	0.082875
	60	0.277242	0.265888	0.242128	0.206274	0.158862	0.109591	0.082875
	75	0.240201	0.231036	0.211993	0.184736	0.148564	0.105447	0.082875
	90	0.210772	0.208115	0.197328	0.178139	0.145882	0.105447	0.082875
	105	0.236556	0.230203	0.213231	0.187997	0.153069	0.110005	0.082875
	120	0.274133	0.262947	0.239838	0.207487	0.166692	0.118913	0.082875
	135	0.309137	0.296245	0.27022	0.232589	0.185356	0.127821	0.082875
	150	0.333312	0.320331	0.29231	0.25041	0.196941	0.134865	0.082875
	165	0.344194	0.333317	0.306295	0.261938	0.204128	0.139008	0.082875
	180	0.346606	0.335815	0.308522	0.264213	0.206381	0.14108	0.082875

Table A A-3 - f_p values of the adult manikin with its arms raised, calculated using the parallel ray method

A-M Raised arms								
f_p		β(°)						
		0	**15**	**30**	**45**	**60**	**75**	**90**
α(°)	**0**	0.332656	0.322964	0.298003	0.258241	0.202075	0.140695	0.095577
	15	0.330764	0.320953	0.295583	0.254841	0.202279	0.139905	0.095577
	30	0.326469	0.316506	0.291333	0.251369	0.197777	0.137336	0.095577
	45	0.315732	0.305972	0.280709	0.239867	0.186727	0.13042	0.095577
	60	0.286434	0.277386	0.254031	0.216575	0.168106	0.120737	0.095577
	75	0.232798	0.223179	0.205161	0.179973	0.147131	0.111449	0.095577
	90	0.200995	0.198829	0.191114	0.174041	0.143038	0.1073	0.095577
	105	0.236326	0.229743	0.21248	0.186845	0.153167	0.11303	0.095577
	120	0.286996	0.274422	0.250077	0.214043	0.169743	0.123701	0.095577
	135	0.318135	0.304542	0.277463	0.237335	0.188057	0.133186	0.095577
	150	0.327134	0.315288	0.288559	0.247679	0.196243	0.139905	0.095577
	165	0.331429	0.319735	0.292455	0.252671	0.19921	0.141881	0.095577
	180	0.333372	0.322064	0.295229	0.252381	0.199107	0.143066	0.095577

Table A A-4 - f_p values of the 5-year-old boy manikin with its arms lowered, calculated using the parallel ray method

5-B								
f_p		β(°)						
		0	**15**	**30**	**45**	**60**	**75**	**90**
α(°)	**0**	0.332791	0.331131	0.310697	0.242624	0.174043	0.131704	0.100
	15	0.327846	0.327737	0.303811	0.239811	0.178319	0.131288	0.100
	30	0.325159	0.321450	0.300833	0.246730	0.198310	0.136066	0.100
	45	0.330856	0.323508	0.298165	0.251292	0.200021	0.130665	0.100
	60	0.303983	0.292460	0.276575	0.237073	0.194034	0.127549	0.100
	75	0.252925	0.246276	0.231224	0.202098	0.171584	0.113839	0.100
	90	0.218636	0.222349	0.215900	0.198448	0.166025	0.114877	0.100
	105	0.244165	0.237095	0.232713	0.204835	0.165490	0.114046	0.100
	120	0.288290	0.272484	0.258521	0.215024	0.189437	0.125887	0.100
	135	0.314947	0.311656	0.278560	0.253421	0.201624	0.139390	0.100
	150	0.328760	0.333079	0.313613	0.255245	0.201197	0.145207	0.100
	165	0.354880	0.334247	0.305734	0.268247	0.202693	0.142714	0.100
	180	0.366328	0.317721	0.310449	0.262393	0.201303	0.141467	0.100

APPENDIX B
PROJECTED AREA FACTORS OF SEATED OCCUPANTS – CHAPTER 4

Table A B-1 - f_p for the Youssef-*float* manikin

Youssef-*float*														
f_p		**β**												
		-90	**-75**	**-60**	**-45**	**-30**	**-15**	**0**	**15**	**30**	**45**	**60**	**75**	**90**
α	**0**	0.185062	0.165161	0.152321	0.164005	0.210764	0.253917	0.280799	0.297537	0.304518	0.291675	0.267318	0.233415	0.179567
	15	0.185062	0.169440	0.159855	0.180218	0.225080	0.263776	0.287941	0.303956	0.306627	0.294024	0.267872	0.234057	0.179567
	30	0.185062	0.179496	0.181791	0.206065	0.243933	0.275985	0.295526	0.309803	0.309120	0.293084	0.265102	0.231918	0.179567
	45	0.185062	0.191478	0.199960	0.230503	0.258504	0.278908	0.296412	0.309516	0.307075	0.288150	0.259342	0.226141	0.179567
	60	0.185062	0.198967	0.214694	0.242722	0.261955	0.270482	0.283291	0.293753	0.291928	0.274678	0.246158	0.219722	0.179567
	75	0.185062	0.204530	0.222117	0.240763	0.246873	0.245950	0.251069	0.263031	0.264064	0.254157	0.234525	0.210949	0.179567
	90	0.185062	0.210521	0.229761	0.245463	0.246170	0.238613	0.236675	0.247726	0.250515	0.242878	0.223779	0.205386	0.179567
	105	0.185062	0.216084	0.236741	0.257995	0.262850	0.257241	0.252121	0.252427	0.248918	0.236377	0.215581	0.199395	0.179567
	120	0.185062	0.219508	0.239732	0.261050	0.270583	0.267903	0.263858	0.257241	0.248023	0.230581	0.210485	0.192120	0.179567
	135	0.185062	0.222289	0.244275	0.265357	0.277101	0.275583	0.272218	0.262572	0.244316	0.220086	0.201954	0.182064	0.179567
	150	0.185062	0.225713	0.248041	0.269274	0.280552	0.279710	0.272716	0.261540	0.238437	0.209433	0.186001	0.170938	0.179567
	165	0.185062	0.229778	0.250257	0.268334	0.276718	0.275526	0.268730	0.256726	0.230959	0.197450	0.170712	0.167086	0.179567
	180	0.185062	0.230634	0.250257	0.267237	0.273331	0.274666	0.264689	0.251567	0.225463	0.194552	0.170601	0.167728	0.179567

Table A B-2 - f_p for the Nour-*float* manikin

Nour-*float*														
f_p		**β**												
		-90	**-75**	**-60**	**-45**	**-30**	**-15**	**0**	**15**	**30**	**45**	**60**	**75**	**90**
α	**0**	0.182886	0.165933	0.147213	0.156065	0.198187	0.243538	0.277426	0.298561	0.307088	0.296689	0.274033	0.238982	0.177510
	15	0.182886	0.170660	0.158560	0.176435	0.216861	0.253322	0.282985	0.305468	0.311709	0.300150	0.274589	0.239842	0.177510
	30	0.182886	0.179683	0.182923	0.201760	0.235279	0.267251	0.290935	0.311281	0.315302	0.302824	0.274144	0.236834	0.177510
	45	0.182886	0.191071	0.203169	0.225748	0.249910	0.269956	0.290101	0.308173	0.312350	0.296453	0.268359	0.233396	0.177510
	60	0.182886	0.199020	0.217520	0.240612	0.255172	0.263337	0.277981	0.294072	0.296885	0.284341	0.257457	0.226306	0.177510
	75	0.182886	0.206755	0.227198	0.242815	0.246380	0.242847	0.248128	0.265984	0.272435	0.265308	0.245999	0.219431	0.177510
	90	0.182886	0.214704	0.236209	0.249578	0.248755	0.237724	0.232618	0.248315	0.255750	0.251623	0.233539	0.213415	0.177510
	105	0.182886	0.221794	0.243663	0.262949	0.265504	0.256430	0.248517	0.251883	0.250167	0.242264	0.223527	0.206540	0.177510
	120	0.182886	0.226736	0.248335	0.267982	0.274296	0.267826	0.259747	0.253955	0.246188	0.234242	0.214405	0.195797	0.177510
	135	0.182886	0.230388	0.253786	0.273881	0.283344	0.276229	0.266085	0.256660	0.240412	0.220164	0.204949	0.182262	0.177510
	150	0.182886	0.231462	0.255900	0.276319	0.285783	0.280028	0.269365	0.257178	0.233353	0.206007	0.186594	0.167437	0.177510
	165	0.182886	0.233396	0.256345	0.275061	0.281932	0.279165	0.265418	0.248833	0.221802	0.189726	0.165791	0.159488	0.177510
	180	0.182886	0.233826	0.256456	0.274510	0.277761	0.276229	0.261582	0.245207	0.219107	0.187446	0.166013	0.159058	0.177510

Table A B-3 - f_p for the Adam-*float* manikin

Adam-*float*														
f_p		**β**												
		-90	**-75**	**-60**	**-45**	**-30**	**-15**	**0**	**15**	**30**	**45**	**60**	**75**	**90**
α	**0**	0.157928	0.136596	0.128880	0.157346	0.214962	0.257779	0.295691	0.316200	0.318628	0.306112	0.276012	0.231386	0.165366
	15	0.157928	0.142507	0.137406	0.172880	0.218872	0.260606	0.294435	0.313994	0.314907	0.301707	0.271858	0.231597	0.165366
	30	0.157928	0.154963	0.160580	0.193359	0.234699	0.273162	0.297712	0.313372	0.312637	0.297379	0.264097	0.229064	0.165366
	45	0.157928	0.166152	0.181021	0.211752	0.244094	0.275989	0.298040	0.313146	0.308665	0.286019	0.252291	0.220619	0.165366
	60	0.157928	0.177130	0.195341	0.224890	0.248698	0.268524	0.288644	0.299629	0.296116	0.277518	0.240376	0.207530	0.165366
	75	0.157928	0.183885	0.209223	0.231381	0.241824	0.252180	0.264117	0.271974	0.272785	0.262448	0.231632	0.196763	0.165366
	90	0.157928	0.190852	0.220482	0.242124	0.246365	0.245902	0.245381	0.252689	0.249959	0.244751	0.222340	0.188319	0.165366
	105	0.157928	0.197186	0.231194	0.259512	0.269569	0.266036	0.259966	0.255121	0.243527	0.230841	0.208458	0.179874	0.165366
	120	0.157928	0.204152	0.237097	0.268863	0.285712	0.285264	0.276736	0.261511	0.242518	0.224040	0.200150	0.171852	0.165366
	135	0.157928	0.210275	0.243000	0.272031	0.287919	0.290694	0.280232	0.264226	0.239807	0.214843	0.187579	0.164041	0.165366
	150	0.157928	0.217875	0.250433	0.278059	0.293153	0.290863	0.279740	0.258514	0.231988	0.199774	0.169871	0.151374	0.165366
	165	0.157928	0.221464	0.255352	0.283314	0.294288	0.291259	0.254940	0.254046	0.222655	0.184626	0.158612	0.145252	0.165366
	180	0.157928	0.221675	0.255898	0.287101	0.298323	0.294709	0.279522	0.254159	0.218115	0.180994	0.155879	0.145463	0.165366

Table A B-4 - f_p for the Youssef-*stool* manikin

Youssef-*stool*														
f_p		**β**												
		-90	**-75**	**-60**	**-45**	**-30**	**-15**	**0**	**15**	**30**	**45**	**60**	**75**	**90**
α	**0**	0.136234	0.118687	0.116972	0.143458	0.199617	0.249465	0.279854	0.296630	0.303190	0.290491	0.266427	0.228698	0.178457
	15	0.136234	0.124048	0.125633	0.163476	0.217167	0.261300	0.287567	0.303639	0.305368	0.291747	0.265761	0.228698	0.178457
	30	0.136234	0.133698	0.147396	0.185849	0.234013	0.273019	0.294170	0.309556	0.308378	0.291590	0.263429	0.227840	0.178457
	45	0.136234	0.143562	0.164051	0.205631	0.244262	0.274570	0.296056	0.309499	0.305240	0.286252	0.256323	0.223122	0.178457
	60	0.136234	0.151283	0.175377	0.216543	0.247208	0.265953	0.281851	0.293068	0.290700	0.273456	0.243887	0.214330	0.178457
	75	0.136234	0.154499	0.181706	0.212853	0.231195	0.240044	0.250334	0.262219	0.263093	0.253360	0.232006	0.206610	0.178457
	90	0.136234	0.159003	0.187702	0.215444	0.228697	0.232346	0.236573	0.246708	0.249130	0.241585	0.221013	0.200605	0.178457
	105	0.136234	0.161362	0.192033	0.225649	0.243557	0.251476	0.251444	0.251706	0.247849	0.234755	0.213463	0.195459	0.178457
	120	0.136234	0.164578	0.192699	0.226120	0.249706	0.260381	0.262985	0.256934	0.247144	0.228946	0.207911	0.187739	0.178457
	135	0.136234	0.167152	0.197140	0.230045	0.253485	0.267217	0.271586	0.261932	0.243877	0.219055	0.199694	0.177660	0.178457
	150	0.136234	0.168224	0.195697	0.223451	0.245671	0.257508	0.261986	0.256187	0.236575	0.208065	0.184149	0.166508	0.178457
	165	0.136234	0.172942	0.197029	0.223686	0.244454	0.257106	0.258435	0.251017	0.228633	0.196368	0.169048	0.162648	0.178457
	180	0.136234	0.177231	0.198584	0.224314	0.240739	0.255038	0.253663	0.244927	0.222740	0.193620	0.168715	0.163506	0.178457

Table A B-5 - f_p for the Adam-*stool* manikin

Adam-*stool*														
f_p		**β**												
		-90	**-75**	**-60**	**-45**	**-30**	**-15**	**0**	**15**	**30**	**45**	**60**	**75**	**90**
α	**0**	0.106619	0.086794	0.094141	0.142294	0.207416	0.255113	0.294277	0.314716	0.316978	0.304645	0.274141	0.229432	0.164128
	15	0.106619	0.092062	0.103304	0.159725	0.213772	0.259064	0.293350	0.312401	0.313705	0.300017	0.270541	0.228800	0.164128
	30	0.106619	0.105125	0.124250	0.176384	0.227931	0.271030	0.296512	0.312401	0.311629	0.294850	0.262141	0.225850	0.164128
	45	0.106619	0.116502	0.141814	0.188339	0.233595	0.272836	0.296894	0.311216	0.307035	0.283667	0.250141	0.218265	0.164128
	60	0.106619	0.127036	0.154905	0.199599	0.236427	0.265329	0.287571	0.298122	0.294952	0.276494	0.238796	0.205202	0.164128
	75	0.106619	0.132514	0.166577	0.204227	0.228497	0.248679	0.262494	0.270635	0.271605	0.260914	0.229959	0.194879	0.164128
	90	0.106619	0.137571	0.175632	0.213173	0.232399	0.241454	0.244558	0.250993	0.248383	0.242790	0.219487	0.186872	0.164128
	105	0.106619	0.144102	0.184250	0.228213	0.253040	0.261548	0.258950	0.253871	0.242531	0.229755	0.206832	0.177391	0.164128
	120	0.106619	0.150844	0.188505	0.234074	0.266256	0.279101	0.275523	0.259911	0.241461	0.223122	0.198759	0.169385	0.164128
	135	0.106619	0.155690	0.193305	0.232917	0.262417	0.279383	0.275360	0.260249	0.237559	0.213327	0.185886	0.161379	0.164128
	150	0.106619	0.163696	0.196359	0.229910	0.254110	0.263918	0.261676	0.245179	0.225099	0.197979	0.168541	0.149159	0.164128
	165	0.106619	0.166857	0.201814	0.235231	0.256690	0.265442	0.260531	0.241059	0.215660	0.183325	0.157086	0.142627	0.164128
	180	0.106619	0.166646	0.203777	0.238779	0.259963	0.265894	0.258841	0.237165	0.207353	0.178698	0.154468	0.142627	0.164128

Table A B-6 - f_p for the Youssef-*chair* manikin

Youssef-*chair*														
f_p		**β**												
		-90	**-75**	**-60**	**-45**	**-30**	**-15**	**0**	**15**	**30**	**45**	**60**	**75**	**90**
α	**0**	0.053284	0.080958	0.091557	0.137699	0.200653	0.254802	0.285013	0.301810	0.309198	0.298711	0.279393	0.259811	0.186842
	15	0.053284	0.085604	0.096039	0.151381	0.213078	0.264305	0.292280	0.308032	0.311216	0.299948	0.279284	0.260444	0.186842
	30	0.053284	0.095529	0.113642	0.169005	0.226575	0.274940	0.298618	0.313576	0.313676	0.299870	0.277207	0.259178	0.186842
	45	0.053284	0.104397	0.124248	0.179672	0.231621	0.272734	0.297525	0.310691	0.309513	0.294459	0.270537	0.253899	0.186842
	60	0.053284	0.107142	0.128621	0.178899	0.224052	0.256329	0.278566	0.291288	0.291097	0.279154	0.257964	0.246508	0.186842
	75	0.053284	0.106931	0.127090	0.167381	0.201032	0.226179	0.243871	0.257687	0.260886	0.257047	0.245718	0.237428	0.186842
	90	0.053284	0.105453	0.125997	0.163053	0.193778	0.215997	0.229829	0.241678	0.245875	0.243829	0.234894	0.232149	0.186842
	105	0.053284	0.102286	0.121077	0.158801	0.192139	0.218542	0.230430	0.235909	0.238496	0.234399	0.226257	0.227081	0.186842
	120	0.053284	0.095529	0.106535	0.136694	0.165397	0.189184	0.201472	0.201912	0.201978	0.204794	0.209529	0.217157	0.186842
	135	0.053284	0.088771	0.087949	0.102142	0.121878	0.140253	0.153336	0.153320	0.154359	0.160734	0.179571	0.200475	0.186842
	150	0.053284	0.083915	0.070236	0.068749	0.076152	0.084817	0.094600	0.097205	0.103272	0.112422	0.139664	0.180837	0.186842
	165	0.053284	0.082225	0.063786	0.054526	0.050545	0.048671	0.050125	0.052687	0.061078	0.073773	0.108066	0.170490	0.186842
	180	0.053284	0.081381	0.061490	0.050352	0.040390	0.039620	0.038378	0.037810	0.047896	0.063106	0.103583	0.169857	0.186842

Table A B-7 - f_p for the Adam-*chair* manikin

Adam-*chair*														
f_p		**β**												
		-90	**-75**	**-60**	**-45**	**-30**	**-15**	**0**	**15**	**30**	**45**	**60**	**75**	**90**
α	**0**	0.037253	0.033383	0.067773	0.130005	0.199937	0.251198	0.292172	0.312950	0.315127	0.303511	0.273403	0.229863	0.163750
	15	0.037253	0.041108	0.071665	0.138872	0.201559	0.255561	0.291470	0.310209	0.311697	0.298695	0.269727	0.230698	0.163750
	30	0.037253	0.052592	0.089504	0.152783	0.214842	0.266021	0.295036	0.310433	0.309826	0.293880	0.261187	0.226731	0.163750
	45	0.037253	0.062197	0.103234	0.163866	0.219146	0.267027	0.294550	0.309426	0.305335	0.283103	0.249943	0.219632	0.163750
	60	0.037253	0.071384	0.111126	0.168834	0.218273	0.258973	0.286067	0.296058	0.293049	0.275306	0.238267	0.206686	0.163750
	75	0.037253	0.074725	0.115775	0.166006	0.205987	0.240011	0.261269	0.269041	0.270036	0.259867	0.230483	0.197499	0.163750
	90	0.037253	0.078275	0.119992	0.164706	0.198378	0.226083	0.237713	0.245996	0.244716	0.241293	0.219455	0.188103	0.163750
	105	0.037253	0.080989	0.122154	0.169598	0.207171	0.230446	0.239172	0.236655	0.228688	0.221573	0.203779	0.178498	0.163750
	120	0.037253	0.083077	0.114586	0.165471	0.206548	0.233019	0.238794	0.227537	0.213907	0.204681	0.192643	0.169311	0.163750
	135	0.037253	0.085165	0.113181	0.156681	0.193950	0.221608	0.225341	0.214225	0.198752	0.187254	0.176643	0.160750	0.163750
	150	0.037253	0.087879	0.115559	0.151177	0.184096	0.203485	0.208160	0.195151	0.181290	0.165241	0.155453	0.150937	0.163750
	165	0.037253	0.089759	0.117829	0.149878	0.177610	0.197612	0.200002	0.181950	0.166072	0.147585	0.143993	0.144882	0.163750
	180	0.037253	0.087253	0.112748	0.146744	0.174492	0.193920	0.194329	0.179936	0.162642	0.146515	0.140965	0.144255	0.163750

LIST OF BIBLIOGRAPHICAL REFERENCES

Alfano, F. R. d'Ambrosio, Dell'isola, M., Ficco, G., Palella, B. I., & Riccio, G. (2021). On the measurement of the mean radiant temperature by means of globes: An experimental investigation under black enclosure conditions. *Building and Environment*, *193*, 107655. https://doi.org/10.1016/J.BUILDENV.2021.107655

Alfano, F. R. d'Ambrosio, Ficco, G., Frattolillo, A., Palella, B. I., & Riccio, G. (2021). Mean Radiant Temperature Measurements through Small Black Globes under Forced Convection Conditions. *Atmosphere 2021, Vol. 12, Page 621*, *12*(5), 621. https://doi.org/10.3390/ATMOS12050621

Alfano, F. R. d'Ambrosio, Ianniello, E., & Palella, B. I. (2013). PMV-PPD and acceptability in naturally ventilated schools. *Building and Environment*, *67*, 129–137. https://doi.org/10.1016/J.BUILDENV.2013.05.013

Alfano, F. R. d'Ambrosio, Pepe, D., Riccio, G., Vio, M., & Palella, B. I. (2023). On the effects of the mean radiant temperature evaluation in the assessment of thermal comfort by dynamic energy simulation tools. *Building and Environment*, *236*, 110254. https://doi.org/10.1016/J.BUILDENV.2023.110254

Amorim, P. R. dos S. (2007). *Energy expenditure and physical activity patterns in children: applicability of simultaneous methods*. Queensland University of Technology.

Ansys. (2010). *Ansys FLUENT 12.0 User's Guide - 13.3.3 Setting Up the S2S Model*. https://www.afs.enea.it/project/neptunius/docs/fluent/html/ug/node475.htm#sec-s2s-viewfactorsmethod

Arens, E., Hoyt, T., Zhou, X., Huang, L., Zhang, H., & Schiavon, S. (2015). Modeling the comfort effects of short-wave solar radiation indoors. *Building and Environment*, *88*, 3–9. https://doi.org/10.1016/J.BUILDENV.2014.09.004

ASHRAE. (2017). 2017 ASHRAE handbook. Fundamentals. In *2017 ASHRAE HANDBOOK*. ASHRAE, [2017].

ASHRAE-55. (2017). Thermal environmental conditions for human occupancy. *ANSI/ASHRAE Standard - 55*, *7*, 1–14.

Bedford, T. (1935). The effective radiating surface of the human body. *Journal of Hygiene*, *35*(3), 303–306. https://doi.org/10.1017/S0022172400032319

Blender Documentation Team. (2025, October 4). *Blender 4.5 Manual*. https://docs.blender.org/manual/en/latest/index.html

Calvino, F., Gennusa, M. La, Nucara, A., Rizzo, G., & Scaccianoce, G. (2005). Evaluating human body area factors from digital images: A measurement tool for a better evaluation of the ergonomics of working places. *Occupational Ergonomics*, *5*, 173–185.

Calvino, F., La Gennusa, M., Rizzo, G., Scaccianoce, G., & Simone, A. (2009). Measurements of projected areas of seated and standing people of southern Italy based on a statistical analysis. *Applied Ergonomics*, *40*(2), 239–250. https://doi.org/10.1016/j.apergo.2008.04.013

Cannistraro, G., Franzitta, G., Giaconia, C., & Rizzo, G. (1992). Algorithms for the calculation of the view factors between human body and rectangular surfaces in parallelepiped environments. *Energy and Buildings*, *19*(1), 51–60. https://doi.org/10.1016/0378-7788(92)90035-F

cgtrader.com user Rafor. (2023, January 31). *Chair and school desk Free low-poly 3D model*.

Chen, Y., He, Y., & Li, N. (2024). *A Novel Model for Calculating Human-Body Angle Factor in Radiant Heat Transfer: Balancing Computation Accuracy and Speed*. https://doi.org/10.3390/buildings14020366

Cheng, W., & Brown, R. D. (2020). An energy budget model for estimating the thermal comfort of children. *International Journal of Biometeorology*, *64*(8), 1355–1366. https://doi.org/10.1007/S00484-020-01916-X

Colley, R. C., Lang, J. J., Saunders, T. J., Roberts, K. C., Butler, G. P., & Prince, S. A. (2022). How sedentary are Canadian adults? It depends on the measure. *Health Reports*, *33*(10), 14–27. https://doi.org/10.25318/82-003-X202201000002-ENG

Conceição, E. Z. E., & Lúcio, M. M. J. R. (2008). Thermal study of school buildings in winter conditions. *Building and Environment*, *43*(5), 782–792. https://doi.org/10.1016/J.BUILDENV.2007.01.029

Cumber, P. S. (2022). View factors-when is ray tracing a good idea? *International Journal of Heat and Mass Transfer*, *189*, 122698. https://doi.org/10.1016/J.IJHEATMASSTRANSFER.2022.122698

De Dear, R., Kim, J., Candido, C., & Deuble, M. (2015). Adaptive thermal comfort in australian school classrooms. *Building Research and Information*, *43*(3), 383–398. https://doi.org/10.1080/09613218.2015.991627

De Giuli, V., Da Pos, O., & De Carli, M. (2012). Indoor environmental quality and pupil perception in Italian primary schools. *Building and Environment*, *56*, 335–345. https://doi.org/10.1016/J.BUILDENV.2012.03.024

Dijken, F. V., Bronswijk, J. V., & Sundell, J. (2005). Indoor environment in Dutch primary schools and health of the pupils. *Indoor Air*, *15(1)*, 623–627. https://www.researchgate.net/publication/254837674_Indoor_environment_in_Dutch_primary_schools_and_health_of_the_pupils

Du Bois, D., & Du Bois, E. F. (1916). A Formula to Estimate the Approximate Surface Area if Height and Weight be Known. *Nutrition*, *5(5)*, 303–311. https://www.researchgate.net/publication/20636456_A_Formula_to_Estimate_the_Approximate_Surface_Area_if_Height_and_Weight_be_Known

Emberson, L., & Owen, D. (2025). *The stock of computing power from NVIDIA chips is doubling every 10 months*. Epoch.Ai. https://epoch.ai/data-insights/nvidia-chip-production

Fabbri, K. (2013). Thermal comfort evaluation in kindergarten: PMV and PPD measurement through datalogger and questionnaire. *Building and Environment*, *68*, 202–214. https://doi.org/10.1016/J.BUILDENV.2013.07.002

Fan, Y., & McColl, K. A. (2024). Widespread outdoor exposure to uncompensable heat stress with warming. *Communications Earth and Environment*, *5*(1). https://doi.org/10.1038/S43247-024-01930-6

Fanger, P. O. (1970). *Thermal comfort. Analysis and applications in environmental engineering.* Copenhagen: Danish Technical Press. https://www.cabdirect.org/cabdirect/abstract/19722700268

Flouris, A. D., Dinas, P. C., Ioannou, L. G., Nybo, L., Havenith, G., Kenny, G. P., & Kjellstrom, T. (2018). Workers' health and productivity under occupational heat strain: a systematic review and meta-analysis. *The Lancet Planetary Health*, *2*(12), e521–e531. https://doi.org/10.1016/S2542-5196(18)30237-7

Folkerts, M. A., Gerrett, N., Kingma, B. R. M., Zuurbier, M., & Daanen, H. A. M. (2020). Care provider assessment of thermal state of children in day-care centers. *Building and Environment*, *179*. https://doi.org/10.1016/J.BUILDENV.2020.106915

Fountain, M. (1987). *UC Berkeley Indoor Environmental Quality (IEQ) Title Instrumentation for thermal comfort measurements: The globe thermometer*. https://escholarship.org/uc/item/1qx8c7sm

Francisco, S. C., Raimundo, A. M., Gaspar, A. M., & Quintela, D. A. (2012). Numerical evaluation of radiative heat exchanges between human beings and cooling radiant systems. *Proceedings of 7th Windsor Conference: The Changing Context of Comfort in an Unpredictable World. Cumberland Lodge, Windsor, UK, 12-15 April 2012.*, 1–12.

https://www.researchgate.net/publication/267843905_Numerical_evaluation_of_radiative_heat_exchanges_between_human_beings_and_cooling_radiant_systems

Fredriks, A. M., Van Buuren, S., Van Heel, W. J. M., Dijkman-Neerincx, R. H. M., Verloove-Vanhorick, S. P., & Wit, J. M. (2005). Nationwide age references for sitting height, leg length, and sitting height/height ratio, and their diagnostic value for disproportionate growth disorders. *Archives of Disease in Childhood*, *90*(8), 807–812. https://doi.org/10.1136/ADC.2004.050799

free3d.com user ksalk3d. (2019, November 20). *Wood Stool 3D Model*. https://free3d.com/3d-model/wood-stool-303532.html

free3d.com user printable_models. (2019, November 20). *Office Chair v1 3D Model*. https://free3d.com/3d-model/office-chair-v1--160271.html

Frisancho, A. R. (2008). *Anthropometric standards: an interactive nutritional reference of body size and body composition for children and adults*. University of Michigan Press.

Gao, S., Oh, W., Lin, C., & Feng, C. (2024). A review of thermal comfort of 4- to 14-year-old children via field experiments: Experimental designs and methods. *Energy and Buildings*, *322*, 114687. https://doi.org/10.1016/J.ENBUILD.2024.114687

Gerber, B., & Pienaar, A. E. (2025). Age-Related Changes in Predictors of BMI in 6, 9 and 12-Year-Old Boys and Girls: The NW-CHILD Study. Journal of functional morphology and kinesiology, 10(3), 320. https://doi.org/10.3390/jfmk10030320

Habibi, P., Razmjouei, J., Moradi, A., Mahdavi, F., Fallah-Aliabadi, S., & Heydari, A. (2024). Climate change and heat stress resilient outdoor workers: findings from systematic literature review. *BMC Public Health*, *24*(1), 1711. https://doi.org/10.1186/S12889-024-19212-3

Haddad, S., Osmond, P., & King, S. (2013). Metabolic rate estimation in the calculation of PMV for children. *Cutting Edge: 47th International Conference of the Architectural Science Association*. https://www.researchgate.net/publication/265051186_Metabolic_rate_estimation_in_the_calculation_of_PMV_for_children

Haddad, S., Osmond, P., King, S., & Heidari, S. (2014, April 10). Developing assumptions of metabolic rate estimation for primary school children in the calculation of the Fanger PMV model. *Proceedings of 8th Windsor Conference: Counting the Cost of Comfort in a Changing World.* https://www.researchgate.net/publication/265051274_Developing_assumptions_of_metabolic_rate_estimation_for_primary_school_children_in_the_calculation_of_the_Fanger_PMV_model

Halawa, E., Van Hoof, J., & Soebarto, V. (2014). The impacts of the thermal radiation field on thermal comfort, energy consumption and control - A critical overview. *Renewable and Sustainable Energy Reviews*, *37*, 907–918. https://doi.org/10.1016/J.RSER.2014.05.040

Harrell, J. S., Mcmurray, R. G., Baggett, C. D., Pennell, M. L., Pearce, P. F., & Bangdiwala, S. I. (2005). Energy costs of physical activities in children and adolescents. *Medicine and Science in Sports and Exercise*, *37*(2), 329–336. https://doi.org/10.1249/01.MSS.0000153115.33762.3F

Havenith, G. (2007). Metabolic rate and clothing insulation data of children and adolescents during various school activities. *Taylor & Francis*, *50*(10), 1689–1701. https://doi.org/10.1080/00140130701587574

Havgaard Vorre, M., Lund Jensen, R., & Le Dréau, J. (2015). Radiation exchange between persons and surfaces for building energy simulations. *Energy and Buildings*, *101*, 110–121. https://doi.org/10.1016/j.enbuild.2015.05.005

Haycock, G. B., Schwartz, G. J., & Wisotsky, D. H. (1978). Geometric method for measuring body surface area: A height-weight formula validated in infants, children, and adults. *The Journal of Pediatrics*, *93*(1), 62–66. https://doi.org/10.1016/S0022-3476(78)80601-5

Hooshmand, S. M., Zhang, H., Javidanfar, H., Zhai, Y., & Wagner, A. (2023). A review of local radiant heating systems and their effects on thermal comfort and sensation. *Energy and Buildings*, *296*, 113331. https://doi.org/10.1016/J.ENBUILD.2023.113331

Hope, D., Bates, T. C., Dykiert, D., Der, G., & Deary, I. J. (2013). Bodily symmetry increases across human childhood. *Early Human Development*, *89*(8), 531–535. https://doi.org/10.1016/J.EARLHUMDEV.2013.01.003

Horikoshi, T., Tsuchikawa Kobayashi, T. Y., & Miwa Kurazumi K Hirayama, E. Y. (1990). The Effective Radiation Area and Angle Factor Between Man and a Rectangular Plane Near Him. *ASHRAE Transactions*, 60–66.

Howell, J. R., Menguc, M. P., & Siegel, R. (2015). Thermal Radiation Heat Transfer. *Thermal Radiation Heat Transfer*. https://doi.org/10.1201/B18835

Hu, R., & Niu, J. L. (2012). A review of the application of radiant cooling & heating systems in Mainland China. *Energy and Buildings*, *52*, 11–19. https://doi.org/10.1016/J.ENBUILD.2012.05.030

Humphreys, M. A. (1977). The optimum diameter for a globe thermometer for use indoors. *Academic.Oup.ComMA HumphreysThe Annals of Occupational Hygiene,*

1977•academic.Oup.Com, *20*(2), 135–140. https://academic.oup.com/annweh/article-abstract/20/2/135/178618

Imhoff, M. L., Zhang, P., Wolfe, R. E., & Bounoua, L. (2010). Remote sensing of the urban heat island effect across biomes in the continental USA. *Remote Sensing of Environment*, *114*(3), 504–513. https://doi.org/10.1016/J.RSE.2009.10.008

Incropera, F. P., DeWitt, D. P., Bergman, T. L., & Lavine, A. S. (2011). *Fundamentals of Heat and Mass Transfer-Incropera.pdf*. https://books.google.com/books/about/Fundamentals_of_Heat_and_Mass_Transfer.html?id=vvyIoXEywMoC

ISO. (1994). *ISO 7730: Moderate Thermal Environments-Determination of the PMV and PPD Indices and Specification of the Conditions for Thermal Comfort*.

ISO 7726. (1998). International Organization for Standardization: Ergonomics of the thermal environment — Instruments for measuring physical quantities. *ISO Standard*, *1998*(1), 1–56. https://doi.org/ISO 7726:1998 (E)

ISO 7730. (2005). *International Organization for Standardization: Ergonomics of the thermal environment — Analytical determination and interpretation of thermal comfort using calculation of the PMV and PPD indices and local thermal comfort criteria*. https://www.iso.org/standard/39155.html

ISO 9920. (2007). *9920: Estimation of the thermal insulation and evaporative resistance of a clothing ensemble*.

Jones, B., Hong, S., & McCullough, E. (1998). Detailed projected area data for the human body. *ASHRAE Trans 104(2)*, 1327–1339.

Kalisperis, L. N., Steinman, M., & Summers, L. H. (1991). Angle Factor Graphs for a Person to Inclined Surfaces. *ASHRAE Trans., 97(2)*, 809–839. https://subscriptions.techstreet.com/products/566485

Kántor, N., & Unger, J. (2011). The most problematic variable in the course of human-biometeorological comfort assessment-the mean radiant temperature. *Cent. Eur. J. Geosci.* •, *3*(1), 90–100. https://doi.org/10.2478/s13533-011-0010-x

Kramer, S. C., Gritzki, R., Perschk, A., Rösler, M., & Felsmann, C. (2015). Fully parallel, OpenGL-based computation of obstructed area-to-area view factors. *Journal of Building Performance Simulation*, *8*(4), 266–281. https://doi.org/10.1080/19401493.2014.917700;WEBSITE:WEBSITE:TFOPB;PAGEGROUP:STRING:PUBLICATION

Kubaha, K., Fiala, D., Toftum, J., & Taki, A. H. (2004). Human projected area factors for detailed direct and diffuse solar radiation analysis. *International Journal of Biometeorology*, *49*(2), 113–129. https://doi.org/10.1007/s00484-004-0214-6

Kurazumi, Y., Tsuchikawa, T., Matsubara, N., & Horikoshi, T. (2008). Effect of posture on the heat transfer areas of the human body. *Building and Environment*, *43*(10), 1555–1565. https://doi.org/10.1016/j.buildenv.2007.09.001

La Gennusa, M., Nucara, A., Pietrafesa, M., & Rizzo, G. (2007). A model for managing and evaluating solar radiation for indoor thermal comfort. *Solar Energy*, *81*(5), 594–606. https://doi.org/10.1016/j.solener.2006.09.005

La Gennusa, M., Nucara, A., Pietrafesa, M., Rizzo, G., & Scaccianoce, G. (2008). Angle Factors and Projected Area Factors for Comfort Analysis of Subjects in Complex Confined Enclosures: Analytical Relations and Experimental Results. *Indoor and Built Environment*, *17*(4), 346–360. https://doi.org/10.1177/1420326X08094621

La Gennusa, M., Nucara, A., Rizzo, G., & Scaccianoce, G. (2005). The calculation of the mean radiant temperature of a subject exposed to the solar radiation - A generalised algorithm. *Building and Environment*, *40*(3), 367–375. https://doi.org/10.1016/j.buildenv.2004.06.019

Larsen, M. E., & Howell, J. R. (1986). Least-Squares Smoothing of Direct-Exchange Areas in Zonal Analysis. *Journal of Heat Transfer*, *108*(1), 239–242. https://doi.org/10.1115/1.3246898

Li, Z., Feng, X., Fan, X., Sun, J., & Fang, Z. (2022). Effect of direct solar projected area factor on outdoor thermal comfort evaluation: A case study in Shanghai, China. *Urban Climate*, *41*, 101033. https://doi.org/10.1016/j.uclim.2021.101033

Liu, G., Nagano, K., Ye, M., & Liu, H. (2025). Optimization of a radiant heating system in a net Zero energy house (nZEH) to maintain a comfortable indoor environment while minimizing energy consumption. *Energy and Buildings*, *328*, 115208. https://doi.org/10.1016/J.ENBUILD.2024.115208

Lo Curcio FP. (2009). *Scambi termici tra corpo umano ed ambiente indoor: verifi ca della validità degli algoritmi per il calcolo del fattore di area proiettata* [Degree Thesis]. University of Palermo (in Italian).

Looney, D. P., Sanford, D. P., Li, P., Santee, W. R., Doughty, E. M., & Potter, A. W. (2020). Formulae for calculating body surface area in modern U.S. Army Soldiers. *Journal of Thermal Biology*, *92*, 102650. https://doi.org/10.1016/J.JTHERBIO.2020.102650

Luo, M., Wang, Z., Ke, K., Cao, B., Zhai, Y., & Zhou, X. (2018). Human metabolic rate and thermal comfort in buildings: The problem and challenge. *Building and Environment*, *131*, 44–52. https://doi.org/10.1016/J.BUILDENV.2018.01.005

Manabe, M., Yamazaki, H., & Sakai, K. (2004). Shape factor simulation for the thermal radiation environment of the human body and the VRML visualization. *Building and Environment*, *39*(8), 927–937. https://doi.org/10.1016/J.BUILDENV.2004.01.017

Martinez-Molina, A., Boarin, P., Tort-Ausina, I., & Vivancos, J. L. (2017). Post-occupancy evaluation of a historic primary school in Spain: Comparing PMV, TSV and PD for teachers' and pupils' thermal comfort. *Building and Environment*, *117*, 248–259. https://doi.org/10.1016/J.BUILDENV.2017.03.010

Matthews, C. E., Chen, K. Y., Freedson, P. S., Buchowski, M. S., Beech, B. M., Pate, R. R., & Troiano, R. P. (2008). Amount of Time Spent in Sedentary Behaviors in the United States, 2003–2004. *American Journal of Epidemiology*, *167*(7), 875. https://doi.org/10.1093/AJE/KWM390

Mcdowell, M. A., Fryar, C. D., Ogden, C. L., & Flegal, K. M. (2008). *Anthropometric reference data for children and adults: United States, 2003–2006. National health statistics reports; no 10.* (Vol. 22). http://www.cdc.gov/nchs/data/nhanes/

Miyazaki, Y. (1995). A study on evaluation of Non-uniform thermal environments by human body model Part 1. *Journal of Human and Living Environment*. https://cir.nii.ac.jp/crid/1571698599527152512

Modest, M., & Mazumder, S. (2021). *Radiative heat transfer*. https://books.google.com/books?hl=en&lr=&id=j2Q0EAAAQBAJ&oi=fnd&pg=PP1&ots=8Y-qtpeyOM&sig=PZfePgXkxDV90KRo4z0nTjmAZwU

Montazami, A., Gaterell, M., Nicol, F., Lumley, M., & Thoua, C. (2017). Impact of social background and behaviour on children's thermal comfort. *Building and Environment*, *122*, 422–434. https://doi.org/10.1016/J.BUILDENV.2017.06.002

Montazami, A., & Nicol, F. (2013). Overheating in schools: Comparing existing and new guidelines. *Building Research and Information*, *41*(3), 317–329. https://doi.org/10.1080/09613218.2013.770716

Mors, S. ter, Hensen, J. L. M., Loomans, M. G. L. C., & Boerstra, A. C. (2011). Adaptive thermal comfort in primary school classrooms: Creating and validating PMV-based comfort charts. *Building and Environment*, *46*(12), 2454–2461. https://doi.org/10.1016/J.BUILDENV.2011.05.025

Nam, I., Yang, J., Lee, D., Park, E., & Sohn, J. R. (2015). A study on the thermal comfort and clothing insulation characteristics of preschool children in Korea. *Building and Environment*, *92*, 724–733. https://doi.org/10.1016/J.BUILDENV.2015.05.041

Natural Resources Canada. (2024). *Fact sheet: Reducing Electric Heating Costs With Radiant Floors*. https://publications.gc.ca/collections/collection_2025/rncan-nrcan/M154-170-2024-eng.pdf

Nucara, A., Pietrafesa, M., Rizzo, G., Scaccianoce, G., & Scaccianoce, G. (2012). *Handbook of Anthropometry: Physical Measures of Human Form in Health and Disease*. https://doi.org/10.1007/978-1-4419-1788-1_4

Oliveira, A. V. M., Raimundo, A. M., Gaspar, A. R., & Quintela, D. A. (2019). Globe Temperature and Its Measurement: Requirements and Limitations. *Annals of Work Exposures and Health*, *63*(7), 743–758. https://doi.org/10.1093/ANNWEH/WXZ042

Park, S., & Tuller, S. E. (2011). Human body area factors for radiation exchange analysis: Standing and walking postures. *Article in International Journal of Biometeorology*. https://doi.org/10.1007/s00484-010-0385-2

Rhee, K. N., & Kim, K. W. (2015). A 50 year review of basic and applied research in radiant heating and cooling systems for the built environment. *Building and Environment*, *91*, 166–190. https://doi.org/10.1016/J.BUILDENV.2015.03.040

Rizzo, G., Franzitta, G., & Cannistraro, G. (1991). Algorithms for the calculation of the mean projected area factors of seated and standing persons. *Energy and Buildings*, *17*(3), 221–230. https://doi.org/10.1016/0378-7788(91)90109-G

Rusek, W., Baran, J., Leszczak, J., Adamczyk, M., Baran, R., Weres, A., Inglot, G., Czenczek-Lewandowska, E., & Pop, T. (2021). Changes in Children's Body Composition and Posture during Puberty Growth. Children (Basel, Switzerland), 8(4), 288. https://doi.org/10.3390/children8040288

Rykaczewski, K., Bartels, L., Martinez, D. M., & Viswanathan, S. H. (2022). Human body radiation area factors for diverse adult population. *International Journal of Biometeorology*, *66*(11), 2357–2367. https://doi.org/10.1007/s00484-022-02362-7

Schofield, W. (1985). Predicting basal metabolic rate, new standards and review of previous work. *Human Nutrition. Clinical Nutrition*, *39*, 5–41. https://www.researchgate.net/publication/312921374_Predicting_basal_metabolic_rate_new_standards_and_review_of_previous_work

Schweiker, M., Huebner, G. M., Kingma, B. R. M., Kramer, R., & Pallubinsky, H. (2018). Drivers of diversity in human thermal perception–A review for holistic comfort models. *Temperature*, *5*(4), 308–342. https://doi.org/10.1080/23328940.2018.1534490

Sönmez, F. F., Ziar, H., Isabella, O., & Zeman, M. (2019). Fast and accurate ray-casting-based view factor estimation method for complex geometries. *Solar Energy Materials and Solar Cells*, *200*, 109934. https://doi.org/10.1016/J.SOLMAT.2019.109934

Souza, J., Nogueira, B. L., Lima, A. V. P., & Leder, S. (2020). Thermal Comfort Analysis in Both Naturally Ventilated and Air-Conditioned Classrooms in a Warm and Humid Climate. *IOP Conference Series: Earth and Environmental Science*, *503*(1). https://doi.org/10.1088/1755-1315/503/1/012044

Tanabe, S., Narita, C., Ozeki, Y., & Konishi, M. (2000). Effective radiation area of human body calculated by a numerical simulation. *Energy and Buildings*, *32*(2), 205–215. https://doi.org/10.1016/S0378-7788(00)00045-1

Tartarini, F., Schiavon, S., Cheung, T., & Hoyt, T. (2020). CBE Thermal Comfort Tool: Online tool for thermal comfort calculations and visualizations. *SoftwareX*, *12*. https://doi.org/10.1016/j.softx.2020.100563

Teli, D., Dalenbäck, J.-O., & Ekberg, L. E. (2016, July). Winter thermal comfort and indoor air quality in Swedish grade school classrooms, as assessed by the children. *Conference: 14th International Conference of Indoor Air Quality and Climate*. https://www.researchgate.net/publication/305999701_Winter_thermal_comfort_and_indoor_air_quality_in_Swedish_grade_school_classrooms_as_assessed_by_the_children

Teli, D., Jentsch, M. F., & James, P. A. B. (2012). Naturally ventilated classrooms: An assessment of existing comfort models for predicting the thermal sensation and preference of primary school children. *Energy and Buildings*, *53*, 166–182. https://doi.org/10.1016/J.ENBUILD.2012.06.022

TheGlobalEconomy.com. (2025). *Percent children by country, around the world*. Https://Www.Theglobaleconomy.Com/Rankings/Percent_children/#:~:Text=Population%20ages%200%2D14%2C%20percent,Download%20data%20from%20our%20database. https://www.theglobaleconomy.com/rankings/percent_children/

Trebilcock, M., Soto, J., & Figueroa, R. (2014). Thermal comfort in primary schools: a field study in Chile. *Proceedings of 8th Windsor Conference: Counting the Cost of Comfort in a Changing World*, 421–431. https://www.researchgate.net/publication/278038413_Thermal_comfort_in_primary_schools_a_field_study_in_Chile

Underwood, & Ward. (1966). The Solar Radiation Area of Man. *Ergonomics*, *9*(2), 155–168. https://doi.org/10.1080/00140136608964361

United States Environmental Protection Agency. (2025). *Improving Your Indoor Environment US EPA*. Improving Your Indoor Environment. https://www.epa.gov/indoor-air-quality-iaq/improving-your-indoor-environment#text

University of Michigan Transportation Research Institute. (2020). *UMTRI BioHuman: 3d human shapes*. http://humanshape.org/

Vignerov, J. (2009). Anthropometric Standards. An Interactive Nutritional Reference of Body Size and Body Composition for Children and Adults. A. Roberto Frisancho, 2008, ISBN 13: 978-0-472-11591-4, ISBN 10: 0-472-11591-X, published in USA by The University of Michigan Press, price 85 USD, 335 pp., 143 growth references tables, 89 growth charts, complementary tables and figures, CD. *Economics & Human Biology*, *7*(1), 130–131.

Walker, T., Xue, S. C., & Barton, G. W. (2010). Numerical determination of radiative view factors using ray tracing. *Journal of Heat Transfer*, *132*(7), 1–6. https://doi.org/10.1115/1.4000974

Wang, D., Jiang, J., Liu, Y., Wang, Y., Xu, Y., & Liu, J. (2017). Student responses to classroom thermal environments in rural primary and secondary schools in winter. *Building and Environment*, *115*, 104–117. https://doi.org/10.1016/J.BUILDENV.2017.01.006

Wang, J., & Hihara, E. (2004). Human body surface area: A theoretical approach. *European Journal of Applied Physiology*, *91*(4), 425–428. https://doi.org/10.1007/S00421-003-1011-3

Wang, Y., Li, N., Hu, J., He, Y., Yongga, A., Yuan, C., & Wang, M. (2020). Influence of the Shade from Other Occupants on the Angle Factor between a Human Body and Radiant Surface in Buildings. *Environmental Science and Engineering*, 749–757. https://doi.org/10.1007/978-981-13-9528-4_76

Wang, Y., Meng, X., Zhang, L., Liu, Y., Long, E., Wang, Y., Long, Á. E., Meng, X., Zhang, L., & Liu, Y. (2014). Angle Factor Calculation for the Thermal Radiation Environment of the Human Body. *Lecture Notes in Electrical Engineering*, *261*. https://doi.org/10.1007/978-3-642-39584-0_51

Wei, Q., Transactions, Y. J.-A., & 2004, undefined. (2004). Simple Approach to Evaluate the View Factors between Internal Heat Sources and Their Environment. *ASHRAE Transactions*. https://search.ebscohost.com/login.aspx?direct=true&profile=ehost&scope=site&authtype=crawler&jrnl=00012505&AN=15565090&h=FMpJ6SzO%2BRKW3EI0tVHUXyZBnB9JU5cnkfIjz0A9qm2bF0UwbNBatf4cBfQjhr%2FuBOThvQiC%2FYgBv0dHa8ztew%3D%3D&crl=c

Xu, J., Psikuta, A., Li, J., Annaheim, S., & Rossi, R. M. (2019). Influence of human body geometry, posture and the surrounding environment on body heat loss based on a validated numerical model. *Building and Environment*, *166*. https://doi.org/10.1016/j.buildenv.2019.106340

Yang, B., Olofsson, T., Wang, F., & Lu, W. (2018). Thermal comfort in primary school classrooms: A case study under subarctic climate area of Sweden. *Building and Environment*, *135*, 237–245. https://doi.org/10.1016/J.BUILDENV.2018.03.019

Yousaf, R., Fiala, D., & Wagner, A. (2008). Numerical simulation of human radiation heat transfer using a mathematical model of human physiology and computational fluid dynamics (CFD). In *High Performance Computing in Science and Engineering '07: Transactions of the High Performance Computing Center, Stuttgart (HLRS) 2007* (pp. 647–666). Springer Berlin Heidelberg. https://doi.org/10.1007/978-3-540-74739-0_42

Youssef, N., & D'Avignon, K. (2021). Evaluating Thermal Comfort of Children: A Perspective on Commonly Used Methods. *ASHRAE Transactions*, *127*.

Youssef, N., & D'Avignon, K. (2023). Investigation into the pertinence of using child-specific radiation data for thermal comfort calculations. *ASHRAE Transactions*, *129*(2).

Youssef, N., & D'Avignon, K. (2025). Considering child-specific view factors in human thermal balance. *Science and Technology for the Built Environment*. https://doi.org/10.1080/23744731.2025.2518734/ASSET/9868D75C-5D96-4658-8BFC-10DB8C707A68/ASSETS/GRAPHIC/UHVC_A_2518734_F0012_C.JPG

Yun, H., Nam, I., Kim, J., Yang, J., Lee, K., & Sohn, J. (2014). A field study of thermal comfort for kindergarten children in korea: An assessment of existing models and preferences of children. *Building and Environment*, *75*, 182–189. https://doi.org/10.1016/J.BUILDENV.2014.02.003

Zeiler, W., & Boxem, G. (2009). Effects of thermal activated building systems in schools on thermal comfort in winter. *Building and Environment*, *44*(11), 2308–2317. https://doi.org/10.1016/J.BUILDENV.2009.05.005

Zeng, Y., Liang, Y., Luo, M., Zhou, X., Zhai, Y., Zhang, H., Mohammad Hooshmand, S., & Wagner, A. (2024a). Calculating the local and overall view factors of a multi-segment human model. *Energy and Buildings*, *325*, 114967. https://doi.org/10.1016/J.ENBUILD.2024.114967

Zeng, Y., Liang, Y., Luo, M., Zhou, X., Zhai, Y., Zhang, H., Mohammad Hooshmand, S., & Wagner, A. (2024b). Calculating the local and overall view factors of a multi-segment human model. *Energy and Buildings*, 114967. https://doi.org/10.1016/J.ENBUILD.2024.114967